

Mechanisms of Lipid Homeostasis in the Endoplasmic Reticulum and Lipid Droplets

By

Clark W Peterson

A dissertation submitted in partial satisfaction of the

requirements for the degree of

Doctor of Philosophy

in

Metabolic Biology

in the

Graduate Division

of the

University of California, Berkeley

Committee in charge:

Professor James A. Olzmann, Chair

Professor Andreas Stahl

Professor Joseph Napoli

Fall 2020



## ABSTRACT

### Mechanisms of Lipid Homeostasis in the Endoplasmic Reticulum and Lipid Droplets

By

Clark W Peterson

Doctor of Philosophy in Metabolic Biology

University of California, Berkeley,

Professor James A. Olzmann, Chair

The endoplasmic reticulum (ER) serves as the entry point to the secretory system where nearly one-third of the cellular proteome must undergo synthesis, folding, and maturation events before being deployed<sup>1-3</sup>. Proteins that fail to successfully navigate these processes and achieve their native conformation are detained by endoplasmic reticulum-associated degradation (ERAD), a quality-control mechanism responsible for targeting misfolded proteins for degradation by the cytosolic 26S proteasome<sup>4</sup>. Recent studies have demonstrated that treatment with the long chain acyl-CoA synthetase inhibitor triacsin c disrupts lipid droplet (LD) biogenesis and ERAD, suggesting a functional connection between the processes<sup>142</sup>. However, whether LDs are involved in ERAD remains an outstanding question.

LDs are highly dynamic neutral lipid storage organelles that function as central hubs of lipid metabolism charged with storing lipids and maintaining energy homeostasis of the cell. The specific metabolic role of LDs is dictated by the cell type and the metabolic state of the cell, which can fluctuate in response to a number of cellular stimuli<sup>1,15</sup>. LD functions are regulated by a complement of integral and peripheral proteins that associate with the bounding LD phospholipid monolayer. The ability to define a high-confidence LD proteome is paramount to understanding LD functions and dynamics. However, accurate analysis of the LD proteome composition has remained a challenge due to the presence of contaminating proteins in LD-enriched buoyant fractions.

In chapter one, we discuss the connection between protein and lipid regulatory systems within the ER and LDs, highlighting the importance of ERAD and lipophagy in maintaining cellular homeostasis. In chapter two, we use chemical and genetic approaches to disrupt LD biogenesis to explore a potential role for LDs in ERAD, ultimately providing evidence that LDs are dispensable for mammalian ERAD. Instead, our results suggest that triacsin c causes global alterations to the lipid landscape that disrupt ER proteostasis by interfering with the glycan trimming and dislocation steps of ERAD. Finally, in chapter three we develop a proximity labeling strategy that exploits LD-targeted APEX2 to biotinylate LD proteins in living cells. We apply this approach to two different cell types and are able to identify the vast majority of previously validated LD

proteins, exclude common contaminating proteins, and identify the autophagy adaptor p62 as a mediator of hepatic lipophagy. Together these studies advance our understanding of the mechanisms that regulate lipid dynamics in the ER and LDs and their contribution towards maintaining cellular homeostasis.



## DEDICATION

First and foremost, I would like to thank my mentor, Dr. James Olzmann. There has been no greater influence on the scientist that I am and where I am today in my career than you. I have learned so much from you, in terms of how to think like a scientist, soaking up your endless passion for science, learning how to be a good mentor and to always pay it forward, and so much more. I wish everyone could be as lucky to have such an incredible mentor as I did. I am forever grateful for you and what you have meant to me and my career.

To my family – You’ve been there with me through every step of this journey and your support has meant everything. I truly would not be here without you, in so many different ways. When I was down and began to doubt myself, you were my strength that I could always lean on. You’ve always believed in me and seen the best in me, and let me know that no matter what happens you’ll always be proud of me. I appreciate that more than I could ever put into words. You make me constantly strive to be the best version of myself that I can be.

To the Olzmann lab family – You really made my grad school experience what it was and what I will always remember the most. You turned the daily grind into talking science with my friends and something where I truly looked forward to coming to lab every day. Truc, your endless positivity was something that I knew I could count on each and every morning and set the tone for every day. You don’t know how big of a difference that made, and how much I appreciate you. Melissa, I can’t believe how far we’ve come together. From palmitoylation to the nice GSI to late night fractionations with big mama plates full of droppy poppies, you’ve been there with me since day one and I wouldn’t have it any other way. Joe, your passion for science and life is infectious and you truly embody everything that is great about my Berkeley experience. Our conversations ranging from science raps to the meaning of life are things that I will always cherish and remember the most fondly about my time at Berkeley.

To Mary, Melanie, Robson, and the English family - Your support was the foundation that made this entire journey possible. Without you, I never would have been in a position to be at Berkeley and make my dreams of having a doctorate a reality. You made me a part of the family and believed in me when I had nothing, continuously supporting me and putting me in positions to succeed. You are some of the kindest, most good-hearted people that I have been fortunate enough to cross paths with and you have meant more to me during this stage of my life than you may ever know. I appreciate you all and everything that you have done to help me get to where I am today.

## TABLE OF CONTENTS

Chapter One: Protein and lipid regulatory systems in the endoplasmic reticulum and lipid droplets	1
Introduction	2
The endoplasmic reticulum	2
Endoplasmic reticulum-associated degradation	3
Regulation of ER lipid metabolism	3
Lipid droplet dynamics	3
Biogenesis in the ER	4
Proteome composition	4
Protein targeting and association	5
Organelle contacts	6
Mobilization of stored lipids within lipid droplets by lipolysis and lipophagy	7
Lipolysis	7
Adipose triglyceride lipase	7
Hormone sensitive lipase	7
Monoacylglycerol lipase	8
Autophagy	8
Autophagic process	8
Selective autophagy	9
Lipophagy	9
Lipolysis-lipophagy crosstalk	10
Chapter Two: Lipid disequilibrium disrupts ER proteostasis by impairing ERAD substrate glycan trimming and dislocation	11
Introduction	12
Results	13
Inhibition of long-chain acyl-CoA synthetases with triacsin C impairs select ERAD pathways	13
Triacsin C does not generally inhibit the ubiquitin-proteasome system	14
Triacsin C does not impair protein secretion	15
Triacsin C impairs CD147 glycan trimming	15
Triacsin C disrupts CD147 delivery to the Hrd1 dislocation complex	16
Triacsin C impairs the dislocation of a luminal glycosylated ERAD substrate	17
Lipid droplets are dispensable for CD147 ERAD	17
Metabolomic profiling reveals global alterations in the cellular lipid landscape of triacsin C-treated cells	18
Triacsin C activation of the PERK and IRE1 arms of the UPR has opposing effects on cell viability	19
Discussion	20
Materials and methods	22

Figures	27
Chapter Three: A proximity labeling strategy provides insight into the composition and dynamics of lipid droplet proteomes	45
Introduction	46
Results	47
Generation and characterization of LD-targeted APEX2	47
Identification of a high-confidence LD proteome	48
An integrated U2OS and Huh7 high-confidence proteome	49
p62 is required for successful lipophagy in hepatocytes	50
Discussion	50
Materials and methods	51
Figures	56
Conclusion	71
References	74

## LIST OF FIGURES

Figure 2-1	Triacsin C inhibits a subset of ERAD pathways	28
Figure 2-2	Triacsin C does not generally inhibit the ubiquitin-proteasome system or protein secretion	30
Figure 2-3	Triacsin C impairs ERAD substrate glycan trimming	31
Figure 2-4	Triacsin C impairs substrate delivery to and dislocation from the Hrd1 complex	33
Figure 2-5	Lipid droplet biogenesis is dispensable for CD147 ERAD	34
Figure 2-6	Triacsin C alters the cellular lipid landscape	36
Figure 2-7	Triacsin C activates opposing arms of the UPR	38
Figure 2-S1	Analysis of CD147 maturation and NHK secretion	40
Figure 2-S2	Proteasome inhibition causes accumulation of CD147 in a deglycosylated form	41
Figure2-S3	Analysis of glucosidases and mannosidases in CD147 glycan trimming and degradation	42
Figure 2-S4	Triacsin C and DGAT1 reduce the amount of PLIN2-positive lipid droplets	43
Figure 2-S5	Characterization of a CHOP::GFP reporter cell line	44
Figure 3-1	Lipid Droplet-Targeted APEX2 Biotinylates Proteins on Lipid Droplets	57
Figure 3-2	Proteomic Analysis of Biotinylated LD Proteins	59
Figure 3-3	Illustration of the High-Confidence LD Proteome	61
Figure 3-4	Combined High-Confidence LD Proteomes from U2OS and Huh7 Cells	62
Figure 3-5	p62 is required for LD catabolism in hepatocytes	63
Figure 3-S1	Lipid droplet-targeted APEX2 biotinylates lipid droplet proteins in Huh7 cells	64
Figure 3-S2	Proteomic analysis of biotinylated lipid droplet proteins in Huh7 cells	65
Figure 3-S3	Spectral profiles of validated lipid droplet proteins and select contaminants in Huh7 cells	67
Figure 3-S4	Illustration of the high confidence lipid droplet proteome in Huh7 cells	68
Figure 3-S5	Calculation of LD confidence score	70

# **Chapter One: Protein and lipid regulatory systems in the endoplasmic reticulum and lipid droplets**

## Introduction

Lipids are essential, highly diverse building blocks that have numerous functions in cellular metabolism, including as substrates for energy homeostasis, ligands in signaling pathways, and core structural components in cellular membranes<sup>1</sup>. The majority of lipids are synthesized in the endoplasmic reticulum (ER) before being distributed throughout the cell via the secretory pathway or the action of lipid transfer proteins present at organelle contact sites. ER-synthesized neutral lipids can be packaged directly into ER-derived lipid storage organelles known as lipid droplets (LDs)<sup>2</sup>. The ER is similarly recognized as the site of secretory protein synthesis, modification, and quality control<sup>2-4</sup>. As mature LDs bud off from the ER and enter the cytosol, a subset of ER proteins remain associated with the LD surface through the presence of various hydrophobic topologies that facilitate their integration into the LD monolayer<sup>1,15</sup>. The other remaining proteins that collectively make up the LD proteome are instead synthesized in the cytosol and later targeted to the LD surface through different mechanisms. The composition of proteins that comprise the overall LD proteome are able to collectively govern LD functions. As LDs are considered cellular hubs of lipid metabolism, many of the proteins that are found within the LD proteome belong to a number of lipid metabolic pathways, such as those involved in lipid synthesis, lipid storage, or lipolysis<sup>1,9</sup>. Identifying the LD proteome has typically been challenging due to the high degree of organelle interactions maintained by LDs that can produce false positives, as well as limitations inherent to the methods of subcellular separation and organelle purification. Recent advancements in proteomic labeling techniques has greatly improved our ability to successfully identify high-confidence LD proteins while increasing our understanding of the complex mechanisms that regulate LD proteome dynamics.

## The endoplasmic reticulum

The endoplasmic reticulum (ER) is a multifunctional membranous organelle that plays a central role in protein and lipid metabolism. Approximately one-third of all proteins are targeted to the secretory pathway and must initially pass through the ER at the point of entry<sup>4</sup>. The ER contains specialized machinery that is tasked with ensuring the proper synthesis, folding, and modification of proteins prior to trafficking to downstream organelles<sup>5</sup>. Misfolded proteins that are unable to achieve their proper conformation must be recognized and removed by a process known as ER-associated degradation (ERAD), in which folding-defective proteins are retrotranslocated back into the cytosol and ultimately degraded by the ubiquitin-proteasome system<sup>6</sup>. The ER is also regarded as a primary site for lipid synthesis<sup>2,8</sup>. A large portion of ER-resident enzymes involved in lipid metabolism integrate directly into the ER bilayer through the utilization of hydrophobic transmembrane domains<sup>10</sup>, such as the TAG synthesis enzymes glycerol phosphate acyltransferase (GPAT) and acylglycerolphosphate acyltransferase (AGPAT; also known as LPAAT)<sup>8,81</sup>. Alternatively, other proteins may peripherally associate with the outer ER membrane domain through protein-protein interactions, including the AAA+ ATPase valosin-containing protein (VCP/p97) which gets recruited to the ER through its interaction with the membrane-embedded UBX-domain containing protein 8 (UBXD8)<sup>4</sup>.

### **Endoplasmic reticulum-associated degradation**

Newly synthesized secretory proteins translocated into the ER must be correctly folded into specific three-dimensional native conformations with the help of resident chaperones in order to attain proper function<sup>3</sup>. Upon reaching their native conformation, proteins are transported out of the ER and trafficked to various downstream organelles or secreted from the cell<sup>5</sup>. However, proteins that misfold and fail to reach their native conformation remain trapped in the ER and possess an inherent propensity towards forming cytotoxic aggregates, a pathology associated with the progression of many debilitating diseases including cystic fibrosis, Alzheimer's, and Parkinson's disease<sup>5,6</sup>. ERAD has evolved as a mechanism allowing cells to identify potentially misfolded proteins and target them for degradation to preserve the fidelity of the secretory proteome<sup>4</sup>. ERAD facilitates the transfer of a substrate from the ER lumen to the cytoplasmic 26S proteasome through a series of four spatially and temporally coupled steps: recognition of the substrate by ER-resident chaperones and lectins; retrotranslocation of the substrate across the lipid bilayer into the cytoplasm; ubiquitination by ER-resident E3 ligases; and targeting of the protein for degradation by the 26S proteasome<sup>4-6</sup>.

### **Regulation of ER lipid metabolism**

The ER is a central hub of lipid metabolism, serving as the primary site of biosynthesis of numerous lipid species, including phospholipids, cholesterol, and neutral lipids such as triacylglycerol (TAG) and cholesteryl esters (CE)<sup>7,8</sup>. These lipids can then be transported out from the ER to other cellular compartments via the secretory system or by non-vesicular lipid transport at membrane contact sites<sup>9,10</sup>. The majority of lipid synthesis enzymes are ER-resident transmembrane proteins, allowing the ER to rapidly detect and respond to fluctuations in lipid levels to maintain homeostasis<sup>7,10</sup>. Multiple regulatory mechanisms exist in concert to coordinately modulate the activity of ER-resident enzymes<sup>11,12</sup>. An important example of such a system is presented in the opposing regulatory effects of insulin-induced genes (Insig-1 and Insig-2) on the cholesterol synthesis pathway through altered trafficking of sterol regulatory-element binding protein (SREBP) and targeted degradation of 3-hydroxy-3-methylglutaryl-CoA reductase (HMGCR), the rate-limiting enzyme in cholesterol biosynthesis<sup>12</sup>. SREBP is a transcription factor that preferentially regulates the expression of genes involved in cholesterol synthesis and uptake<sup>11</sup>. When cholesterol levels in the cell reach a sufficient threshold, inactive SREBP is retained in the ER through its interactions with SREBP cleavage-activating protein (SCAP) and Insig-1/2<sup>12</sup>. A decrease in cholesterol levels induces a conformational change in SCAP causing it to dissociate from the Insigs, allowing the SCAP-SREBP complex to traffic to the Golgi where proteolytic cleavage releases the active form of SREBP, which subsequently enters the nucleus to activate transcription of cholesterologenic genes, including HMGCR<sup>11,12,74</sup>. Once cellular cholesterol levels have been restored, sterol-induced binding of Insig-1/2 to HMGCR facilitates its delivery to the gp78 and Trc8 complexes for degradation, thereby creating a feedback loop in which lipid species are able to influence their own biosynthesis through employment of ERAD<sup>11,12</sup>.

### **Lipid droplet dynamics**

LDs play an essential role in maintaining metabolic homeostasis by providing a reservoir of energy-rich lipids that can be readily mobilized for cellular energy, membrane synthesis, and lipid signaling pathways during conditions of increased cellular need<sup>1</sup>. Conversely, LDs also serve to protect the cell from lipotoxicity during periods of nutrient excess by sequestering potentially harmful fatty acids (FAs) in the form of TAG<sup>13</sup>. Apart from their role in lipid storage, LDs have been implicated in many cellular processes, including the ER stress response<sup>4,7</sup>, protein degradation<sup>15</sup>, histone regulation<sup>16</sup>, and multiple stages of the hepatitis C virus life cycle<sup>17,18</sup>. Dysregulation of LD metabolism and physiological function has been implicated in the development of several human pathologies, including neutral lipid storage disease (NLS), cardiovascular disease, obesity, and non-alcoholic fatty liver disease (NAFLD)<sup>7,15</sup>.

### **Biogenesis in the ER**

The process of LD biogenesis begins in the ER where the enzymes catalyzing neutral lipid synthesis are located<sup>19</sup>. An essential step for TAG synthesis is the initial activation of fatty acids by the acyl-CoA synthetase (ACSL) family of enzymes<sup>20</sup>. ACSLs utilize ATP to catalyze the formation of fatty acyl-CoA, thereby allowing for incorporation in the sequential acylation reactions catalyzed by GPAT, LPAAT, and acyl-CoA:diacylglycerol acyltransferase (DGAT) required to convert glycerol to TAG<sup>20</sup>. Similarly, the acyl-CoA:cholesterol O-acyltransferases (ACAT1 and ACAT2) require activated fatty acyl-CoA to catalyze the esterification of a FA to sterols to produce sterol esters<sup>21</sup>. As the concentration of neutral lipids increases they begin to aggregate between the leaflets of the ER bilayer due to phase separation, leading to the formation of a lens-like structure<sup>20</sup>. Continued deposition of neutral lipids drives the cumulative growth of the lens until eventual budding of the nascent LD into the cytoplasm begins to occur. The mechanisms that govern directional budding of LDs remain incompletely understood, but key proteins such as seipin likely regulate this process. At this stage, the phospholipid monolayer of the nascent LD often remains continuous with the ER membrane, thus allowing for direct trafficking of proteins from the ER to the LD to occur<sup>22</sup>.

### **Proteome Composition**

LDs are highly conserved organelles found in nearly every organism and cell type<sup>5</sup>. The size and number of LDs can vary dramatically between cell types as well as within individual cells. The LD proteome is also highly dynamic<sup>4</sup>, as the overall function of the LD is determined by the collection of proteins associated with its surface and LD function must be able to adapt to the changing metabolic demands of the cell<sup>21</sup>. The LD proteome has been studied extensively over the last decade across bacteria, yeast, insects, plants and mammals<sup>22-23</sup>. Although protein composition can vary across different organisms and tissues, several highly conserved functional classes of proteins were shown to be present across species<sup>21</sup>. These included enzymes associated with lipid storage and metabolism, as well as those involved in membrane trafficking, protein degradation and cell signaling. Histones or histone-like proteins have similarly been found in the majority of LD proteomes<sup>22,23</sup>, indicating a conserved role in DNA maintenance and potential roles in antibacterial responses<sup>102</sup>.

The mammalian LD proteome contains over 100 proteins in a typical cell<sup>2</sup>. The perilipin (PLIN) family of proteins consists of five isoforms (PLIN1-5) that are inherently found on the surfaces of



LDs, with each family member exhibiting separate expression patterns dependent on the tissue<sup>24</sup>. PLIN proteins are generally classified as proteins that contribute to the overall structure of the LD, although studies have also identified various other roles involved in regulating lipolysis, LD formation, lipid signaling pathways, and mediating LD-organelle interactions. The latter is evidenced by the unique ability of PLIN5 to promote LD-mitochondrial association and increase fatty acid channeling to mitochondria for oxidation<sup>28,29</sup>. PLIN1 was the first protein to be identified on the surface of LDs and was shown to regulate TAG storage in adipocytes<sup>25,26</sup>. PLIN2 is ubiquitously expressed in all tissues and considered a primary marker protein for LDs, though it is also widely known as a prominent hepatic LD protein involved in LD formation and lipid storage<sup>29</sup>. A large percentage of the LD proteome is comprised of proteins involved in various aspects of lipid metabolism<sup>34</sup>. These include enzymes involved in TAG synthesis, such as the acyl-CoA synthetase ACSL3 and the acyltransferases GPAT4 and DGAT2, as well as enzymes that facilitate TAG hydrolysis such as the rate-limiting lipase ATGL and its regulator comparative gene identification-58 (CGI-58)<sup>32</sup>. The localization of these central lipid metabolic enzymes to the LD surface allows for rapid and precise regulation of neutral lipid stores in response to changes in cellular demand. During physiological conditions that promote LD growth, neutral lipid synthesis must be coordinated with a concomitant increase in phosphatidylcholine (PC) to maintain an appropriate volume-to-surface area ratio and prevent LD coalescence<sup>35</sup>. Low levels of PC in the expanding phospholipid monolayer leads to the LD-localization and activation of CTP:phosphocholine cytidyltransferase (CCT), an enzyme catalyzing the rate-limiting step in PC synthesis, ultimately leading to an increase in PC to facilitate LD expansion<sup>36</sup>.

### **Protein targeting and association**

Due to the unique ultrastructure of the LD, proteins targeted to the LD surface are faced with several constraints limiting their interaction. The hydrophobic neutral lipid interior of LDs is an energetically unfavorable environment that prevents the direct insertion of hydrophilic protein residues<sup>34</sup>. Furthermore, the presence of a phospholipid monolayer rather than a typical lipid bilayer precludes the option of using a transmembrane domain as a binding motif, thus excluding the presence of bitopic and polytopic transmembrane proteins from the LD surface<sup>34</sup>. In spite of these challenges, proteins are able to associate with the LD monolayer through adopting one of four potential topologies: membrane insertion of an amphipathic helix, membrane integration via a monotopic hairpin loop, membrane insertion of a covalent fatty acid modification employed as a lipid anchor, and peripheral binding via protein-protein interactions with stably integrated LD proteins<sup>37</sup>. In addition to the method of membrane integration, integral LD proteins can be broadly classified based on their trafficking pathways: Class I LD proteins initially insert into the ER membrane and traffic laterally to LDs, while Class II LD proteins are targeted from the cytosol and insert directly into the LD monolayer.

Class I LD proteins contain a functionally diverse assortment of proteins, including the acyl-CoA synthetase ACSL3 and acyltransferases GPAT4 and DGAT2 involved in TAG biosynthesis, the ERAD components AUP1 and UBXD8, and caveolin-1, a caveolae membrane component known to have a role in modulating lipid droplet formation<sup>38,39</sup>. A common feature among Class I LD proteins is the presence of a hydrophobic domain flanked by hydrophilic N- and C- termini exposed to the cytosol, forming an embedded hairpin structure in the membrane<sup>40,41</sup>. Importantly, these

proteins lack the luminal domains typically found in transmembrane proteins, allowing for their integration in both the ER bilayer and LD monolayer membranes.

Class II LD proteins bypass initial insertion into the ER and are instead recruited to LDs directly from the cytoplasm. Most proteins in this group tend to associate with the LD surface via amphipathic helices. However, insertion into the monolayer using a lipid anchor and direct protein-protein interactions with integral LD proteins have also been observed. Examples of this class include CCT, the perilipin family of proteins (PLIN1-5), and cell death activator A (CIDEA), a protein present in brown adipocytes that promotes the enlargement of LDs through targeted LD-LD fusion events<sup>42</sup>. The binding of Class II proteins to the LD surface appears to involve the inherent ability of the amphipathic helices to sense packing defects in the phospholipid monolayer that form ideal binding sites for amphipathic helices to integrate into the membrane<sup>43</sup>. One example of this is PLIN3 (also known as TIP47), whose structure is comprised of four amphipathic helices. In the unbound state, the four helices form a closed pocket and sequester the hydrophobic regions in its core. When PLIN3 comes in contact with LDs the amphipathic helices unfold, exposing the hydrophobic regions which become preferentially embedded in the LD monolayer while the hydrophilic regions of the helices remain exposed to the aqueous environment of the cytosol<sup>44</sup>.

### **Organelle contacts**

LDs are dynamic storage organelles primarily responsible for regulating lipid metabolism and maintaining cellular energy homeostasis. Being a major metabolic hub of the cell requires LDs to take part in a multitude of processes throughout the cell often requiring intimate contact with various other organelles, including the ER, mitochondria, peroxisomes<sup>33</sup>, and lysosome<sup>37-40</sup>. In order to engage organelles located in different regions of the cell, LDs utilize interactions with the cytoskeletal network and associated motor proteins to navigate their transport along microtubules throughout the cell<sup>45</sup>. The ER serves as the initial site of LD biogenesis, and some LDs that do not fully bud off into the cytoplasm will retain this connection throughout their existence<sup>46</sup>. The presence of continuous lipid bridges between the outer leaflet of the ER membrane and the LD monolayer allows for protein trafficking to occur between the two organelles, with the majority of LD-associated proteins believed to have originated in the ER prior to being targeted to LDs<sup>9</sup>.

Contact sites between LDs and mitochondria are highly dynamic and frequent occurrences. The coordinated hydrolysis of TAG stores in LDs leads to the release of free FAs which can be coupled with direct transport into the mitochondria to generate ATP through  $\beta$ -oxidation<sup>47</sup>. LDs have been shown to maintain increasingly close proximity to mitochondria in oxidative tissues that have a high demand for FA oxidation-driven energy production<sup>48</sup>, though the specific mechanism of LD-mitochondria contact has remained elusive. Several proteins have been reported to play a role in LD-mitochondrial contact sites, including the SNARE protein SNAP23, PLIN1, and the mitochondrial fusion GTPase mitofusion 2 (MFN2)<sup>50</sup>, although the most well-studied LD-mitochondrial interactor is PLIN5<sup>47-49</sup>. PLIN5 is highly expressed in oxidative tissues and has been shown to improve hepatic lipotoxicity by inhibiting lipolysis<sup>51</sup>. In addition, overexpression of PLIN5 has been shown to induce mitochondrial recruitment to LDs, lending support to its role in

mediating LD-mitochondrial contact sites. However, it is presently unclear whether PLIN5 does indeed function as a LD-mitochondrial tether or if the increased association is driven through an indirect mechanism<sup>49,52</sup>.

## **Mobilization of stored lipids within lipid droplets by lipolysis and lipophagy**

Neutral lipid reservoirs stored within LDs provide an excellent source of readily available TAG that can be rapidly mobilized in response to increased cellular demands to produce a pool of free FAs that can be utilized as fuel. Cells have evolved two seemingly distinct pathways that function to mediate LD breakdown and TAG hydrolysis: lipolysis and targeted autophagy of LDs, better known as “lipophagy”<sup>14</sup>.

### **Lipolysis**

Lipolysis is defined as the hydrolytic cleavage of ester bonds in TAG, resulting in the generation of FAs and glycerol<sup>60</sup>. Although the term “lipolysis” is used to refer specifically to the breakdown of TAG stored within LDs, similar hydrolytic reactions also occur that are catalyzed by alternate sets of enzymes that selectively target other esterified lipid species, namely cholesterol esters and phospholipids. Regarding the breakdown of cholesterol esters, a vast number of cholesterol ester hydrolases have been identified throughout the cell<sup>61</sup>, including include lysosomal acid lipase (LAL)<sup>62</sup> and hormone-sensitive lipase (HSL)<sup>57,61</sup>, previously known as cholesteryl ester hydrolase (CEH). HSL is an important component in lipid metabolism capable of hydrolyzing a variety of esterified lipids, including its role in catalyzing the second step in TAG hydrolysis<sup>63</sup>. Efficient lipolysis of TAG involves three sequential rounds of hydrolysis with each requiring a different enzyme to catalyze the removal of an additional FA, thereby also generating a different lipid species to be acted on after each step.

### **Adipose triglyceride lipase**

Adipose triglyceride lipase (ATGL) catalyzes the first and rate-limiting step of lipolysis by hydrolyzing one of the ester bonds in TAG to yield DAG and a FA<sup>57</sup>. The activity of ATGL is regulated through the binding of its cofactor CGI-58, with CGI-58 interaction being required for efficient ATGL activity<sup>60</sup>. ATGL is present across nearly all tissue types with the highest expression levels occurring in adipose tissue<sup>58</sup>. Inhibition of ATGL activity leads to significantly increased levels of TAG accumulation throughout cells while, alternatively, overexpression of ATGL is sufficient to induce a marked decrease in the presence of TAG storage in LDs<sup>59</sup>.

### **Hormone sensitive lipase**

HSL is known to interact with various lipid regulatory pathways<sup>63-66</sup> although its primary function is regarded to be its role in catalyzing the second step in lipolysis. Here, HSL is responsible for the hydrolytic cleavage of DAG to remove a FA and generate MAG. HSL exhibits broad substrate specificity and is able to confer hydrolytic activity against multiple lipid species, including MAG, TAG, CE, and retinoid esters<sup>63</sup>. Although HSL does possess the hydrolase activity required to catalyze the initial step of lipolysis as well, its activity has been shown to be 11-fold greater towards DAG than towards TAG, indicating an inherent preference towards DAG as a substrate<sup>63</sup>.

### **Monoacylglycerol lipase**

Monoacylglycerol lipase (MGL) catalyzes the terminal step in lipolysis by hydrolyzing MAG to glycerol and a FA. In addition to a role in lipolysis, MGL utilizes its hydrolytic activity to serve as a key regulator of the cannabinoid receptors CB1 and CB2 by degrading the endocannabinoid ligand 2-arachidonoyl glycerol<sup>67</sup>. Global deletion of MGL in mouse models was shown to produce a leaner phenotype with delayed lipid absorption and decreased levels of circulating lipids<sup>68</sup>. In the absence of MGL, HSL is able to partially compensate for catalyzing MAG hydrolysis during the terminal step of lipolysis, albeit impairments in lipolysis still persist<sup>69</sup>.

### **Autophagy**

Autophagy is a self-targeted catabolic process utilized by all eukaryotic cell types in which cytoplasmic material such as damaged or non-essential organelles, misfolded proteins, or cellular pathogens are delivered to the lysosome for degradation<sup>70-72</sup>. Starvation and other forms of cellular stress induce autophagy as a form of cell survival in order to acquire nutrients from internal components or eliminate harmful material<sup>73</sup>. The highly acidic environment of the autolysosome contains over 50 hydrolases functioning together to degrade a wide range of sequestered material from nucleic acids, lipids, and proteins to entire bacterial organisms, and recycle the components back into the cytosol for reuse by the cell<sup>70-73</sup>.

There are three types of autophagy: macroautophagy, microautophagy, and chaperone-mediated autophagy (CMA). Macroautophagy is the main autophagic pathway (referred to simply as “autophagy”) in which a substrate becomes enveloped by a double membrane vesicular structure, known as an autophagosome, which ultimately fuses with the lysosome to form an autolysosome<sup>70</sup>. Microautophagy is similar to macroautophagy, however, instead of forming an autophagosome the cytosolic components are sequestered directly by the lysosome through invagination of the lysosomal membrane<sup>76</sup>. In CMA, targeted substrates become bound by chaperone proteins and delivered to the lysosomal membrane, where interaction with the CMA receptor lysosome-associated membrane protein (LAMP)-2A results in their unfolding and translocation across the lysosomal membrane for degradation<sup>77</sup>.

### **Autophagic process**

Initiation of autophagy is controlled by the unc-51-like kinase 1 (ULK1) complex<sup>78</sup>. When nutrients are limited, inactivation of mTOR prevents the subsequent phosphorylation of ULK1, thereby activating the complex<sup>78</sup>. The active ULK1 complex translocates to the ER membrane where its activation of the phosphatidylinositol 3 kinase (PI3K) complex leads to nucleation of the phagophore<sup>70</sup>. PI3K then recruits ubiquitin-like conjugate system 1, consisting of autophagy-related (ATG) proteins ATG5-12-16, which enables elongation of the phagophore membrane and recruitment of microtubule-associated protein 1A/1B-light chain 3 (LC3)<sup>78</sup>. The presence of LC3 on both sides of the autophagosomal membrane is important for facilitating membrane elongation and closure as well as serving as the binding site for autophagic adapter proteins, such as sequestosome-1 (p62/SQSTM1)<sup>79</sup>. Following sequestration of cytoplasmic cargo, the autophagosome undergoes fusion with the lysosome to form an autolysosome in a process that is mediated by a set of SNARE proteins including syntaxin-17 (STX17), synaptosomal-associated protein 29 (SNAP29), and vesicle-associated membrane protein 8 (VAMP8)<sup>80,81</sup>.

## Selective autophagy

Autophagy was traditionally considered to be a nonselective process intended for general degradation of proteins and organelles to maintain energy homeostasis of the cell. However, multiple scenarios involving selective degradation of cytoplasmic components have since been discovered<sup>82</sup>, including targeting of protein aggregates (aggrephagy)<sup>83</sup>, mitochondria (mitophagy)<sup>84,85</sup>, peroxisomes (pexophagy)<sup>86</sup>, ribosomes (ribophagy)<sup>87</sup>, sections of the ER (reticulophagy)<sup>88</sup>, and LDs (lipophagy)<sup>14,55,56</sup>. Selective autophagy is mediated through the involvement of specific proteins known as autophagy adapters that act as cargo receptors for the degradation of ubiquitinated substrates<sup>81</sup>. Common autophagy adapters include p62<sup>79,89</sup>, neighbor of BRCA1 gene 1 (NBR1)<sup>90</sup>, nuclear dot protein 52 (NDP52)<sup>91</sup>, and optineurin (OPTN)<sup>85</sup>. Most autophagy adapters have a set of core structural components, including a ubiquitin-associated domain (UBA), which facilitates the binding to ubiquitinated substrates, and an LC3-interacting region (LIR) that is required for recruitment to the autophagosome through its binding of LC3<sup>89-91</sup>. The AAA+ ATPase valosin-containing protein (VCP/p97) similarly contains both UBA and LIR domains and has been implicated in selective autophagy<sup>92</sup>.

## Lipophagy

The selective autophagy of LDs, or “lipophagy”, serves as an intracellular mechanism to regulate lipid storage and energy homeostasis through mobilization of TAG. The process was discovered in 2009 by researchers studying the regulation of lipid metabolism by autophagy in hepatocytes<sup>93</sup>. They found that key autophagic pathway components (ATG5, ATG7, LC3) localized to the surface of LDs and that pharmacological and genetic inhibition of autophagy led to an increase in TAG and LDs that was due to a decrease in TAG breakdown as opposed to increased lipid synthesis. Additionally, inhibition of autophagy increased LD content both in the basal state and following a brief stimulus of exogenous free FAs indicating that lipophagy is a constitutive process<sup>93</sup>. While lipophagy is strongly induced by prolonged starvation, intriguingly, brief exposure to FAs such as oleic acid is also a sufficient stimulus<sup>93,94</sup>. Conversely, deleting *Atg7* in mice blocks autophagy and leads to an increase in hepatic lipid accumulation similar to human fatty liver disease<sup>93</sup>.

Since its discovery, lipophagy has been observed in numerous cell types, including hepatocytes<sup>14</sup>, brown adipocytes<sup>55,101</sup>, enterocytes<sup>13</sup>, cardiomyocytes<sup>30</sup>, macrophages<sup>95</sup>, and neurons<sup>94</sup>. The mechanisms underlying lipophagy have been shown to similarly follow those required in macroautophagy<sup>55,96</sup>, although the exact machinery involved in LD recognition remains unknown. The ubiquitination factor ancient ubiquitous protein 1 (AUP1) is a protein known to recruit the E2 ubiquitin-conjugating enzyme UBE2G2 and that also has been shown localizing to LDs<sup>97,98</sup>. This suggests that recruitment of a larger ubiquitination complex to LDs is possible, perhaps to facilitate ubiquitination of LD proteins as a target for autophagic machinery. A recent study showed that treatment with the autophagic activator rapamycin resulted in the association of p62 with LDs and the predominant LD protein PLIN2<sup>99</sup>. A separate study used the expression of a fusion protein consisting of p62 attached to the LD-binding domain of TIP47/PLIN3 to generate a forced lipophagy system capable of inducing a reduction in both LD size and number<sup>100</sup>. These studies provide evidence suggesting that p62 or perhaps other autophagic adapters might be

involved in recognizing LDs as substrates for autophagy. Future studies involving genetic manipulation of autophagic adapters as well as members of the lipophagic pathway are needed to determine the full complement of factors that are involved in the initiation of lipophagy.

### **Lipolysis-lipophagy crosstalk**

Although the independent roles of lipolysis and lipophagy in TAG mobilization have been well studied, whether their contributions to lipid catabolism are complementary to one another has only recently been explored. In one example, ATGL was shown to be recruited to LC3 on LDs through the presence of an internal LIR domain following cold-induced lipophagy in brown adipocytes<sup>101</sup>. Mutation of the LIR domain was sufficient to disrupt ATGL colocalization while also blocking lipolysis, indicating that ATGL activity is dependent on its interaction with LC3. Further evidence of cooperation between the two catabolic systems came from the discovery that lipolysis and lipophagy appear to act sequentially on LDs depending on size, with lipolysis targeting larger LDs upstream of lipophagy in hepatocytes<sup>14</sup>. Whether this sophisticated tandem approach to lipid homeostasis represents a universal system governing all cell types or is unique to hepatocytes has yet to be determined, though it uncovers exciting potential for future discoveries in lipid biology.

## **Chapter Two: Lipid disequilibrium disrupts ER proteostasis by impairing ERAD substrate glycan trimming and dislocation**

Contents in this chapter are modified with permission from the previously published research article:

To M\*, Peterson CW\*, Roberts MA, Counihan JL, Wu TT, Forster MS, Nomura DK, Olzmann JA. Lipid disequilibrium disrupts ER proteostasis by impairing ERAD substrate glycan trimming and dislocation. *Mol Biol Cell*. 2017 Jan 15;28(2)270-284.

\*These authors contributed equally

## Introduction

As the entry point into the secretory pathway, the endoplasmic reticulum (ER) is host to an extensive cohort of enzymes and chaperones that coordinate the folding, modification, and deployment of a large fraction of the proteome. Failure of secretory proteins to achieve their native structure due to mutations, errors in transcription or translation, protein damage, or inefficient folding can have dire consequences for cellular physiology and has been implicated in the etiology of numerous human diseases<sup>105</sup>. Incorrect protein folding not only can result in a reduction in protein activity (i.e., loss of function), but it can also lead to the generation of cytotoxic protein aggregates (i.e., gain of function). To ensure the fidelity of the secretory proteome, the ER has evolved a quality control system that detects terminally misfolded and unoligomerized proteins and targets them for clearance via a process known as ER-associated degradation<sup>106-108</sup> (ERAD). The cell also responds to perturbations in ER homeostasis by activating the unfolded protein response<sup>108,109</sup> (UPR), a set of signaling pathways that enhance the overall folding capacity of the ER.

ERAD involves a series of spatially and temporally coupled steps that mediate substrate recognition, dislocation (also known as retrotranslocation) across the ER membrane into the cytoplasm, ubiquitination, and targeting to the proteasome for proteolysis<sup>106-108</sup>. Although the mechanism by which substrates are triaged for degradation is incompletely understood, it is clear that the structure of substrate-conjugated N-linked glycans provides a “molecular code” that plays a determining role in the fate of secretory proteins<sup>110</sup>. During insertion into the ER, the majority of the secretory proteome is modified by covalent attachment of a triantennary glycan moiety<sup>111</sup>. Progressive trimming by ER-resident mannosidases exposes an  $\alpha$ -1,6-linked mannose, which acts as a signal for ERAD and is recognized by the mannose 6-phosphate receptor homology (MRH) domain of the ER lectin, OS-9, and possibly a second ER lectin, XTP3-B<sup>112</sup>. These two ER lectins interact with the Hrd1 luminal adaptor SEL1L<sup>113-115</sup>, facilitating substrate delivery for dislocation. Most models posit that the AAA ATPase VCP (also known as p97) then extracts substrates from proteinaceous pores in the membrane, possibly formed by the E3 ubiquitin ligase Hrd1<sup>116-118</sup>, the derlin family of proteins<sup>119-122</sup> or, in some cases, the Sec 61 translocon<sup>123,124</sup>.

In addition to its role as a protein-folding compartment, the ER functions as a major site of lipid metabolism, mediating the synthesis of important lipids (e.g., phospholipids, sterols, and neutral lipids) and the biogenesis of lipid storage organelles called lipid droplets<sup>125-127</sup> (LDs). LDs are ubiquitous, conserved organelles composed of a neutral lipid core (e.g., triacylglycerol [TAG] and sterol esters) encircled by a phospholipid monolayer. Whereas the hydrophobic core of LDs is devoid of proteins, the bounding phospholipid monolayer is decorated with a unique proteome that regulates LD growth, breakdown, and trafficking. LDs function as dynamic repositories of lipids, protecting the cell from fatty acid-induced toxicity<sup>128</sup> and providing the cell with an “on-demand” source of lipids for membrane biogenesis<sup>129</sup>, energy production via  $\beta$ -oxidation<sup>130</sup>, and use as ligands in lipid signaling pathways<sup>131-132</sup>. Several unexpected roles have also been identified for LDs, such as the regulation of the hepatitis C life cycle<sup>133,134</sup>, the sequestration of histones<sup>135,136</sup>, and the control of cytosolic inclusion body clearance<sup>137</sup>.



Reports have identified a number of intriguing links between ERAD and LDs. A subset of proteins implicated in ERAD, including UBXD8, UBXD2, VCP, AUP1, and Ube2g2, were identified in proteomic analyses of buoyant, LD-enriched biochemical fractions<sup>138-140</sup>, and the localization of these proteins to the LD surface was confirmed by fluorescence microscopy<sup>114,141-146</sup>. This subset of ERAD factors has been implicated in the regulation of LD abundance, size, and clustering<sup>114,141-146</sup>, but whether these effects on LDs are related to their functions in ERAD remains to be determined. ERAD substrates have also been observed on the LD surface (e.g., ApoB100<sup>144,147</sup>) and in ER subdomains that are closely juxtaposed to LDs (e.g., 3-hydroxy-3-methylglutaryl-coenzyme A reductase [HMGCR]<sup>148</sup>). In addition, ER stress induces LD biogenesis<sup>149,150</sup> and loss of LDs activates the UPR<sup>151-154</sup>.

Indirect experimental evidence supporting a functional role for LDs in ERAD came from studies employing triacsin C, a polyunsaturated fatty acid analogue that inhibits long-chain acyl-CoA synthetases (ACSLs)<sup>155,156</sup> and blocks LD biogenesis<sup>157,158</sup>. These studies found that triacsin C impaired the degradation kinetics of several ERAD substrates, including the null Hong Kong (NHK) mutant of  $\alpha$ -1 antitrypsin<sup>142</sup>, a truncated variant of ribophorin I<sup>142</sup>, class I MHC heavy chain<sup>142</sup>, and HMGCR<sup>145,148</sup>. Together these findings led to multiple models of how LDs might be involved in ERAD<sup>142,144,145,148,150,159</sup>: 1) LD biogenesis is coupled to the dislocation of luminal ERAD substrates via the formation of transient pores in the membrane or the dislocation of integral membrane ERAD substrates via capture in the membrane of an exiting LD, 2) ERAD substrate dislocation and ubiquitination preferentially occur in LD-associated ER subdomains, and/or 3) ERAD substrates are sequestered on the surface of LDs as an intermediate step en route to the proteasome. Although these models are attractive, triacsin C is not a specific inhibitor of LD biogenesis, as it also affects unrelated processes that require activated fatty acids (e.g., de novo phospholipid synthesis<sup>156</sup>). Moreover, the degradation kinetics of several ERAD substrates was unaffected in a strain of yeast lacking LDs<sup>153,160</sup>, indicating either that LD formation is not essential for ERAD or that there are unrecognized differences between the ERAD process in yeast and mammalian cells. Thus, the functional relationship between ERAD and LDs remains unresolved.

In this study, we focused our attention on the effect of triacsin C on ERAD and the potential requirement of LDs for ERAD in mammalian cells. Our results demonstrate that, as in yeast<sup>153,160</sup>, LDs are dispensable for ERAD in mammalian cells. However, our data indicate that triacsin C causes widespread changes in the cellular lipid composition, impairs ERAD substrate glycan trimming and dislocation, and induces the UPR, culminating in cell death. These findings support a fundamental connection between fatty acid metabolism and ER proteostasis.

## Results

### **Inhibition of long-chain acyl-CoA synthetases with triacsin C impairs select ERAD pathways**

Triacsin c has been shown to be a potent inhibitor of ACSLs 1, 3 and 4 at a concentration of 5  $\mu$ M, although it does not inhibit ACSL 5 or 6<sup>252</sup>. Therefore, to ensure broad inhibition across all ACSL isoforms present, we chose to examine the effects of triacsin C in HEK293 cells, in which ACSL5 and ACSL6 are not physiologically detectable<sup>253,254</sup>. To examine the effect of triacsin C on ERAD,

we analyzed the degradation kinetics of a panel of substrates that reflect a range of topologies and use distinct degradation pathways (Figure 2-1A). The panel included an endogenous ERAD substrate, CD147, which is a glycosylated type I transmembrane protein that is recognized as an unassembled subunit of an oligomeric complex and is constitutively degraded by a Hrd1/SEL1L pathway<sup>115</sup>. We also tested two exogenously expressed mutant substrates: the NHK mutant of  $\alpha$ -1 antitrypsin—a soluble, luminal substrate degraded by a Hrd1/SEL1L pathway<sup>113,161</sup>—and the  $\Delta$ F508 mutant cystic fibrosis transmembrane conductance regulator (CFTR $\Delta$ F508)—a polytopic integral membrane substrate degraded by multiple E3 ligase pathways<sup>162-164</sup>.

To determine the kinetics of triacsin C treatment on ERAD disruption, we performed a time course of triacsin C incubation and analyzed the degradation of CD147 during emetine translation shutoff (Figure 2-1, B–D). As expected<sup>115,165</sup>, CD147 migrated as two primary species: a high-molecular weight plasma membrane form bearing complex glycans (CD147(mature [Mat.])) and a lower-molecular weight ER form bearing the core-glycan structure (CD147(CG); Figure 2-1C). CD147(CG) was degraded during the 6-h emetine chase (Figure 2-1, C and D). Addition of triacsin C at time 0 of the emetine chase had no effect on CD147(CG) degradation (Figure 2-1, C and D). Increasing stabilization of CD147(CG) was observed as the triacsin C preincubation time was lengthened, with a maximal stabilization occurring after a 16-h triacsin C pretreatment (Figure 1, C and D). Using the 16-h triacsin C pretreatment, we analyzed the degradation kinetics of our full panel of ERAD substrates (Figure 2-1, E–J). The Hrd1 substrate CD147(CG) was stabilized by triacsin C pretreatment (Figure 2-1, E and F). Although the majority of newly synthesized CD147 is degraded by ERAD, a small fraction can correctly assemble and mature by trafficking through the Golgi to the plasma membrane<sup>115,165</sup>. To account for both fates of CD147, we performed radioactive pulse-chase experiments (Supplemental Figure S2-1A). Over the 6-h time course of our experiment, no CD147 maturation was detected, and triacsin C pretreatment stabilized CD147(CG). These results indicate that the effect of triacsin C is due to impairment of CD147 degradation rather than maturation. The Hrd1 luminal substrate NHK–green fluorescent protein (GFP) was also stabilized by triacsin C pretreatment (Figure 2-1, G and H). No secretion of NHK-GFP was observed in this cell line (Supplemental Figure S2-1B). In contrast to CD147 and NHK-GFP, CFTR $\Delta$ F508 degradation kinetics was unaffected by the triacsin C pretreatment (Figure 2-1, I and J). These data demonstrate that treatment with the ACSL inhibitor triacsin C impairs select ERAD pathways.

### **Triacsin C does not generally inhibit the ubiquitin-proteasome system**

Our finding that triacsin C inhibits the degradation of a subset of ERAD substrates suggests that triacsin C treatment does not generally inhibit the ubiquitin-proteasome system (UPS). In agreement with this notion, ubiquitinated proteins accumulated in cells treated with the proteasome inhibitor MG-132, but not with triacsin C (Figure 2-2A). To assess more directly the effect of triacsin C on the degradation of cytosolic proteins, we used flow cytometry to measure the degradation kinetics of a cytosolic UPS reporter (Figure 2-2B). This reporter consists of the Venus fluorescent protein fused to a destabilized domain (Venus-DD), a variant FK506-binding domain from FKBP12 that, in the absence of the small molecule shield-1, is misfolded and rapidly degraded via the UPS<sup>166-168</sup>. Triacsin C had no significant effect on the constitutive degradation

of Venus-DD (Figure 2-2B), indicating that triacsin C does not generally affect the degradation of cytosolic UPS substrates.

After dislocation, ERAD substrates are deglycosylated by the cytosolic peptide:*N*-glycanase (PNGase) and cleared by the UPS<sup>106,110</sup>. Thus, the presence and accumulation of a deglycosylated form of ERAD substrates reflect inefficient coupling of dislocation with proteasomal degradation. Incubation with the proteasome inhibitor MG-132 during an emetine chase resulted in the accumulation of deglycosylated CD147 (CD147(-CHO)), indicating the buildup of cytosolically dislocated CD147 (Figure 2-2C). CD147 deglycosylated *in vitro* by incubation with the glycosidase PNGase F resolved at the same molecular weight as the CD147 band that accumulated in MG-132-treated cells, and no additional lower-molecular weight forms appeared (Supplemental Figure S2-2), confirming the identity of the CD147(-CHO) species. A portion of CD147 also migrated in a high-molecular weight smear, likely representing ubiquitinated CD147 (Figure 2C). In contrast to MG-132, triacsin C pretreatment solely stabilized CD147(CG); deglycosylated CD147 and ubiquitinated CD147 were absent (Figure 2-2C). Together, these data indicate that triacsin C impairs ERAD upstream of the proteasome and does not cause a global defect in the UPS.

#### **Triacsin C does not impair protein secretion**

Dysregulated lipid metabolism can alter organelle morphology and function<sup>169-171</sup>, and disruptions in ER-to-Golgi trafficking reduce the degradation of some ERAD substrates<sup>172-174</sup>. To examine the function of the secretory pathway, we analyzed the secretion of hemagglutinin-tagged transthyretin (TTR-HA), a tetrameric protein that is normally secreted into the serum, where it functions as a carrier of the thyroid hormone thyroxine. Similar levels of TTR-HA were immunoprecipitated from media isolated from cells incubated in the presence or absence of triacsin C (Figure 2-2, D and E), indicating that triacsin C pretreatment does not affect TTR secretion. Furthermore, the overall morphology of the ER (Figure 2-2F) and Golgi complex (Figure 2-2G) remained unperturbed by a triacsin C pretreatment at the resolution of fluorescence deconvolution microscopy. Together, these results indicate that the secretory system remains functionally and morphologically intact after a 16-h triacsin C treatment.

#### **Triacsin C impairs CD147 glycan trimming**

Our initial results indicated that triacsin C affects ERAD upstream of the proteasome (Figure 2-2). To determine more precisely the steps in ERAD that are compromised, we focused our attention on the degradation of the endogenous substrate CD147, which was strongly stabilized by triacsin C (Figure 2-1). Glycan trimming is often believed to be one of the most upstream events in ERAD, potentially acting as a timing mechanism that releases a substrate from futile calnexin/calreticulin folding cycles and facilitates targeting for degradation by enabling direct interactions with the ERAD-implicated lectins<sup>110</sup>. The various trimmed CD147(CG) glycoforms are not resolved on small SDS-PAGE gels. Therefore, to examine a potential effect of triacsin C on CD147(CG) glycan trimming, we separated CD147 on large-format SDS-PAGE gels (Figure 2-3A). On these larger gels, the variety of CD147 glycoforms becomes evident, and CD147(CG) is resolved as approximately five bands (Figure 2-3A). Treatment of lysates *in vitro* with PNGase F collapsed all CD147 forms into a single band of ~29 kDa (Figure 2-3D), consistent with the

conjecture that the variations in the CD147 banding pattern reflect the diversity of CD147 glycoforms.

During the course of an emetine translation shutoff experiment, the upper CD147(CG) bands were rapidly lost (Figure 2-3, A and B, vehicle), whereas the lower bands displayed a slight lag period before clearance (Figure 2-3, A and C, vehicle). These results are consistent with the conversion of CD147(CG) from a slower-migrating, untrimmed form into a faster-migrating, trimmed form before degradation. Treatment with the mannosidase inhibitor kifunensine (Figure 2-3, A–C, kifunensine) or the glucosidase inhibitor deoxynojirimycin (Supplemental Figure S2-3) stabilized CD147(CG) in the slower-migrating form, providing evidence that these bands represent an untrimmed form of CD147(CG). It is worth noting that CD147(CG) continued to be degraded in the presence of kifunensine (Figure 2-3A, kifunensine), albeit at a slower rate, indicating either that glycan trimming is not a strict requirement for CD147(CG) degradation or that kifunensine inhibition of glycan trimming is incomplete. Cotreatment with kifunensine and deoxynojirimycin did not result in additional stabilization (Supplemental Figure S2-3). Analysis of CD147(CG) in cells pretreated with triacsin C revealed a significantly reduced rate of CD147(CG) conversion from untrimmed to the trimmed glycoform (Figure 2-3, A–C, triacsin C), similar to the effect of kifunensine. In contrast, blocking CD147(CG) degradation at a downstream step with the VCP inhibitor CB-5083 resulted in the accumulation of a lower-molecular weight, presumably highly trimmed form of CD147(CG) (Figure 2-3, A–C, CB-5083). These data suggest that triacsin C impairment in ERAD is caused, at least in part, through inhibition of substrate glycan trimming.

### **Triacsin C disrupts CD147 delivery to the Hrd1 dislocation complex**

CD147 is degraded via an ERAD pathway that requires Hrd1, SEL1L, and, to some extent, the lectins OS-9 and XTP3-B<sup>115</sup>. The Hrd1 dislocation complex is a membrane-embedded, macromolecular complex<sup>114,175</sup>. Several properties of membrane lipids can influence the interactions and functions of membrane-embedded protein complexes<sup>176,177</sup>. To determine whether ACSL inhibition affects the composition of the Hrd1 dislocation complex, we used a quantitative triple stable isotope labeling with amino acids in cell culture (SILAC) strategy to measure the dynamics of Hrd1 interactions in response to triacsin C treatment (Figure 2-4A). The results from this experiment are displayed in a two-dimensional plot (Figure 2-4A), which groups nonspecific background, as well as constitutive and dynamic interactors. Of the 145 proteins detected, 15 passed our criteria for high-confidence interactors (SILAC ratio M:L > 2-fold). In addition to the identification of Hrd1 itself (the bait), the strongest interactors (SILAC ratio M:L > 20-fold) were known members of the Hrd1 complex—SEL1L, FAM8A1, ERLIN2, OS-9, and XTP3-B. Other noteworthy interactors that were captured included proteins involved in protein folding and degradation, such as VCP, PDI, GRP94, Hsp47, calnexin, and ubiquitin. The significance of Hrd1 association with RPN1 (also known as ribophorin I), PGRC1, and EMD is unknown. These proteins are not known to be involved in protein quality control and may represent endogenous substrates of the Hrd1 complex. Several previously reported Hrd1 complex members (UBXD8, AUP1, derlin-1, derlin-2) were not detected in our SILAC experiment, possibly due to their lower abundance. Therefore, we examined the association of these interactors with Hrd1 by immunoblotting of affinity purified S-tagged Hrd1 complexes (Figure 2-4B). Analysis of the results from both the SILAC (Figure 2-4A) and immunoblotting (Figure 2-4B) experiments indicate that

few Hrd1 interactions were affected by triacsin C treatment. The core Hrd1 complex, characterized by SEL1L, FAM8A1, XTP3-B, OS-9, and ERLIN2, remained intact after triacsin C treatment. There were minor trends toward increased associations with VCP and ubiquitin, as well as decreased association with Hsp47.

To examine a potential effect of triacsin C on the delivery of CD147 to the Hrd1 complex, we analyzed endogenous Hrd1 complexes immunoprecipitated from vehicle- and triacsin C-treated cells. Hrd1 bound only the ER-localized core glycosylated form of CD147 (Figure 2-4, C and D), supporting the specificity of the interaction with CD147. Of interest, triacsin C treatment caused a pronounced decrease in the amount of CD147(CG) that coprecipitated with Hrd1 (Figure 2-4, C and D). Thus, our results indicate that whereas the overall composition of the Hrd1 dislocation complex is mostly unaffected, triacsin C treatment reduces the delivery of the substrate CD147 to the Hrd1 complex.

### **Triacsin C impairs the dislocation of a luminal glycosylated ERAD substrate**

Given the effects of triacsin C on CD147 glycan trimming (Figure 2-3) and association with Hrd1 (Figure 2-4, C and D), we predicted that triacsin C would affect substrate dislocation. The accumulation of deglycosylated CD147 in response to MG-132 treatment provides one potential method to assess dislocation. However, MG-132 also stabilized CD147(CG), and the appearance of deglycosylated CD147 was minimal and difficult to detect (Figure 2-2C). Therefore, to assess quantitatively the effects of triacsin C on dislocation, we used a more sensitive and robust fluorescent ERAD dislocation assay based on the reconstitution of split Venus (Figure 2-4E)<sup>179</sup>. In this assay, the N-terminal half of deglycosylation-dependent Venus is fused to the H2-K<sup>b</sup> signal sequence (SS-dgdV1Z), targeting it to the ER lumen<sup>179</sup>. SS-dgdV1Z is glycosylated, recognized as an aberrant protein, and dislocated into the cytosol for degradation<sup>179</sup>. In the presence of MG-132, SS-dgdV1Z accumulates in the cytosol and associates with the C-terminal half of Venus (VZ2), reconstituting the mature fluorescent protein and enabling dislocation to be measured by flow cytometry<sup>179</sup>. Of importance, the fluorescence is deglycosylation dependent, ensuring that any fluorescence detected results from the dislocation of dgdV1Z from the ER lumen into the cytosol.

Incubation of 293T.FluERAD cells stably expressing SS-dgdV1Z and VZ2 with MG-132 resulted in a large increase in Venus fluorescence (Figure 2-4F, 16.4-fold increase). In agreement with a role for VCP in SS-dgdV1Z dislocation<sup>179</sup>, coincubation with CB-5083 and MG-132 nearly completely blocked the increase in fluorescence (Figure 2-4F, 1.6-fold increase). Similar to the effect of kifunensine treatment (Figure 2-4F, 7.6-fold), triacsin C treatment partially blocked the increase in fluorescence in response to MG-132 (Figure 2-4F, 7.3-fold). Thus, triacsin C significantly reduces the dislocation of a luminal glycosylated ERAD substrate.

### **Lipid droplets are dispensable for CD147 ERAD**

The observation that triacsin C inhibits ERAD<sup>142,145,148</sup> (Figure 2-1) is in agreement with a role for LDs in ERAD; however, triacsin C is not a selective inhibitor of LD biogenesis (Figure 2-5A). Although a selective inhibitor of LD biogenesis has not been identified, ablation of the diacylglycerol acyltransferase (DGAT) enzymes (DGAT1 and DGAT2), which catalyze the final and committed step in TAG synthesis (Figure 2-5A), causes a complete blockade of LD biogenesis in

adipocytes<sup>178</sup>. Therefore, to examine a role for LDs in ERAD, we exploited a recently developed DGAT1 inhibitor, T863 (DGAT1i)<sup>180</sup>, and mouse embryonic fibroblast (MEF) cell lines lacking DGAT2 (DGAT2<sup>-/-</sup>)<sup>178,181</sup> to simultaneously disrupt both DGAT enzymes. The DGAT2<sup>-/-</sup> MEFs exhibited a low amount of LDs under basal conditions, which increased dramatically after a 6-h treatment with 200  $\mu$ M oleate (Figure 2-5, B and C), indicating that DGAT2<sup>-/-</sup> MEFs are still able to generate LDs in response to an oleate challenge, due to the presence of DGAT1. Treatment with either triacsin C or DGAT1i reduced the amount of LDs in non-oleate-treated cells and completely blocked the increase in LD biogenesis in response to oleate (Figure 2-5, B and C). The levels of the LD protein perilipin-2 (PLIN2) are known to correlate with LD abundance, and, in the absence of LDs, PLIN2 is degraded by the ubiquitin-proteasome system<sup>182-184</sup>. Analysis of PLIN2 levels and cellular distribution indicate that triacsin C and DGAT1i treatments block oleate-induced increases in PLIN2 levels and PLIN2-immunoreactive LDs (Supplemental Figure S2-4). Together these data demonstrate that the DGAT2<sup>-/-</sup> MEFs provide a facile means to acutely manipulate LD biogenesis at an upstream step (i.e., with triacsin C) or a downstream step (i.e., with DGAT1 inhibitor).

As observed in HEK293 cells, CD147(CG) was degraded in DGAT2<sup>-/-</sup> MEFs during an emetine translation shutoff experiment and was stabilized by a triacsin C pretreatment (Figure 2-5, D and E). The rate of CD147(CG) degradation was greater in the DGAT2<sup>-/-</sup> MEFs than in the HEK293 cells (half-life  $\sim$ 25 min vs.  $\sim$ 2 h). DGAT1i pretreatment, despite inhibiting LD biogenesis (Figure 2-5, B and C), had no effect on the kinetics of CD147 degradation (Figure 2-5, D and E). These results argue against a requirement for LDs in CD147 degradation and suggest that triacsin C affects ERAD through a mechanism independent of LDs.

### **Metabolomic profiling reveals global alterations in the cellular lipid landscape of triacsin C-treated cells**

Long-chain FAs are centrally involved in a number of metabolic pathways, including the synthesis of important biomolecules such as TAG, cholesterol esters, phospholipids, and ceramides, as well as the catabolism of FFAs for energy production via  $\beta$ -oxidation<sup>255</sup>. Thus, since triacsin c inhibits the production of activated FA-CoAs available for such processes, its effects on cellular lipid metabolism may be broader than those directly tied to LD biogenesis. To understand the effects of triacsin C on cellular lipid homeostasis, we performed targeted single reaction monitoring (SRM)-based liquid chromatography-tandem mass spectrometry (LC-MS/MS) steady-state lipidomic profiling of >100 lipid metabolites, encompassing a wide array of lipid classes, including neutral lipids, fatty acids, acyl carnitines (ACs), N-acyl ethanolamines, sterols, phospholipids, sphingolipids, lysophospholipids, and ether lipids (Figure 2-6). Among the 118 lipids, 71 exhibited significant changes ( $p < 0.05$ ) after a 16-h triacsin C treatment (Figure 2-6, A-K). As expected, we observed a prominent decrease in the levels of many neutral lipids—monoacylglycerols (MAGs), diacylglycerols (DAGs), and TAGs (Figure 2-6, B and C). Not all species of TAG were reduced (e.g., C16:0/C20:4/C16:0 TAG and C18:0/C18:0/C18:0 TAG; Figure 2-6, B and C), suggesting that there may be protected pools of TAGs or that some ACSLs that are incompletely inhibited mediate the formation of these specific TAGs<sup>156</sup>. We also observed an anticipated decrease in AC levels, particularly in C16:0 AC (Figure 2-6, B and E). Although free fatty acids might be expected to accumulate due to the inhibition of ACSLs and consequent lack of conversion into the CoA

intermediate for cellular use, no changes in fatty acid levels were detected (Figure 2-6B). This may be due to a compensatory efflux of free fatty acids<sup>156</sup>, which could result in an underestimate of total free fatty acid levels, or increased flux through ACSL enzymes that are not inhibited.

Broad changes in additional cellular lipids were also observed, including decreases in many phospholipids, phospholipid ethers, neutral ether lipids, and lysophospholipid ethers (Figure 2-6, B–K). The decreases in lipid levels presumably resulted from impairments in synthesis caused by the inability of ACSLs to activate fatty acids, a requirement for conjugation. Particularly striking was the general decrease in nearly all phosphatidylinositol and phosphatidylinositol ether lipids (Figure 2-6, B, F, and J). This is interesting, given the recent finding that phosphatidylinositol maintains ER homeostasis in yeast by sequestering fatty acids when LD biogenesis is inhibited<sup>185</sup>. Our results suggest that phosphatidylinositol may represent an especially dynamic phospholipid pool that reflects the levels of fatty acid flux.

Several lipid species displayed significant increases, including many lysophospholipids (Figure 2-6, B, D, and H), which can act as signaling molecules, and several phospholipids (Figure 2-6, B–K). The increase in some lipids is consistent with the possible increased flux of fatty acids through ACSL enzymes that are not inhibited or are incompletely inhibited by triacsin C. The ratio of phosphatidylcholine (PC) to phosphatidylethanolamine (PE) has been implicated in ER homeostasis<sup>171,186,187</sup>, and although we observed alterations in PC and PE levels (Figure 2-6, B and F), the ratio between the two lipid species was relatively unchanged. An increase in ceramides (C16:0 ceramide and C18:0 ceramide) was detected (Figure 2-6, B and G), which is notable, given their role in cellular stress responses and UPR activation<sup>188</sup>. Together our results indicate that triacsin C treatment not only affects the levels of neutral lipids sequestered in LDs, but it also causes widespread alterations in the cellular lipid landscape (Figure 2-6). The levels of several of the altered lipids have been suggested to affect ER homeostasis (e.g., phosphatidylinositol and ceramides).

**Triacsin C activation of the PERK and IRE1 arms of the UPR has opposing effects on cell viability**  
Disruptions in ERAD and in lipid homeostasis can activate the UPR<sup>188,189</sup>. Inositol-requiring enzyme-1 (IRE1), an ER transmembrane serine/threonine kinase and endonuclease, is a primary mediator of the UPR that splices XBP1 mRNA to enable the translation of the XBP1 transcription factor<sup>108</sup>. Analysis using reverse transcription PCR revealed that incubation with triacsin C induced XBP1 splicing (Figure 2-7A). The spliced form of XBP1 was detectable at low levels as early as 8 h, and it became much more prominent at 16 and 24 h (Figure 2-7A). A second arm of the UPR is controlled by the ER-resident kinase PKR-like ER kinase (PERK), which phosphorylates the  $\alpha$  subunit of eukaryotic translation-initiation factor 2 (eIF2 $\alpha$ ). Phosphorylation of eIF2 $\alpha$  represses global translation while simultaneously promoting the translation of the ATF4 transcription factor to up-regulate stress-responsive genes such as the proapoptotic transcription factor C/EBP homologous protein (CHOP)<sup>190</sup>. To examine the potential effect of triacsin C on PERK induction of stress-responsive genes, we exploited a clonal HEK293 reporter cell line expressing an 8.5-kb CHOP gene fragment fused to GFP (CHOP::GFP)<sup>191,192</sup>. Treatment with tunicamycin, an inhibitor of N-linked glycosylation that induces the UPR, resulted in a robust and rapid accumulation in GFP fluorescence (Figure 2-7C and Supplemental Figure 2-S5). Treatment with

triacsin C also caused an increase in GFP fluorescence but with different temporal dynamics. During the first 8 h, no increase in GFP fluorescence was observed (Figure 2-7C). This lag period was followed by an increase in GFP fluorescence levels at 16 and 24 h (Figure 2-7C).

The IRE1 and PERK arms of the UPR play well-characterized protective roles through the induction of genes involved in protein folding and membrane expansion and through the repression of translation<sup>108</sup>. Of note, UPR up-regulation protected yeast from ER trafficking and ERAD defects induced by lipid disequilibrium<sup>171</sup>. However, persistent activation of IRE1 or PERK can lead to cell death<sup>169,192,193</sup>. To determine the role of the IRE1 and PERK pathways in the cellular response to triacsin C treatment, we analyzed the effects of the IRE1 inhibitor 4 $\mu$ 8c (IRE1i) and PERK inhibitor GSK2606414 (PERKi). IRE1i completely blocked triacsin C-induced XBP1 cleavage (Figure 2-7, A and B), and PERKi significantly attenuated the induction of the CHOP::GFP reporter (Figure 2-7D). Inhibition of PERK increased the amounts of cell death induced by triacsin C at 8, 16, and 24 h (Figure 2-7E), indicating that PERK plays a predominantly protective role under these conditions. In contrast, inhibition of IRE1 had little effect during triacsin C treatment and increased the amount of cell death at 24 h (Figure 2-7E). These findings indicate that both the IRE1 and PERK arms of the UPR are induced by triacsin C, but that the outputs of these two signaling pathways have opposing effects on cell viability.

## Discussion

Although there are several intriguing connections between LDs and ERAD, whether LDs are directly involved in the ERAD mechanism has remained an outstanding question. Our data argue that LD biogenesis is not a fundamental requirement for ERAD. Instead, our results support a model (Figure 2-7F) in which triacsin c induces widespread alterations in lipid homeostasis, most likely due to inhibition of ACSL 1, 3 and 4, that impairs specific steps in ERAD, resulting in disruptions in ER proteostasis, activation of the UPR, and eventual cell death. Thus, dysregulated fatty acid metabolism negatively affects ER homeostasis and protein quality control independently of LDs. However, although triacsin c has been demonstrated to inhibit ACSL 1, 3, and 4, it remains possible that it could have other targets. Further studies using genetic approaches to deplete these targets alone or in combination are needed to test our model.

To inhibit LD biogenesis but avoid the broad effects that ACSL inhibition has on lipid homeostasis, we pursued an approach that would disrupt a downstream step in TAG synthesis. To this end, we characterized a combined chemical (DGAT1 inhibition) and genetic (DGAT2<sup>-/-</sup>) approach to inhibit both of the DGAT enzymes, which are required for the conversion of DAG to TAG and the generation of LDs<sup>178,194</sup>. This strategy enabled acute disruption of LD biogenesis, reducing LD abundance under basal and oleate-stimulated conditions as effectively as triacsin C does. In contrast to triacsin C, disruption of LD biogenesis by inhibiting the DGATs had no effect on the kinetics of CD147 ERAD. These results are consistent with previous analyses of ERAD in yeast models of LD disruption<sup>153,160</sup>, which together demonstrate that LD biogenesis is not integral to the ERAD mechanism in yeast or mammalian cells. The possibility that LDs may function in the degradation of specific substrates or in ERAD under specific conditions is still worth consideration. For example, for ApoB100, an extremely large, hydrophobic protein, the



association with LDs might provide a specialized ERAD mechanism to reduce aggregation<sup>144,147</sup>. LDs may also contribute to ERAD only under particular conditions, such as periods of disrupted proteostasis. Under conditions in which proteasomal capacity is limiting, the LD surface could act as a transient site for the sequestration of ERAD and other UPS substrates<sup>147,150</sup>.

Our findings are in agreement with previous reports that triacsin C impairs ERAD<sup>142,145,148</sup>. Indeed, we found that triacsin C inhibited the degradation of two glycosylated Hrd1 substrates—the luminal substrate NHK and the endogenous integral membrane substrate CD147. The highest amount of substrate stabilization required a 16-h pretreatment with triacsin C, suggesting that ACSL activity is not required acutely during ERAD but instead that ACSL activity is required to establish a particular cellular environment conducive for ERAD. To define more precisely the step in ERAD that is affected by triacsin C, we tested individual steps of ERAD in the context of triacsin C treatment. Our results indicate that the triacsin C–induced defect in protein degradation is upstream of the proteasome and is confined to a subset of ERAD pathways. This conclusion is supported by several findings: 1) ubiquitinated proteins did not accumulate in response to triacsin C, 2) triacsin C did not stabilize a cytosolic UPS substrate, 3) triacsin C affected a subset of ERAD substrates—CD147 and NHK—but not CFTR $\Delta$ F508, and 4) triacsin C impaired the dislocation of a luminal glycosylated substrate. Moreover, analyses of the glycosylation state of CD147 during degradation indicate that triacsin C treatment impaired CD147 glycan trimming and delivery to the Hrd1 complex, suggesting that the primary impairment in ERAD is due to the failure to expose the trimmed glycan structure necessary for degradation commitment. Our proteomics data indicate that the composition of the Hrd1 complex is largely unaltered in triacsin C–treated cells; however, it is possible that alterations in the ER lipid composition could modulate the structure and/or function of the complex. The enzymes involved in the trimming of CD147’s glycans are unknown, but this step is most likely catalyzed by ER-resident mannosidases ERManI and/or EDEM1-3. Disruptions in lipid composition could influence substrate localization to ERManI-containing ER subdomains<sup>195</sup> or could affect EDEM membrane association, which is known to affect EDEM glycan trimming activity toward certain substrates<sup>196</sup>. It is also possible that the inhibition of ACSLs could influence protein acylation, and both calnexin<sup>197,198</sup> and the ERAD E3 ligase gp78<sup>199</sup> have been reported to be palmitoylated. Whether other ERAD factors are regulated by lipid modifications is unknown.

Activation of the UPR initiates signaling pathways with opposing outputs, a protective response that seeks to reestablish ER homeostasis and an apoptotic response that promotes cell death in the face of persistent ER stress<sup>192,200,201</sup>. Consistent with disruptions in ER homeostasis, treatment with triacsin C induced XBP1 splicing (IRE1 arm) and CHOP::GFP expression (PERK arm) and eventually caused cell death. Treatment of cells with the UPR inducer tunicamycin causes a rapid and transient up-regulation of IRE1 signaling that is paralleled by a slower increase in apoptotic PERK signaling at later times<sup>192</sup>. Of interest, in response to triacsin C, we see very different temporal dynamics and effects of UPR induction. Both the PERK and IRE1 arms exhibited similar activation kinetics and, after an initial lag period, steadily increased until the end of our experiments. Despite increasing CHOP reporter expression, PERK actions were overall protective in response to triacsin C. This finding indicates that CHOP expression alone is not conclusive evidence of a proapoptotic signaling output, consistent with the observation that forced CHOP

expression was insufficient to induce cell death<sup>169</sup>. In contrast to PERK, IRE1 signaling appeared to promote cell death, and the inhibition of IRE1 attenuated triacsin C-induced apoptosis, possibly by inhibiting excessive regulated Ire1-dependent decay (RIDD) of important secretory transcripts<sup>193</sup> or activation of a JNK apoptotic signaling pathway<sup>202</sup>. These results highlight the complex relationship between the UPR and cell death and reveal that the mode of UPR activation (e.g., tunicamycin vs. triacsin C) has a profound effect on the ultimate effects of each UPR branch. Alterations in phospholipids can directly induce UPR signaling<sup>188,203</sup> and whether the changes in the lipid environment, the defects in ER protein quality control, or both are responsible for triacsin C activation of the UPR is unclear. In addition, how the UPR is customized to fit a particular ER stressor is not evident. It is possible that the temporal coordination of individual UPR branches influences the end output (i.e., protection vs. cell death) or that different ER stressors provide a unique “second hit” (e.g., disruptions in lipid homeostasis or depletion in ER calcium pools) that sensitizes cells to IRE1- or PERK-dependent cell death pathways.

Our study reveals an intimate relationship between cellular lipid homeostasis and ER protein quality control. Our findings raise the possibility that certain lipid environments and/or modifications may affect ER proteostasis by regulating specific steps of the ERAD process. It is worth noting that a multitude of diseases, ranging from obesity to neurodegenerative diseases, are associated with altered lipid homeostasis and upregulated UPR<sup>204</sup>. In addition, targeting lipid metabolic enzymes to decrease fatty acid availability (e.g., inhibition of FASN) is being actively pursued as a therapeutic strategy for the treatment of cancer<sup>205-207</sup>. Therefore, elucidating the connections between ER lipid and protein homeostasis could have significant ramifications for our understanding of the pathogenic mechanisms underlying a wide number of diseases.

## Materials and Methods

### Plasmids, antibodies, and reagents

The pcDNA3.1(-) plasmids for expression of TTR-HA, the null Hong Kong mutant of  $\alpha$ -1 antitrypsin (NHK-HA and NHK-GFP), and S-tagged Hrd1 (Hrd1-S) were previously described<sup>113</sup>. The CFTR $\Delta$ F508 plasmid was kindly provided by Doug Cyr (University of North Carolina at Chapel Hill, Chapel Hill, NC).

Antibodies employed in this study include anti-CD147 (A-12, G-19, 8D6; Santa Cruz Biotechnology), anti-Hrd1 (A302-946A; Bethyl), anti-HA (HA7; Sigma-Aldrich), anti-S-peptide (EMD Millipore), anti-tubulin (Abcam), anti-glyceraldehyde-3-phosphate dehydrogenase (EMD Millipore), anti-GFP (Roche), anti-CFTR (University of North Carolina at Chapel Hill, CFTR Antibodies Distribution Program), anti-ubiquitin conjugates (FK2; EMD Millipore), anti-AUP1 (Proteintech), anti-SEL1L (T-17; Santa Cruz Biotechnology) and anti-KDEL (Enzo). Anti-derlin-1 and anti-derlin-2 antibodies were kind gifts from Yihong Ye (National Institutes of Health, Bethesda, MD). Rabbit polyclonal anti-UBXD8 antibodies were generated against a histidine-tagged fragment of UBXD8 (amino acids 97–445) by Proteintech Group. All IRDye680- and IRDye800-conjugated secondary antibodies for Western blotting were obtained from LI-COR. Alexa Fluor-conjugated secondary antibodies for immunofluorescence microscopy were obtained from Thermo Fisher Scientific.

Reagents employed in this study include triacsin C (Enzo Life Sciences), emetine dihydrochloride hydrate (Sigma-Aldrich), CB-5083 (Cleave Biosciences)<sup>208</sup>, oleate (Sigma-Aldrich), kifunensine (Cayman Chemical), deoxynojirimycin (Sigma-Aldrich), MG-132 (Selleck Chemicals), T863 (Sigma-Aldrich), 4 $\mu$ 8C (EMD Millipore), GSK2606414 (EMD Millipore), tunicamycin (Cayman Chemical), and PNGase F (New England Biolabs).

### **Cell culture and transfections**

HEK293, HEK293T, MEF, HeLa, and U2OS cells were cultured in DMEM containing 4.5 g/l glucose and L-glutamine (Corning) supplemented with 10% fetal bovine serum (FBS) (Thermo Fisher Scientific and Gemini Bio Products) at 37°C and 5% CO<sub>2</sub>. 293T.FluERAD cells stably expressing a split-Venus system for the analysis of the dislocation step of ERAD<sup>179</sup> were kindly provided by Peter Cresswell (Yale University, New Haven, CT). U2OS cells stably expressing Venus-DD<sup>168</sup> and HEK293 cells stably expressing the CHOP::GFP reporter were kindly provided by Ron Kopito (Stanford University, Stanford, CA). DGAT2<sup>-/-</sup> MEF cells were kindly provided by Robert Farese, Jr. (Harvard University, Cambridge, MA). All plasmid transfections were performed using XtremeGENE HP (Roche) transfection reagent according to the manufacturer's instructions.

### **Immunoblotting analysis**

Cells were washed extensively in phosphate-buffered saline (PBS) and lysed in 1% SDS. Protein amounts were normalized using a bicinchoninic acid (BCA) protein assay (Thermo Fisher Scientific). Proteins were separated on 4–20% polyacrylamide gradient gels (Bio-Rad) and transferred onto low-fluorescence polyvinylidene fluoride or nitrocellulose membranes (Bio-Rad). Large-format gel electrophoresis was performed using 10% acrylamide gels made with acrylamide/bis 19:1. Membranes were incubated in 5% nonfat milk in PBS plus 0.1% Tween-20 (PBST) for 30 min to reduce nonspecific antibody binding. Membranes were then incubated for at least 2 h in PBST containing 5% milk or 1% bovine serum albumin (BSA; Sigma-Aldrich) and primary antibodies, followed by incubation for at least 1 h in PBST containing 1% BSA and fluorescence-conjugated secondary antibodies. Immunoblots were visualized on a LI-COR imager (LI-COR Biosciences), and ImageJ<sup>209</sup> was used for quantification.

### **Immunofluorescence microscopy**

HeLa and MEF cells were plated on poly-L-lysine-coated coverslips. Cells were treated the next day, washed with PBS, and fixed at room temperature with 4% paraformaldehyde in PBS for 10 min. Cells were washed three times with PBS and permeabilized with 0.1% Triton X-100 plus 1% BSA in PBS at room temperature for 30 min. Cells were washed three times with 1% BSA in PBS and incubated for 2 h in primary antibodies, washed three times, and incubated for 1 h with Alexa Fluor-conjugated secondary antibodies, BODIPY493/503 (LD staining; Thermo Fisher Scientific), and 4',6-diamidino-2-phenylindole (DAPI; nuclei staining; Thermo Fisher Scientific). Cells were washed three times and mounted using Fluoromount-G (SouthernBiotech). Cells were visualized using a DeltaVision Elite microscope and acquired images deconvolved and analyzed using SoftWoRx. The abundance of LDs per cell was determined by measuring the area of BODIPY493/503-stained LDs per cell using ImageJ<sup>209</sup>.

### Affinity purifications

HEK293 cells were harvested, washed with PBS, and lysed in immunoprecipitation (IP) buffer (50 mM Tris-HCl, pH 7.5, 150 mM NaCl, 1% digitonin, and protease inhibitor tablets [Thermo Fisher Scientific]) at 4°C for 30 min. Lysates were clarified by centrifugation at  $20,000 \times g$  for 10 min. Protein concentrations were measured using the BCA assay. For the affinity purification of S-tagged protein complexes, lysates were loaded onto S-protein agarose beads (EMD Millipore) at a concentration of 25  $\mu$ l beads per 1 mg of lysate. For endogenous Hrd1 IPs, 2 mg of lysate was incubated with anti-Hrd1 antibodies for 1 h and then loaded onto 25  $\mu$ l of protein G agarose beads (EMD Millipore). Lysates were incubated with the beads rotating at 4°C for 2 h, washed three times with lysis buffer containing 0.1% digitonin, and eluted in loading buffer.

### Radiolabeling and pulse-chase analysis

HEK293 cells plated on poly-L-lysine-coated plates were washed twice with “cold” medium, which lacked L-methionine and L-cysteine and contained 10% dialyzed FBS, and then starved in this medium for 30 min. Cells were radiolabeled in medium containing 125  $\mu$ Ci/ml  $^{35}$ S-labeled cysteine/methionine (Easytag Express Protein Labeling Mix 35S; PerkinElmer) for 30 min, washed twice with Hanks’ buffered saline solution, and then chased in complete medium containing 75  $\mu$ M emetine for the indicated times. Cells were harvested, collected by centrifugation, washed in PBS, and lysed in pulse-chase IP buffer (25 mmol/l 4-(2-hydroxyethyl)-1-piperazineethanesulfonic acid buffer, pH 7.4, 150 mmol/l NaCl, 5 mmol/l  $\text{MgCl}_2$ , 1% 3-[(3-cholamidopropyl)dimethylammonio]-1-propanesulfonate detergent, and protease inhibitors). Lysates were cleared by centrifugation at  $20,000 \times g$  for 15 min at 4°C and protein concentrations determined using the BCA assay. Lysates were precleared with protein G beads (EMD Millipore). CD147 was immunoprecipitated from lysates by incubation with anti-CD147 antibody (8D6; Santa Cruz biotechnology) for 4 h at 4°C with mixing, followed by incubation with protein G beads (EMD Millipore) for an additional 2 h at 4°C with mixing. Immunoprecipitated proteins were washed thrice with the pulse-chase IP buffer and then separated by SDS-PAGE. Gels were dried and exposed to a Storage Phosphor Screen (GE Healthcare Life Sciences) for 16 h at room temperature. Radioactive signals corresponding to CD147(Mat.) and CD147(CG) were detected using a Typhoon 9400 Molecular Imager (GE Healthcare Life Sciences).

### SILAC mass spectrometry

Parental HEK293 cells or HEK293 cells expressing S-tagged Hrd1 were grown in DMEM lacking L-arginine and L-lysine supplemented with 10% dialyzed FBS (Life Technologies) and the appropriate SILAC amino acids: *light*, L-arginine (Arg0) and L-lysine (Lys0); *medium*,  $^{13}\text{C}_6$ -L-arginine (Arg6) and 4,4,5,5- $\text{D}_4$ -L-lysine (Lys4); and *heavy*,  $^{13}\text{C}_6$  $^{15}\text{N}_4$ -L-arginine (Arg10) and  $^{13}\text{C}_6$  $^{15}\text{N}_2$ -L-lysine (Lys8). Cells were cultured for at least seven cell doublings to allow for complete incorporation of the stable isotope-labeled amino acids (Cambridge Isotope Laboratories). Parental HEK293 control cells were *light* SILAC labeled, and S-tagged Hrd1 cells were either *medium* or *heavy* labeled. At 16 h before harvest, the S-tagged Hrd1 cells were incubated with either vehicle (*medium* SILAC labeled) or 1  $\mu$ g/ml triacsin C (*heavy* SILAC labeled). After several washes in PBS, cells were lysed in IP buffer, and 3 mg of protein lysate was loaded onto 75  $\mu$ l of S-protein agarose beads (EMD Millipore). Lysates were rotated at 4°C for 2 h and washed three times with IP buffer containing 0.1% digitonin and twice with 50 mM ammonium

bicarbonate. Beads were resuspended in 75  $\mu$ l of 0.2% RapiGest SF (Waters) in 50 mM ammonium bicarbonate for 15 min at 65°C, followed by incubation with 2.5  $\mu$ g of trypsin (Thermo Fisher Scientific) overnight at 37°C. The affinity purification for each condition was performed separately to prevent exchange of interaction partners during the incubations. After the proteolysis step, equal volumes of digested peptides were combined and acidified with HCl to pH 2.0. RapiGest SF precipitate was removed by centrifugation at 20,000  $\times$  *g* for 30 min and the peptide solution concentrated to 40  $\mu$ l using a SpeedVac. Digested peptides were analyzed by LC-MS/MS on a Thermo Scientific Q Exactive Orbitrap Mass spectrometer in conjunction with a Proxeon Easy-nLC II HPLC (Thermo Fisher Scientific) and Proxeon nanospray source at the University of California, Davis, Proteomics Core Facility. The digested peptides were loaded onto a 100  $\mu$ m  $\times$  25 mm Magic C18 100-Å 5U reverse-phase trap, where they were desalted online before being separated using a 75  $\mu$ m  $\times$  150 mm Magic C18 200-Å 3U reverse-phase column. Peptides were eluted using a 180-min gradient with a flow rate of 300 nl/min. An MS survey scan was obtained for the *m/z* range 300–1600, and MS/MS spectra were acquired using a top 15 method, in which the top 15 ions in the MS spectra were subjected to high-energy collisional dissociation. An isolation mass window of 1.6 *m/z* was used for the precursor ion selection, and a normalized collision energy of 27% was used for fragmentation. A 5-s duration was used for the dynamic exclusion. The acquired MS/MS spectra were searched against a full UniProt database of human protein sequences, and SILAC ratios were determined using MaxQuant. The mass spectrometry proteomics data have been deposited to the ProteomeXchange Consortium via the PRIDE partner repository with the data set identifier PXD005633.

### Lipidomic profiling

HEK293 cells were grown to 70% confluence in a 10-cm dish and treated for 16 h with vehicle or 1  $\mu$ g/ml triacsin C. Cells were washed twice with PBS and harvested, and cell pellets were stored at –80°C. Lipid metabolite extraction and analysis by SRM-based LC-MS/MS was performed as previously described<sup>207,210,211</sup>. Briefly, nonpolar lipid metabolites were extracted in 2:1:1 chloroform/methanol/PBS supplemented with internal standards C12:0 dodecylglycerol (10 nmol) and pentadecanoic acid (10 nmol). The organic and aqueous layers were collected after separation by centrifugation at 1000  $\times$  *g* for 5 min. The aqueous layer was acidified by addition of 0.1% formic acid and subjected to a second chloroform extraction. The resulting organic layers were combined and mixed, dried down under N<sub>2</sub>, and dissolved in 120  $\mu$ l of chloroform. A 10- $\mu$ l aliquot was analyzed by SRM LC-MS/MS. Metabolites were separated using a Luna reverse-phase C5 column (Phenomenex), and MS analysis was performed on an Agilent 6430 QQQ LC-MS/MS. Quantification of metabolites was performed by integrating the area under the peak, normalized to internal standard values, adjusted based on external standard curves, and expressed as relative levels compared with the control sample.

### XBP1 splicing assay

RNA was isolated using TRIzol Reagent (Life Technologies) and cDNA generated using the High-Capacity cDNA Reverse Transcription Kit (Applied Biosystems) according to the manufacturer's directions. XBP1 was amplified using the primers 5'-AAACAGAGTAGCAGCTCAGACTGC-3' and 5'-TCCTTCTGGGTAGACCTCTGGGAG-3'. Amplified products were separated on a 2.5% agarose gel at 80 V for 2 h and visualized using a Gel Doc imaging system (Bio-Rad).

**Cell viability**

Cells were trypsinized, pelleted by centrifugation at  $500 \times g$  for 5 min, washed in PBS, and resuspended in 100  $\mu$ l of PBS containing 2.5  $\mu$ g/ml propidium iodide (BD Biosciences). After a 5-min incubation, cells were diluted with PBS to a final volume of 1 ml and analyzed using a BD Biosciences LSRFortessa. Cell suspensions were stored on ice throughout the procedure. Subsequent data analysis was performed using FlowJo software.

## Figures

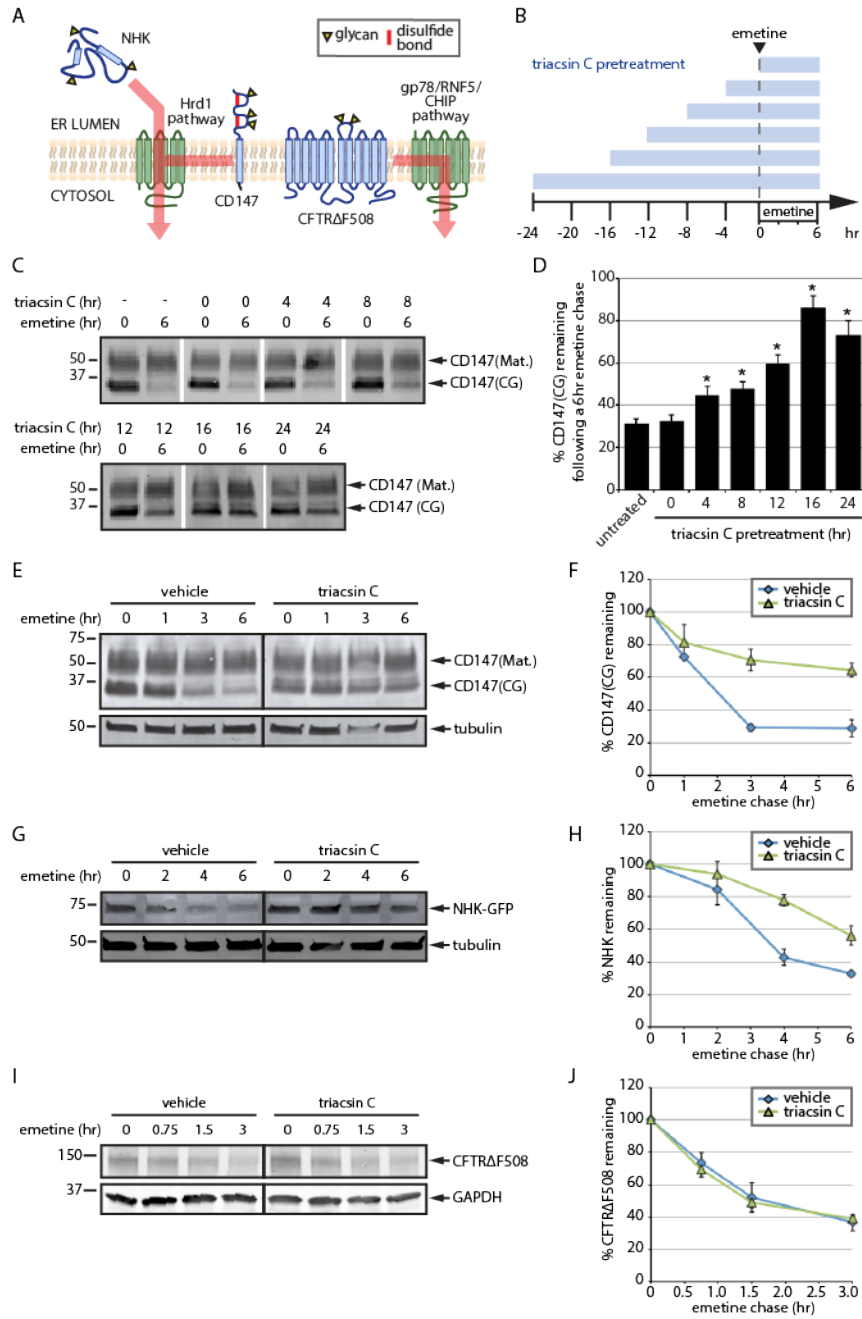




Figure 2-1: Triacsin C inhibits a subset of ERAD pathways. (A) ERAD substrate panel, indicating substrate topology and degradation pathway(s). Substrates are indicated in blue and ERAD components in green. Yellow triangles indicate N-linked glycans. (B) Triacsin C treatment time course. Triacsin C was added for the indicated times (blue bars) and maintained in the medium throughout the emetine chase. (C) HEK293 cells were pretreated with 1  $\mu\text{g}/\text{ml}$  triacsin C for the indicated times (as depicted in B), followed by addition of 75  $\mu\text{M}$  emetine for 6 h. CD147 levels were assessed by immunoblotting of SDS lysates. (D) The relative CD147(CG) levels in C were quantified and are presented as percentage of the levels at time 0 h ( $n = 3$ ). Asterisk indicates significant stabilization ( $p < 0.05$ ). (E) HEK293 cells were pretreated with vehicle or 1  $\mu\text{g}/\text{ml}$  triacsin C for 16 h, followed by 75  $\mu\text{M}$  emetine for the indicated times. CD147 levels were assessed by immunoblotting of SDS lysates. (F) The relative levels of CD147(CG) in E were quantified and are presented as percentage of the levels at time 0 h ( $n = 3$ ). (G) HEK293 cells expressing NHK-GFP were pretreated with vehicle or 1  $\mu\text{g}/\text{ml}$  triacsin C for 16 h, followed by 75  $\mu\text{M}$  emetine for the indicated times. NHK-GFP levels were assessed by immunoblotting of SDS lysates. (H) The relative levels of NHK-GFP in G were quantified and are presented as percentage of the levels at time 0 h ( $n = 3$ ). (I) HEK293 cells expressing CFTR $\Delta\text{F508}$  were pretreated with vehicle or 1  $\mu\text{g}/\text{ml}$  triacsin C for 16 h, followed by 75  $\mu\text{M}$  emetine for the indicated times. CFTR $\Delta\text{F508}$  levels were assessed by immunoblotting of SDS lysates. (J) The relative levels of CFTR $\Delta\text{F508}$  in I were quantified and are presented as percentage of the levels at time 0 h ( $n = 4$ ). Mat., mature; CG, core glycosylated. Error bars indicate SEM.

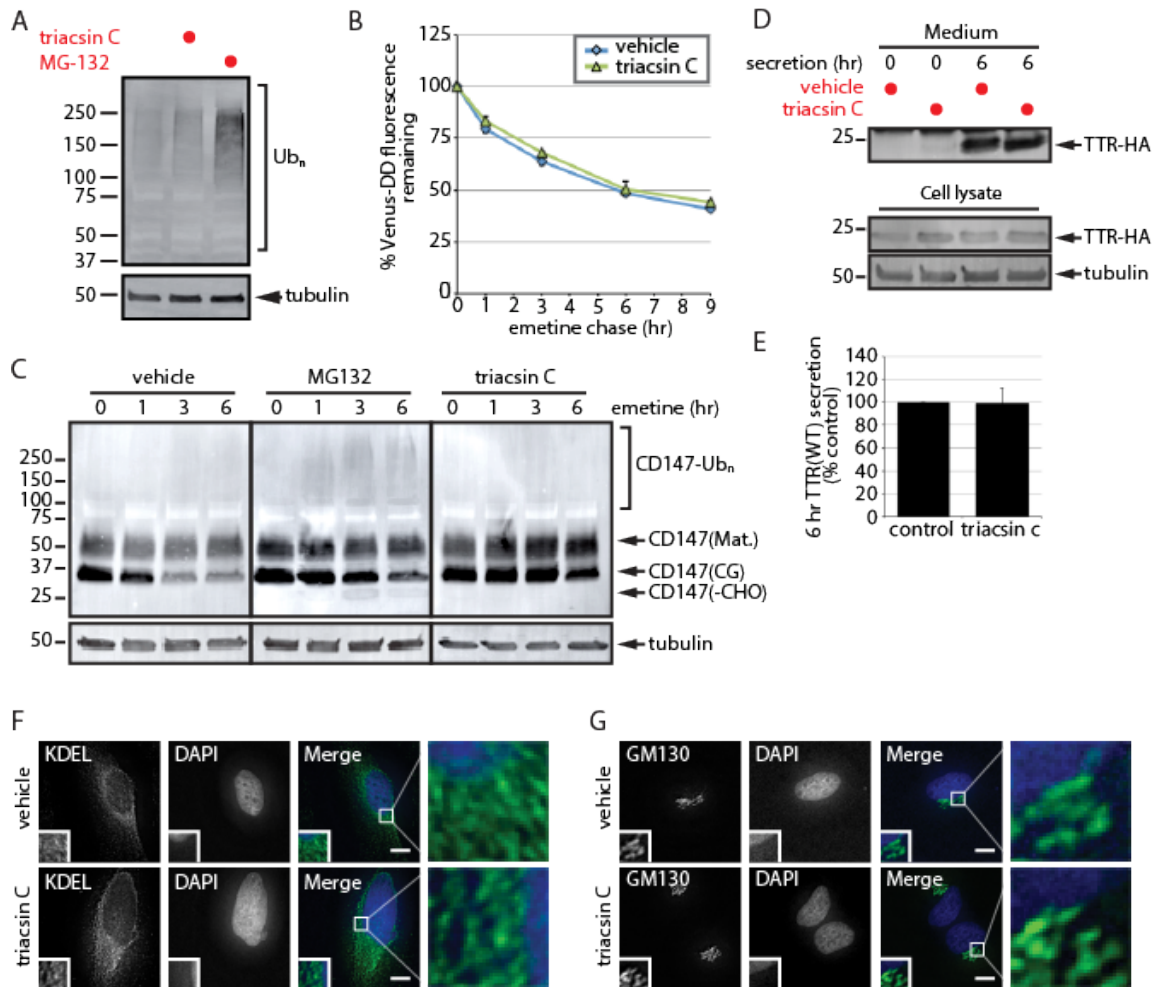


Figure 2-2: Triacsin C does not generally inhibit the ubiquitin-proteasome system or protein secretion. (A) SDS lysates from HEK293 cells incubated with 1  $\mu\text{g}/\text{ml}$  triacsin C for 16 h or 10  $\mu\text{M}$  MG-132 for 6 h were analyzed by immunoblotting. (B) U2OS cells stably expressing Venus-DD were incubated with vehicle or 1  $\mu\text{g}/\text{ml}$  triacsin C for 16 h, followed by emetine treatments for the indicated times. Venus fluorescence levels were monitored by flow cytometry and quantified as the percentage of the levels at time 0 h ( $n = 3$ ). (C) HEK293 cells were incubated with vehicle or 1  $\mu\text{g}/\text{ml}$  triacsin C for 16 h and then treated with 75  $\mu\text{M}$  emetine for the indicated times. Where indicated, 10  $\mu\text{M}$  MG-132 was added at the beginning of the emetine chase. The levels of the different forms of CD147 were assessed by immunoblotting of SDS lysates. (D) HEK293 cells expressing TTR-HA were treated with vehicle or 1  $\mu\text{g}/\text{ml}$  triacsin C for 16 h. Cells were washed with PBS, and the medium was replaced with serum-free OPTI-MEM containing vehicle or 1  $\mu\text{g}/\text{ml}$  triacsin C for the remaining 6 h. Lysates and TTR-HA immunoprecipitated from the media were analyzed by immunoblotting. (E) The levels of TTR-HA in the media were quantified from D and are presented as percentage of the levels in the control sample ( $n = 3$ ). (F, G) The morphology of the ER, anti-KDEL (green) and the Golgi complex, anti-GM130 (green), in HeLa cells treated with vehicle or 1  $\mu\text{g}/\text{ml}$  triacsin C for 16 h was analyzed by immunofluorescence microscopy. Nuclei were stained with DAPI (blue). Scale bar, 10  $\mu\text{m}$ . Mat., mature; CG, core glycosylated; -CHO, deglycosylated. Error bars indicate SEM.

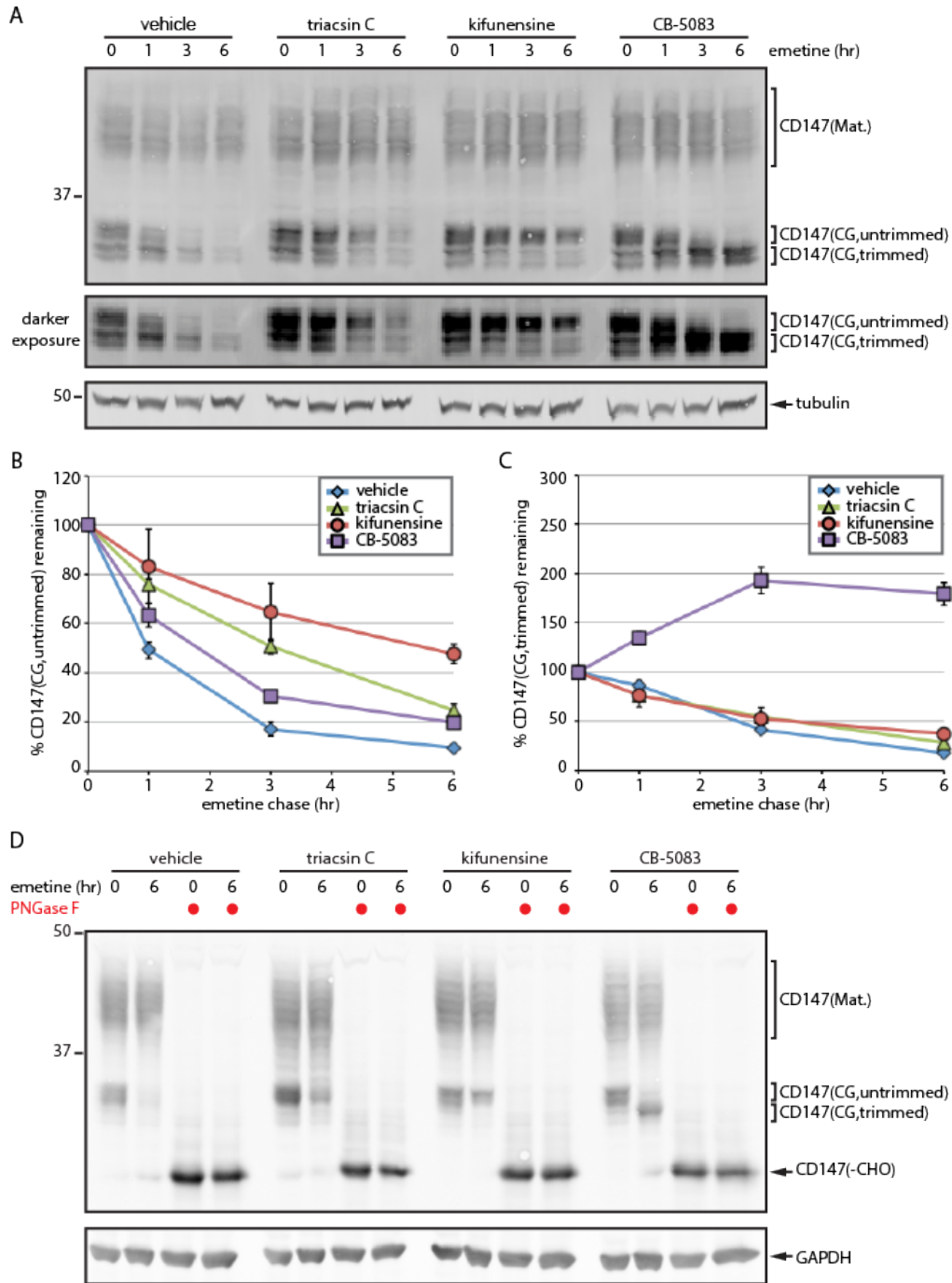


Figure 2-3: Triacsin C impairs ERAD substrate glycan trimming. (A) HEK293 cells were pretreated with vehicle or 1  $\mu\text{g}/\text{ml}$  triacsin C for 16 h, followed by 75  $\mu\text{M}$  emetine for the indicated times. Where indicated, 5  $\mu\text{g}/\text{ml}$  kifunensine and 5  $\mu\text{M}$  CB-5083 were added at the beginning of the emetine chase. SDS lysates were separated on large-format SDS-PAGE gels and analyzed by immunoblotting to visualize the different CD147 glycoforms. A darker exposure of the CD147(CG) bands is provided to facilitate visualization of the different trimmed glycoforms. (B, C) The relative levels of untrimmed CD147(CG) (B) and trimmed CD147(CG) (C) were quantified from A and are presented as percentage of the levels at time 0 h ( $n = 3$ ). (D) Lysates from cells treated as in A were incubated with PNGase F as indicated and analyzed by immunoblotting. Mat., mature; CG, core glycosylated; -CHO, deglycosylated. Error bars indicate SEM.

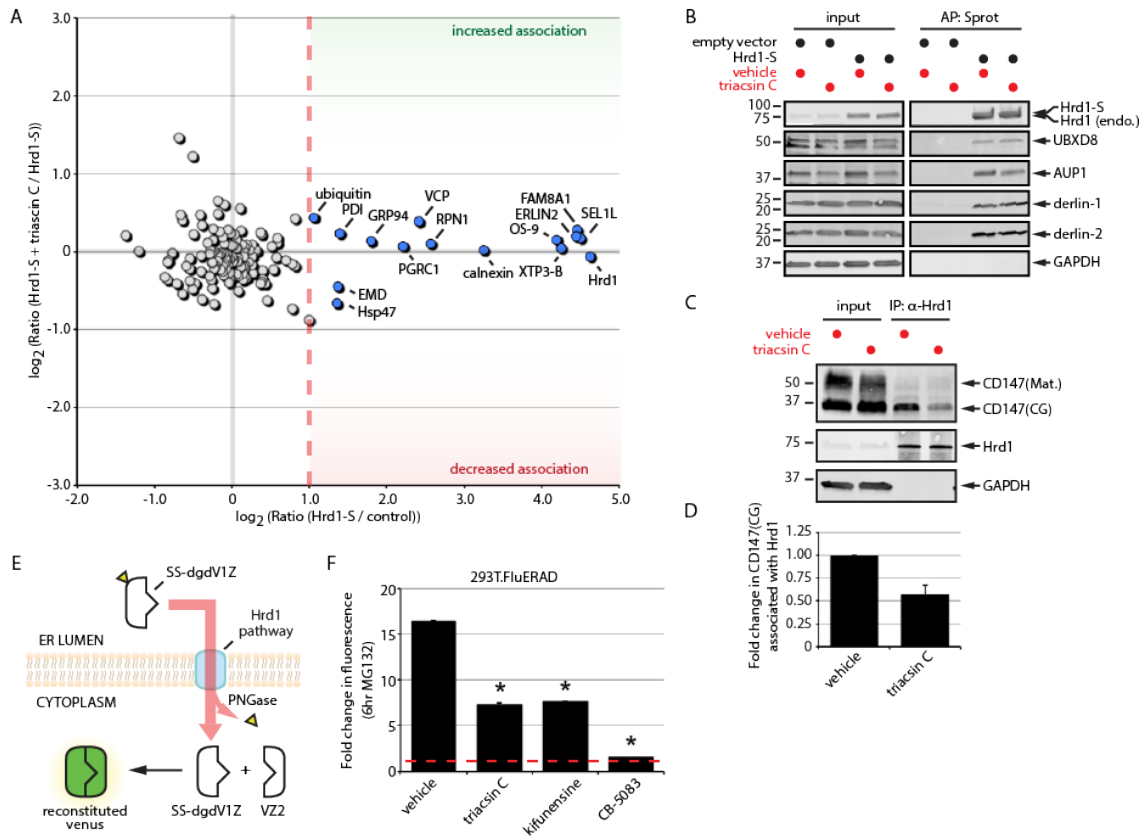


Figure 2-4: Triacsin C impairs substrate delivery to and dislocation from the Hrd1 complex. (A) Two-dimensional plot representing the proteomic analysis of Hrd1-S interactors from a triple SILAC experiment. The ratio of Hrd1-S/control on the x-axis indicates the strength of the interaction under basal conditions. The ratio of Hrd1-S + triacsin C/Hrd1-S on the y-axis indicates the change in the interaction in response to triacsin C treatment. Gray filled circles are nonspecific interactors, and blue filled circles are high-confidence interactors. (B) HEK293 cells expressing an empty vector or S-tagged Hrd1 were pretreated with vehicle or 1  $\mu\text{g/ml}$  triacsin C for 16 h. Affinity-purified complexes were analyzed by immunoblotting with the indicated antibodies. (C) HEK293 cells were pretreated with vehicle or 1  $\mu\text{g/ml}$  triacsin C for 16 h. Endogenous Hrd1 complexes were immunoprecipitated and analyzed by immunoblotting with the indicated antibodies. (D) The fold change in Hrd1-associated CD147(CG) in C was quantified and is presented as a bar graph ( $n = 3$ ). (E) The split-Venus dislocation assay. See text for description. (F) 293T.FluERAD cells, which stably express the deglycosylation-dependent Venus dislocation system, were pretreated with 1  $\mu\text{g/ml}$  triacsin C for 16 h, followed by a 0- or 6-h treatment with 10  $\mu\text{M}$  MG-132. Where indicated, 5  $\mu\text{g/ml}$  kifunensine or 5  $\mu\text{M}$  CB-5083 was added together with 10  $\mu\text{M}$  MG-132 for 0 or 6 h. Venus fluorescence levels were quantified by flow cytometry and are represented as the fold change relative to the 0 h. Asterisk indicates a significant decrease in the fold change in fluorescence levels ( $p < 0.05$ ). AP, affinity purification; CG, core glycosylated; endo., endogenous; IP, immunoprecipitation; Mat., mature; Sprot, S-protein agarose. Error bars indicate SEM.

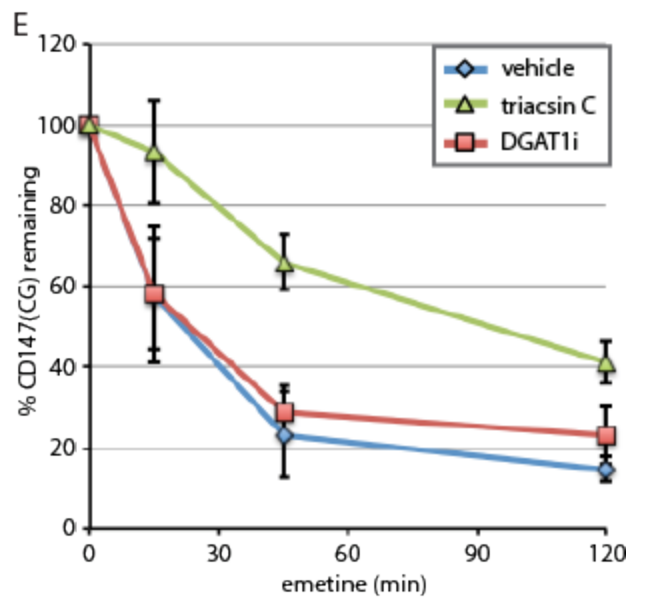
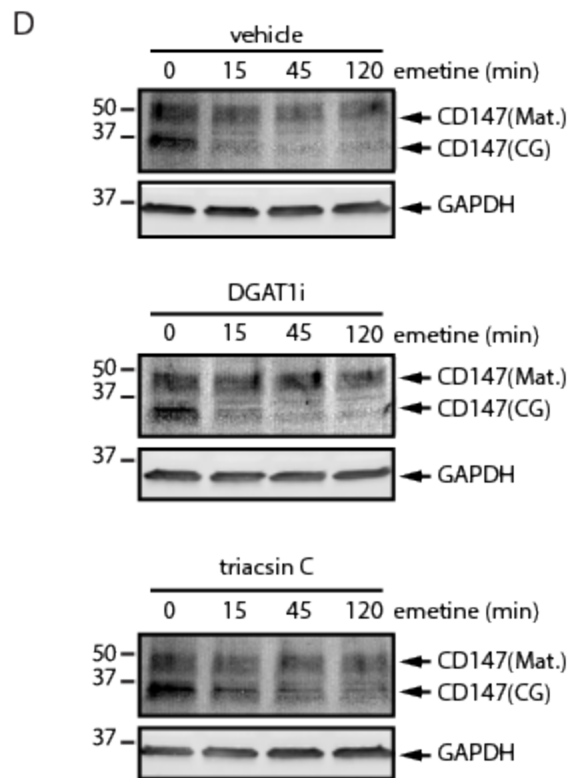
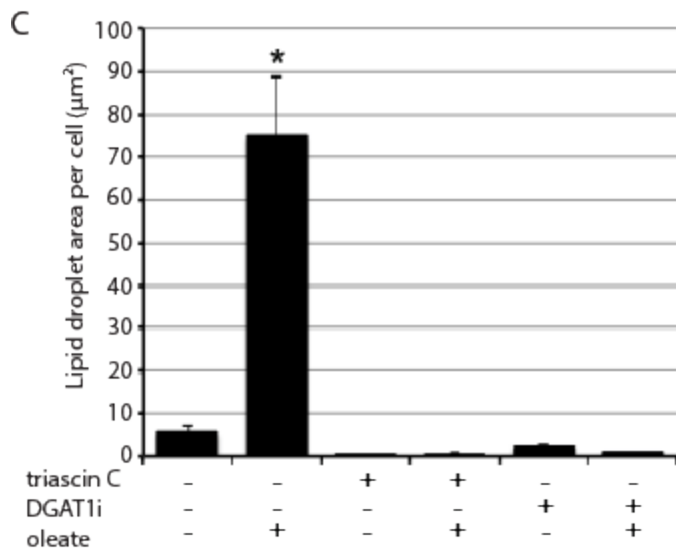
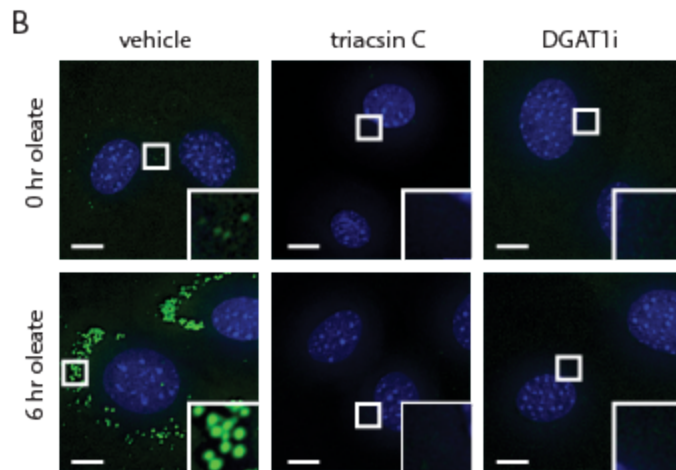
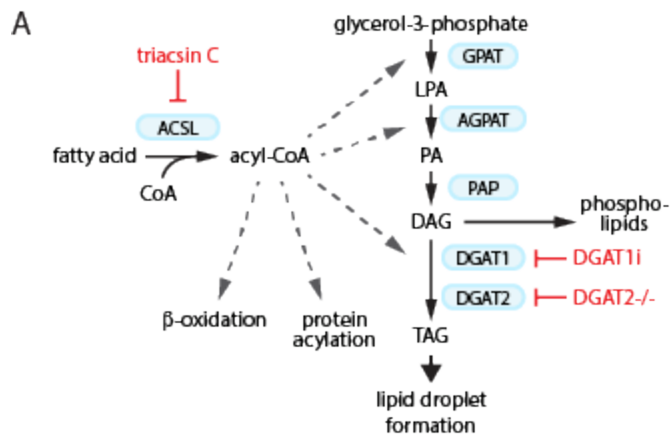


Figure 2-5: Lipid droplet biogenesis is dispensable for CD147 ERAD. (A) The Kennedy pathway of TAG synthesis indicating the enzymes (blue boxes) and metabolites. Select additional pathways that use acyl-CoA are also depicted. Approaches to disrupt LD biogenesis through the inhibition of ACSLs (triaclin C) or the DGAT enzymes (DGAT1i and DGAT2<sup>-/-</sup>) are indicated in red. (B) DGAT2<sup>-/-</sup> MEFs were pretreated with 1 µg/ml triaclin C or 20 µM DGAT1i for 3 h and then incubated with 200 µM oleate for 0 or 6 h as indicated. Fluorescence microscopy was employed to visualize LDs (green) and nuclei (blue). Scale bar, 5 µm. (C) The abundance of LDs was quantified from cells treated as shown in B. Asterisk indicates a significant increase in LD amount relative to untreated cells ( $p < 0.05$ ). (D) DGAT2<sup>-/-</sup> MEFs were pretreated with vehicle, 1 µg/ml triaclin C, or 20 µM DGAT1i for 16 h, followed by 75 µM emetine for the indicated times. CD147 levels were assessed by immunoblotting of SDS lysates. (E) The relative levels of CD147(CG) in D were quantified and are presented as percentage of the levels at time 0 h ( $n = 3$ ). ACSL, long-chain acyl-CoA synthetase; AGPAT, acylglycerolphosphate acyltransferase; DAG, diacylglycerol; DGAT, diacylglycerol acyltransferase; GPAT, glycerol-phosphate acyltransferase; LPA, lysophosphatidic acid; PA, phosphatidic acid; PAP, phosphatidic acid phosphatase; TAG, triacylglycerol. Error bars indicate SEM.

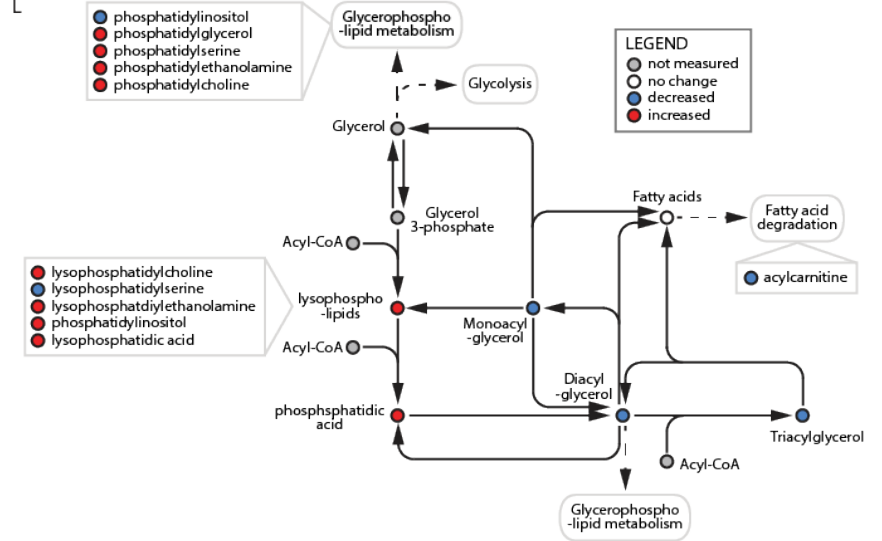
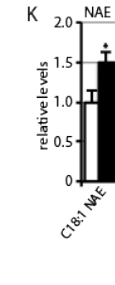
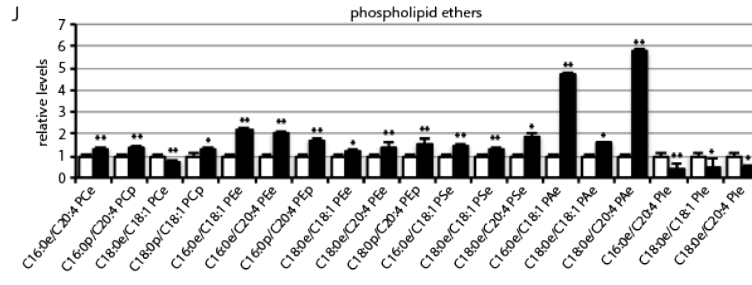
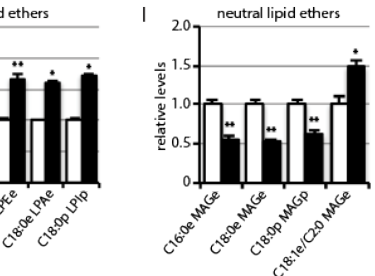
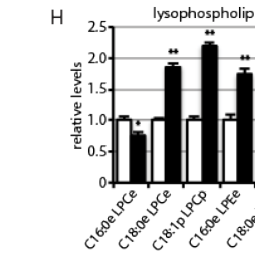
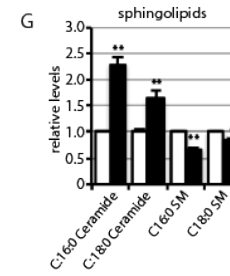
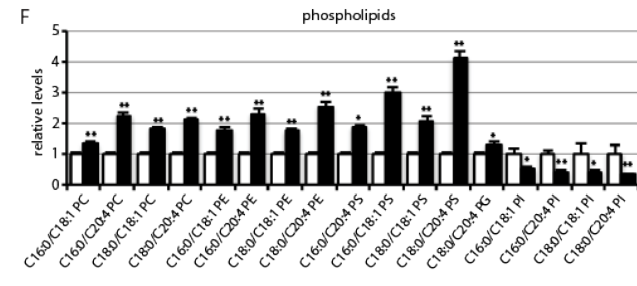
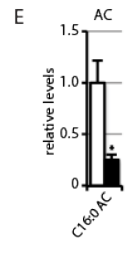
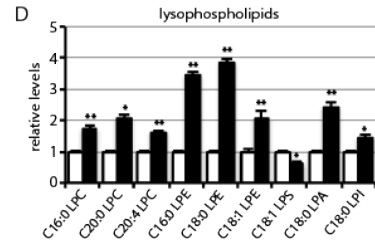
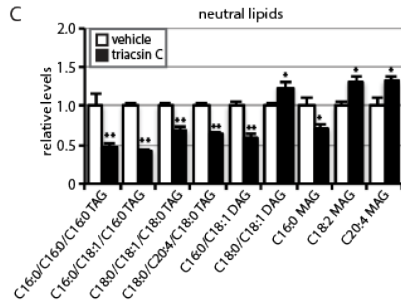
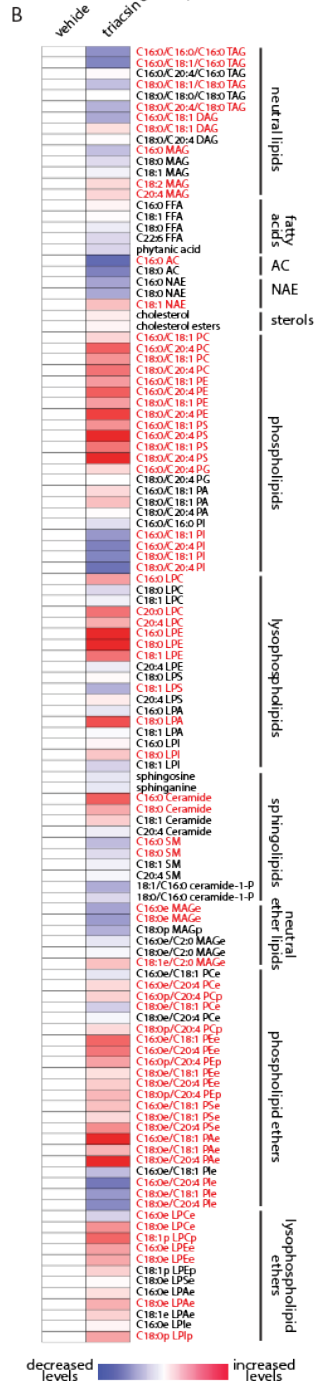
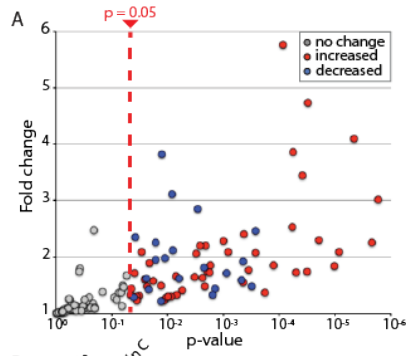




Figure 2-6: Triacsin C alters the cellular lipid landscape. Targeted metabolomic analysis of the nonpolar metabolome of cells treated with 1  $\mu\text{g}/\text{ml}$  triacsin C for 16 h revealed alterations in 71 lipid species, illustrated as a volcano plot (A) and a heat map organized by lipid class (B). Red text in B indicates a significant change ( $p < 0.05$ ). (C–K) Quantification showing the relative levels of significantly altered lipids ( $n = 4$  or 5).  $*p < 0.05$ ,  $**p < 0.01$ . White bars, vehicle; black bars, triacsin C. (L) Pathway map depicting the general effects of triacsin C on neutral lipids and phospholipids. DAG, diacylglycerol; FFA, free fatty acid; MAG, monoacylglycerol; NAE, *N*-acylethanolamine; PA, phosphatidic acid; PC, phosphatidylcholine; PE, phosphatidylethanolamine; PG, phosphatidylglycerol; PI, phosphatidylinositol; PS, phosphatidylserine; TAG, triacylglycerol. “L” before a lipid phospholipid designation indicates lyso-; “e” after a lipid designation indicates an ether lipid; “p” after a lipid designation designates plasmalogen. Error bars indicate SEM.

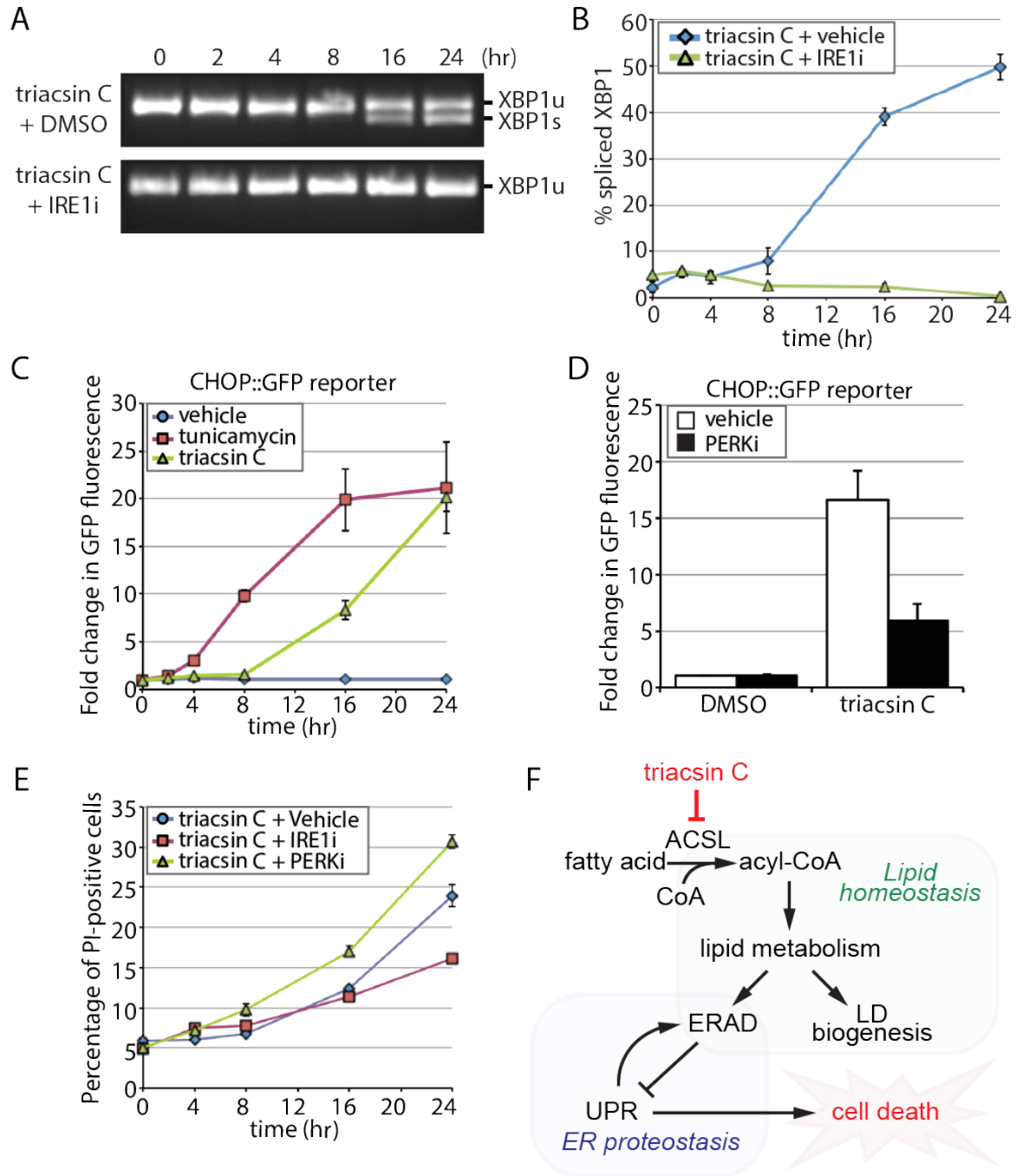


Figure 2-7: Triacsin C activates opposing arms of the UPR. (A) Reverse transcription PCR assay of XBP1 mRNA from HEK293 cells treated with 1  $\mu\text{g}/\text{ml}$  triacsin C for the indicated times in the presence and absence of 100  $\mu\text{M}$  IRE1 inhibitor 4 $\mu\text{8c}$  (IRE1i). XBP1 amplicons were separated on an agarose gel and imaged. XBP1u, unspliced XBP1; XBP1s, spliced XBP1. (B) Quantification of the percentage of spliced XBP1 in A ( $n = 3$ ). (C) HEK293 cells stably expressing a CHOP::GFP construct were treated with vehicle, 1  $\mu\text{g}/\text{ml}$  triacsin C, or 5  $\mu\text{g}/\text{ml}$  tunicamycin as indicated and GFP levels measured using flow cytometry. The fold change in GFP fluorescence relative to time 0 h is shown ( $n = 3$ ). (D) HEK293 cells stably expressing a CHOP::GFP construct were treated with vehicle or 1  $\mu\text{g}/\text{ml}$  triacsin C for 0 and 16 h in the presence and absence of 1  $\mu\text{M}$  PERK inhibitor GSK2606414 (PERKi). GFP levels were measured using flow cytometry. The fold change in GFP fluorescence relative to time 0 h is shown ( $n = 3$ ). (E) HEK293 cells were treated with 1  $\mu\text{g}/\text{ml}$  triacsin C and vehicle, 100  $\mu\text{M}$  IRE1i, or 1  $\mu\text{M}$  PERKi for the indicated times and stained with propidium iodide to identify apoptotic cells. The percentage of apoptotic cells relative to time 0 h is shown ( $n = 3$ ). (F) A model depicting the relationship between fatty acid metabolism and ER proteostasis. Disruptions in fatty acid metabolism result in lipid disequilibrium, causing impairments in ER quality control by inhibiting specific steps in ERAD (independent of LDs). The disruption in ER homeostasis activates the UPR, which protects cells via the PERK pathway and eventually kills cells via the IRE1 pathway. Error bars indicate SEM.

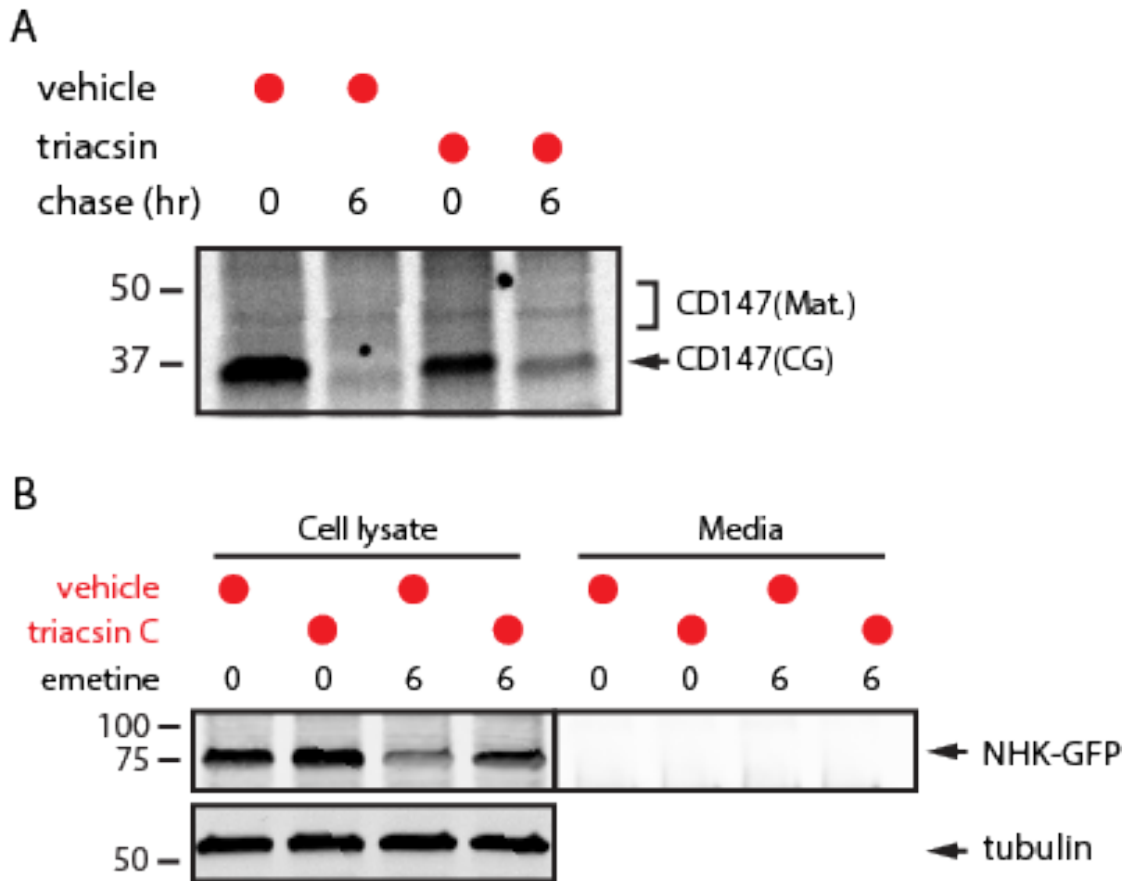


Figure 2-S1: Analysis of CD147 maturation and NHK secretion. (A) HEK293 cells were pretreated with vehicle or 1  $\mu\text{g}/\text{mL}$  triacin C for 16 hr, pulse labeled, and samples collected at 0 hr and 6 hr. CD147 was immunoprecipitated, separated by SDS-PAGE, and radioactivity detected using a Typhoon 9400. (B) HEK293 cells expressing NHK-GFP were treated with vehicle or 1  $\mu\text{g}/\text{mL}$  triacin C for 16 hr. Cells were washed with PBS, and the media was replaced with serum-free OPTI-MEM containing vehicle or 1  $\mu\text{g}/\text{mL}$  triacin C for the remaining 6 hr. Lysates and NHKGFP immunoprecipitated from the media were analyzed by immunoblotting.

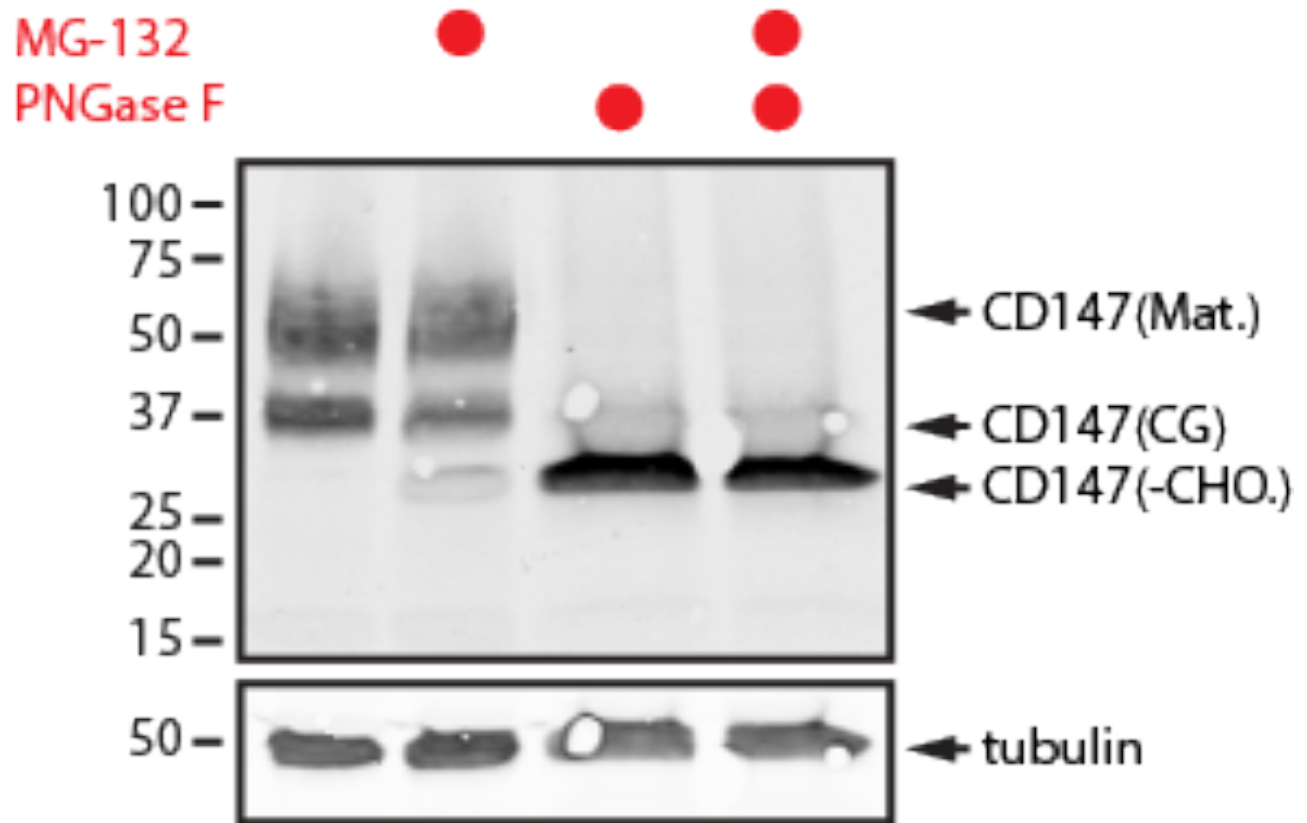


Figure 2-S2: Proteasome inhibition causes accumulation of CD147 in a deglycosylated form. HEK293 cells incubated with vehicle or 10  $\mu$ M MG-132 for 6 hr were lysed in 1% SDS. Lysates were then incubated in the presence and absence of PNGase F for 30 min at 37°C. Proteins were separated by SDS-PAGE and analyzed by immunoblotting.

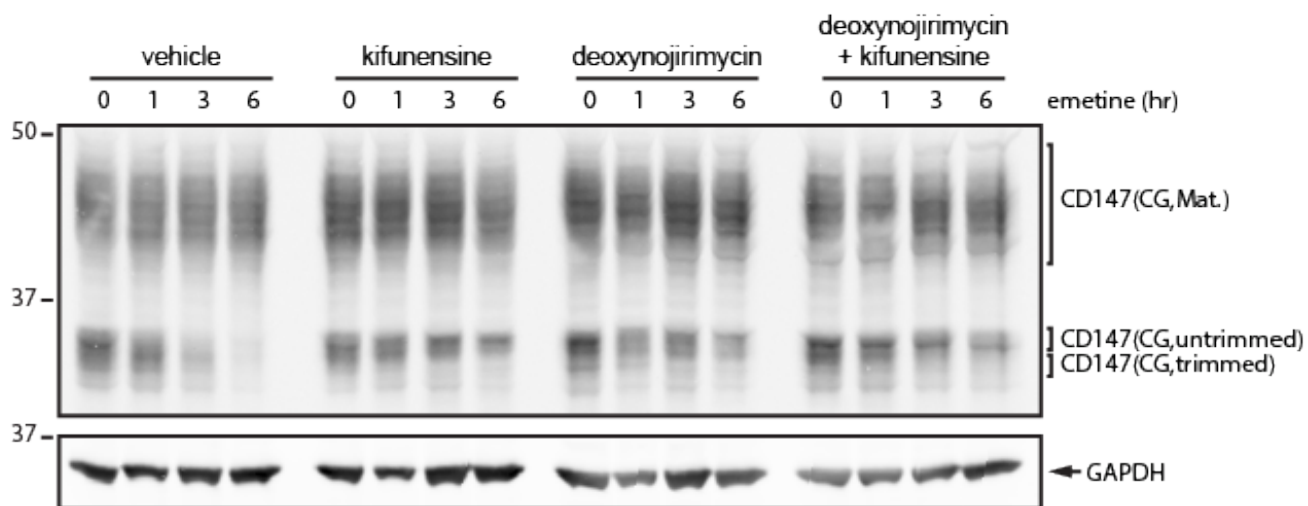


Figure 2-S3: Analysis of glucosidases and mannosidases in CD147 glycan trimming and degradation. HEK293 cells were incubated with 75  $\mu$ M emetine in the presence and absence of 5  $\mu$ g/mL kifunensine and 50  $\mu$ M deoxynojirimycin as indicated. SDS lysates were separated on large format SDS-PAGE gels and analyzed by immunoblotting to visualize the different CD147 glycoforms.

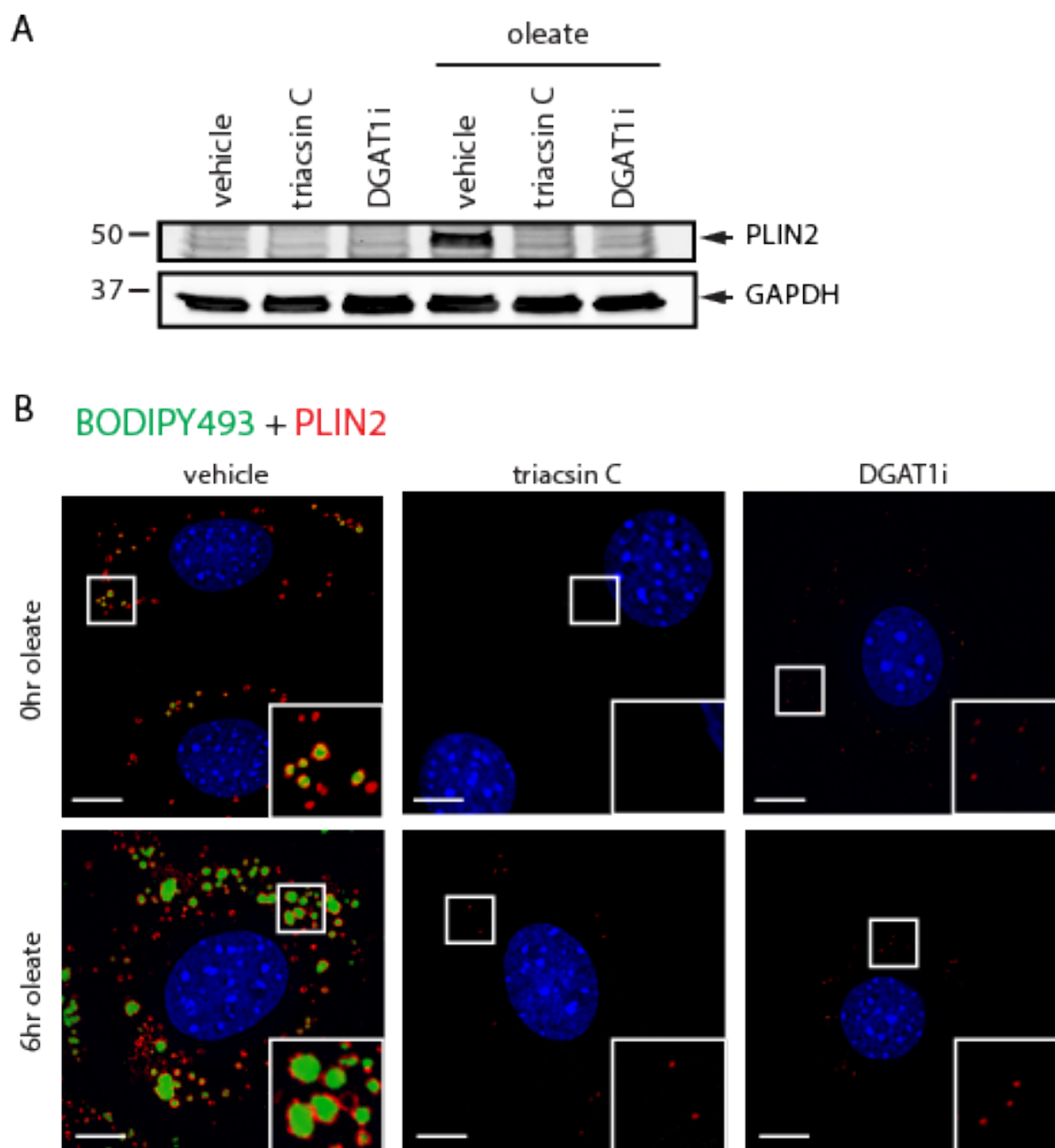


Figure 2-S4: Triacsin C and DGAT1 reduce the amount of PLIN2-positive lipid droplets. (A) DGAT2<sup>-/-</sup> MEFs were pretreated with 1  $\mu$ g/mL triacsin C or 20  $\mu$ M DGAT1i for 3 hr and then incubated with 200  $\mu$ M oleate for 0 hr or 6 hr as indicated. Cells were lysed in 1% SDS and PLIN2 levels were analyzed by immunoblotting. (B) Cells were treated as in panel A and immunofluorescence microscopy employed to visualize PLIN2 (red), LDs (green), and nuclei (blue). Scale bar = 10  $\mu$ m.

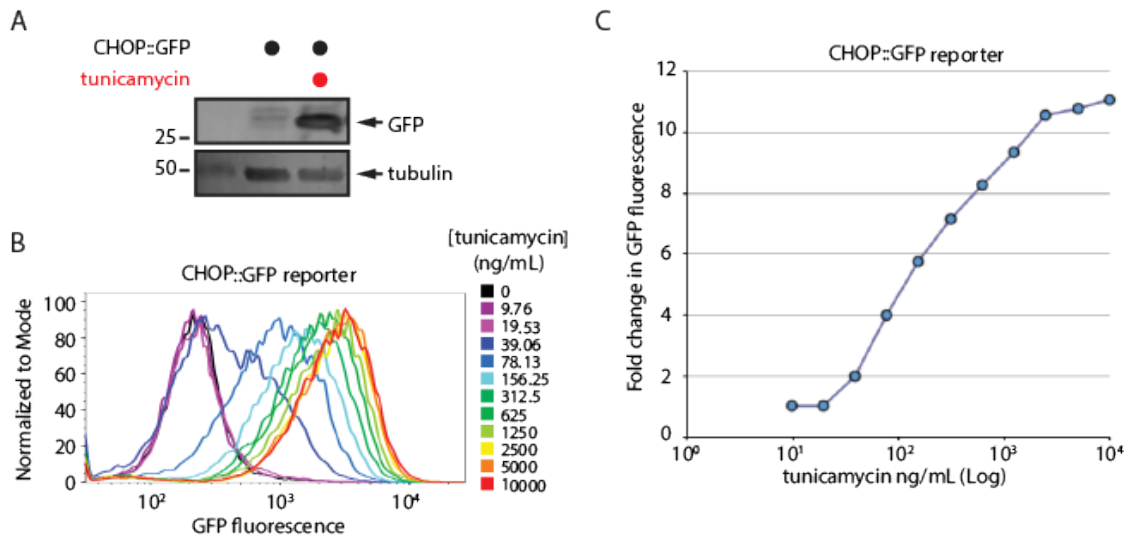


Figure 2-S5: Characterization of a CHOP::GFP reporter cell line. (A) Untransfected HEK293 cells or HEK293 cells stably expressing the CHOP::GFP reporter plasmid were incubated in the presence or absence of 5  $\mu\text{g}/\text{mL}$  tunicamycin as indicated. GFP levels were analyzed by immunoblotting. (B) HEK293 cells stably expressing a CHOP::GFP construct were treated with increasing concentrations of tunicamycin. GFP levels were measured using flow cytometry and are represented as a histogram normalized to the mode. (C) The fold change in GFP fluorescence levels relative to time 0 hr from cells treated as in panel B is shown.



### **Chapter Three: A proximity labeling strategy provides insights into the composition and dynamics of lipid droplet proteomes**

Contents in this chapter are modified with permission from the previously published research article:

Bersuker K, Peterson CWH, To M, Sahl SJ, Savikhin V, Grossman EA, Nomura DK, Olzmann JA. A Proximity Labeling Strategy Provides Insights into the Composition and Dynamics of Lipid Droplet Proteomes. *Dev Cell*. 2018 Jan 8;44(1):97-112.e7.

## Introduction

Lipid droplets (LDs) are conserved neutral lipid (e.g., triacylglycerol and sterols esters) storage organelles that are present in nearly all cells<sup>125-127</sup>. Although the mechanisms of LD biogenesis are not well understood, emerging data suggest that LDs are formed *de novo* through deposition of neutral lipids between the leaflets of the ER, followed by vectorial budding of the nascent LD from the outer leaflet of the ER into the cytoplasm<sup>212</sup>. The mature LD contains a neutral lipid core encircled by a phospholipid monolayer decorated with integral and peripheral proteins that regulate LD functions<sup>34</sup>. LDs are lipid storage depots that can be rapidly accessed to provide cells with fatty acids for energy production, membrane biosynthesis, and lipid signaling<sup>125-127</sup>. In addition, LDs prevent lipotoxicity caused by free fatty acids and their flux into toxic lipid species<sup>47,128,213,214</sup>. The accumulation of LDs in non-adipose tissues is a pathological feature of metabolic disease such as obesity, diabetes, and atherosclerosis<sup>215,216</sup>. A role for LDs in the pathogenesis of metabolic diseases is further supported by the identification of mutations in LD-associated proteins that cause familial lipodystrophies and neutral lipid storage diseases<sup>215,216</sup>.

The hydrophobic core of LDs is an energetically unfavorable environment for hydrophilic protein domains. Thus, proteins are absent from the LD core and are embedded within the bounding phospholipid monolayer through a variety of structural motifs, including hairpin-forming hydrophobic elements, short hydrophobic regions, amphipathic helices, and lipid anchors<sup>34</sup>. Proteins also associate peripherally with LDs by binding to proteins integrated into the LD membrane. LD functions are intrinsically connected to the composition of the LD proteome. For example, LD-associated acyltransferases such as GPAT4, AGPAT3, and DGAT2 regulate TAG synthesis and LD expansion during LD biogenesis<sup>217</sup>. Conversely, LD-associated lipases mediate TAG catabolism and LD degradation<sup>218</sup>. LD metabolism is also controlled by recruitment of proteins to LDs in response to changes in cellular metabolism; e.g., CCT1<sup>36</sup>, GPAT4<sup>217</sup>, and hormone-sensitive lipase (HSL)<sup>219</sup>. Defining a comprehensive inventory of LD proteins, their functions, and their mechanisms of regulation is paramount for understanding the role of LDs in health and disease. Numerous studies have attempted to catalog the LD proteome through proteomic analysis of LD-enriched, biochemically isolated buoyant fractions. The interpretation of these studies has been complicated by the presence of proteins from co-fractionating organelles and/or membrane fragments. Common false positives include ER and mitochondrial proteins whose spatial segregation from LDs (e.g., proteins in the ER lumen) or membrane-integrated motifs (e.g., polytopic proteins integrated into ER and mitochondrial bilayer membranes) prevent them from accessing the LD monolayer<sup>34</sup>. Thus, accurately defining the LD proteome and its mechanisms of regulation remains an outstanding challenge.

The limitations associated with proteomic analysis of biochemically purified organelles spurred the development of proximity labeling strategies to define organelle proteomes<sup>220,221</sup>. Engineered ascorbate peroxidase (APEX), and its more active version, APEX2<sup>222</sup>, have been used to map the proteomes of the mitochondrial matrix<sup>223</sup>, intermembrane space<sup>224</sup>, and outer membrane<sup>225</sup>, as well as the proteomes of the ER outer membrane<sup>225</sup>, the autophagosome lumen<sup>226</sup>, and the primary cilium<sup>227</sup>. In the presence of the APEX2 substrate biotin-phenol (also known as biotin-tyramide), a brief pulse of hydrogen peroxide (H<sub>2</sub>O<sub>2</sub>, <1 min) results in the APEX2-

catalyzed generation of short-lived, membrane-impermeable biotin-phenoxyl radicals that form covalent adducts with electron-rich amino acids in proteins located within a 10–20 nm radius<sup>224,228</sup>. The irreversible conjugation of biotin enables the capture of labeled proteins for proteomic analysis. Labeling of proteins is performed in intact, living cells, thus preserving organelle architecture and minimizing post-lysis artifacts.

In this study, APEX2 targeted to LDs in two cell types labeled the vast majority of previously validated LD proteins and identified proteins whose localization on LDs was not previously established. Importantly, the high-confidence LD proteomes generated using LD-targeted APEX2 are free of common contaminating proteins. We further demonstrate the utility of LD-targeted APEX2 to examine LD proteome dynamics and discover that the composition of the LD proteome is in part regulated by ER-associated degradation (ERAD), a process that mediates ubiquitin-dependent protein quality and quantity control in the early secretory pathway<sup>106,229,230</sup>. These data provide an important LD proteomics resource (<http://dropletproteome.org>) and reveal a mechanism that regulates the composition of LD proteomes.

## Results

### Generation and characterization of LD-targeted APEX2

To target APEX2 to the LD membrane, we generated osteosarcoma (U2OS) Flp-In cell lines that inducibly express V5-tagged APEX2 genetically fused to the C terminus of the perilipin family member PLIN2 (PLIN2-APEX2) and a mutant version of the lipase ATGL (ATGL\*-APEX2) containing an inactivating S47A mutation that prevents ATGL-mediated lipolysis of LDs (Figure 3-1A). Cells expressing a cytosolic version of APEX2 (Cyto-APEX2) were also generated to control for non-specific labeling of cytosolic proteins by LD-targeted APEX2. Incubation of cells with doxycycline induced expression of the APEX2 fusions and the addition of biotin-phenol/H<sub>2</sub>O<sub>2</sub> increased the levels of biotinylated proteins (Figure 3-1B), indicating that the APEX2 fusion proteins are catalytically active.

To confirm that the LD-targeted APEX2 proteins are recruited to LDs, the localization of V5-APEX2 fusions was determined after induction of LD biogenesis with oleate. Both PLIN2-APEX2 and ATGL\*-APEX2 decorated the periphery of LDs labeled by the fluorescent fatty acid BODIPY-C12-568, indicating that APEX2 is recruited to the LD monolayer (Figure 3-1C). In contrast, Cyto-APEX2 was diffusely distributed throughout the cytoplasm and nucleoplasm (Figure 3-1C). Fluorescently labeled streptavidin stained the periphery of LDs in PLIN2-APEX2 and ATGL\*-APEX2 cells treated with biotin-phenol/H<sub>2</sub>O<sub>2</sub> (Figure 3-1D), but not in the Cyto-APEX2 cells, indicating that LD-targeted APEX2 biotinylates proteins on the LD surface. To further verify that LD-targeted APEX2 biotinylates proteins on LDs, we analyzed the distribution of biotinylated proteins in LD-enriched buoyant fractions isolated by sucrose gradient centrifugation (Figures 3-1E - 3-1G). PLIN2-APEX2 and ATGL\*-APEX2 were not exclusively present in the buoyant fraction and, like Cyto-APEX2, biotinylated proteins in the cytosolic fractions (Figures 3-1E - 3-1G, fractions 2–5), and, to a lesser extent, proteins in the membrane fraction (Figures 3-1E – 3-1G, fraction P). Importantly, biotinylated proteins were only observed in LD-enriched buoyant fractions isolated from the

PLIN2-APEX2 and ATGL\*-APEX2 cells (Figures 3-1E – 3-1G, fraction BF). Together, these results demonstrate that LD-targeted APEX2 biotinylates proteins on LDs.

### **Identification of a high-confidence LD proteome**

Non-specific labeling of cytosolic proteins has been reported in previous proteomics studies of organelles in which APEX2 was exposed to the cytosol<sup>224,225</sup>. This limitation can be addressed by using ratiometric stable isotope labeling with amino acids in cell culture (SILAC) to subtract the cytosolic background<sup>224,225</sup>. However, this approach selects against proteins that localize to more than one cellular compartment. Given that several known LD proteins localize to LDs/ER (e.g., UBXD8, GPAT4, and AUP1) and LDs/cytosol (e.g., VCP, UBE2G2, and HSL), we chose to use subcellular fractionation in lieu of SILAC to separate the biotinylated proteins on LDs from those present in the cytosol and on other organelles (Figure 3-2A). Liquid chromatography-tandem mass spectrometry was used to determine the identity and abundance (i.e., normalized total spectral counts) of proteins isolated by affinity purification and of proteins in the total buoyant fraction. The proteins identified in the PLIN2-APEX2 samples (152 proteins) and ATGL\*-APEX2 samples (192 proteins) represented a small subset of the proteins identified in the total buoyant fraction (1,227 proteins) (Figures 3-2B and 3-2C), but the spectral counts from these two samples were highly correlated ( $R^2 = 0.76991$ ) (Figure 3-2D). Fifty-two proteins were also identified in the Cyto-APEX2 samples, accounting for non-specific labeling by LD-targeted APEX2 (Figure 3-2B).

The buoyant fraction contained 44 proteins that were previously observed to localize to LDs by microscopy analyses of endogenous or tagged proteins (Figure 3-2B), all of which were labeled by at least one of the LD-targeted APEX2 proteins (Figure 3-2B). The LD protein SPG20<sup>231</sup> was labeled by APEX2, but was not identified in the buoyant fraction), suggesting that LD-targeted APEX2 can identify low-abundance LD proteins. The relative abundance of biotinylated proteins isolated from the APEX2 lines was used to compute a confidence score (CS) for each identified protein. The CS accounts for protein abundance, identification in replicate experiments, labeling by both LD-targeted APEX2 proteins, and specificity (i.e., absence or low abundance in Cyto-APEX2 control samples) (see the STAR Methods for details). To define a high-confidence LD proteome, we set a threshold CS value that included >85% of previously validated LD proteins, yielding a high-confidence proteome consisting of 153 proteins (Figure 3-2B). The abundant proteins in the buoyant fraction that were not labeled by PLIN2-APEX2 or ATGL\*-APEX2 included many common contaminants identified in previous proteomic studies, including ER luminal proteins (disulfide isomerases PDIA1, PDIA3, and PDIA6), chaperones (GRP78, GRP94, and SerpinA1), and polytopic ER membrane proteins (CALR, CANX, and VAPA) (Figures 3-2E – 3-2G). Thus, the proximity labeling approach discriminates between proteins on LDs and contaminating proteins in the buoyant fraction.

Gene ontology-term analysis of high-confidence LD proteins showed enrichment of pathways that control TAG metabolism, lipid biosynthesis, and sterol biosynthesis (Figure 3-2H). Other pathways included protein and vesicle-mediated transport, small GTPase signaling, oxidation-reduction processes, and membrane organization (Figure 3-2H). To visualize functional relationships between LD proteins, high-confidence proteins were grouped into modules, and physical interactions between proteins were retrieved from the Bio-GRID database (Figure 3-3).

The high-confidence LD proteome contained a group of previously validated LD regulatory scaffold proteins and TAG metabolism enzymes, including the perilipin family members (PLIN2, PLIN3, and PLIN4), acyl-coenzyme A (acyl-CoA) synthetases (ACSL3 and ACSL4), glycerol-3-phosphate acyltransferases (GPAT3 and GPAT4), lipases (PNPLA2, PNPLA3, and LIPE), and the PNPLA2 lipase regulator (ABHD5, also known as CGI-58). Another group within the metabolism-related module contained several enzymes from the cholesterol biosynthesis (SQLE, LSS, and NSDHL) and retinol metabolism (RDH10 and RDH11) pathways. Proteins that function in oxidation-reduction reactions (AIFM2, CYB5R3, HSDL1, and DHRS1) were also identified, the majority of which have not been validated as LD proteins. Surprisingly, half of all human Rab GTPases were present within the vesicular trafficking module, several of which (RAB1A, RAB7A, RAB8A, and RAB11B) were previously demonstrated to have functional roles on LDs. This result suggests that the large number of RAB GTPases identified in previous LD proteomics studies<sup>139,232,233</sup> are present on LDs. Another prominent module has functions related to the ubiquitin system and several of these proteins (FAF2, UBXN4, AUP1, UBE2G2, and VCP) form protein complexes on the ER membrane that function in degrading luminal and membrane ER proteins through the ERAD pathway<sup>175,230</sup>. The identification of UBE2G2 and VCP, which associate with LDs by binding to their membrane-integrated adaptors AUP1<sup>142,143</sup>, and UBXD8<sup>144,146</sup>, respectively, demonstrates that LD-targeted APEX2 can identify peripherally associated LD proteins.

### **An integrated U2OS and Huh7 high-confidence LD proteome**

LDs in different cell types have unique attributes (e.g., differences in size, regulatory mechanisms, or lipid composition) and express distinct LD proteins that specify these features. Liver is a metabolic organ that mediates the packaging and secretion of very low density lipoproteins, *de novo* lipogenesis, and recycling of lipoprotein remnants<sup>234</sup>. The aberrant accumulation of LDs in the liver, or hepatic steatosis, is a feature of many metabolic diseases and a pathogenic hallmark of infection by the hepatitis C virus<sup>234</sup>. Thus, the differences between U2OS and liver cells, as well as the physiological importance of LDs in liver function, led us to investigate the LD proteome in a liver-derived cell model.

To map the liver LD proteome, we introduced the APEX2 proximity biotinylation system into the Huh7 human hepatocellular carcinoma cell line (Figures 3-S1A and 3-S1B), which has been extensively utilized to study hepatocyte function. LDs were more abundant in Huh7 than in U2OS cells, and exhibited a larger heterogeneity in size (Figures 3-1C, 3-S1C, and 3-S1D). Similarly to LD-targeted APEX2 in U2OS cells, PLIN2-APEX2 and ATGL\*-APEX2, but not Cyto-APEX2, localized to LDs and biotinylated proteins in buoyant fractions (Figures 3-S1C–3-S1G). Proteomic analyses identified 197 biotinylated proteins purified from PLIN2-APEX2 and 124 biotinylated proteins purified from ATGL\*-APEX2 cells among 624 total proteins in the Huh7 buoyant fraction (Figures 3-S2A – 3-S2F). Despite the lower number of high-confidence LD proteins identified in Huh7 cells, all 37 previously validated proteins present in the Huh7 buoyant fraction were labeled by at least one version of LD-targeted APEX2 (Figures 3-S3A and 3-S3B). In addition, several validated LD proteins (e.g., CIDEB and MGLL) that were not identified in the buoyant fraction were labeled by LD-targeted APEX2 (Figures 3-S3A and 3-S3B), further supporting the ability of LD-targeted APEX2

to identify low-abundance LD proteins, while avoiding abundant contaminants (e.g., CALR, CANX, and HSPA5) (Figures 3-S2D – 3-S2F and 3-S3C).

When comparing the high-confidence LD proteomes from U2OS and Huh7 cells, we found 63 shared high-confidence LD proteins (Figures 3-S4A and 3-S4B). These proteins included 9 of the 11 new proteins validated in U2OS cells (Figure 3-4). CIDEB, which belongs to a family of CIDE proteins that mediate LD fusion<sup>235</sup>, was only identified in Huh7 cells, consistent with the larger LDs in this cell line. The absence of other CIDE proteins (CIDEA and CIDEF) indicates that CIDEB is the dominant member of this protein family in Huh7 cells and is consistent with the expression pattern of CIDE family genes in mouse tissues (Figure 3-S4C). Interestingly, we identified SQSTM1 (also known as p62) as a Huh7-specific LD protein. p62 mediates selective autophagy by binding ubiquitin-conjugated cargo through its ubiquitin-associated (UBA) domain and autophagosome membranes conjugated to LC3 through its LC3-interacting region (LIR) motifs<sup>81</sup>, thus physically linking cargo to autophagic machinery. Since LDs in Huh7 cells and mouse liver are degraded by a selective autophagy pathway known as lipophagy<sup>93,236</sup>, our data raise the possibility that p62 may be an adapter that targets LDs for degradation by lipophagy.

#### **p62 is required for successful lipophagy in hepatocytes**

To further explore the requirement of p62 in hepatic lipophagy, we initially confirmed the reliance of Huh7 cells on increased lipophagic induction as a response to prolonged starvation, as has previously been reported<sup>236</sup>. Indeed, a significant reduction in both number and size of LDs was observed by fluorescence microscopy following a 48-h serum starve, and this response was blocked by co-treatment with the upstream autophagy inhibitor 3-methyladenine (3-MA) indicating that the reduction in LDs is due to increased lipophagy (Figure 3-5A – 3-5C). To test whether lipophagy is mediated by p62, we established clonal populations in which the CRISPR/Cas9 method was utilized to remove *SQSTM1* (the gene encoding for p62) from the genome and subjected these cells to similar prolonged starvation. We found that in the absence of p62, cells were no longer able to upregulate LD turnover in response to serum starvation (Figure 3-5D – Figure 3-5F). Importantly, when the p62 variant mCherry-p62-HA was reintroduced to cells, they once again regained the capacity to induce a lipophagic response in the presence of prolonged starvation, as evidenced by a similar decrease in LD number and size as was seen in wild type cells (Figure 3-5G – 3-5I). Together these results confirm the role of p62 as a UBA-LIR containing adapter protein required for selective LD autophagy in hepatocytes.

## **Discussion**

LDs are regulators of lipid and energy metabolism that are central to the pathogenesis of human metabolic diseases. Attempts to define the LD proteome through proteomic analysis of biochemically isolated buoyant fractions have been plagued by the presence of contaminating proteins. Recent studies combined fractionation of LDs with protein correlation profiling to yield more specific LD proteomes in *Drosophila* S2 cells<sup>237</sup> and yeast<sup>238</sup>, but potentially failed to detect proteins that localize to multiple cellular compartments. Refined fractionation approaches have further increased the purity of LD preparations, but have been unable to completely separate LDs from other associated organelles<sup>239</sup>. Thus, the inability to accurately define LD proteomes

has remained an obstacle to understanding the role of LD-associated proteins in LD biology. In this study, we implemented a proximity labeling strategy to generate high-confidence LD proteomic maps in two human cell lines and established the utility of this approach to study LD proteome dynamics.

Our results indicate that proximity labeling proteomics identifies a complete and specific LD proteome. LD-targeted APEX2 labeled all proteins in the total buoyant fraction that were previously shown to localize to LDs, and identified previously validated LD proteins (e.g., SPG20, CIDEB, and MGLL) that were not detected in the LD-enriched buoyant fraction. The method also identified a significant number of new proteins on LDs, many of which were identified in both U2OS and Huh7 cells. These proteins may constitute functionally important LD machinery and therefore warrant further investigation. Importantly, LD-targeted APEX2 effectively excluded abundant non-LD proteins that are frequently identified in LD proteomic studies and comprise the vast majority of proteins present in buoyant fractions.

Some limitations have been ascribed to proximity labeling approaches. For example, proteins that are buried within macromolecular complexes may not be accessible for labeling. While this may be a limitation in our study, LD-targeted APEX2 fusions labeled all known LD proteins in the buoyant fraction, suggesting that APEX2 labeling achieves high coverage of the LD proteome. Recent APEX2 studies using ratiometric SILAC to subtract cytosolic background labeling reported that some proteins that localize to more than one cellular compartment may be filtered out, contributing to the incomplete coverage of organelle proteomes: 53% coverage of the outer mitochondrial membrane proteome<sup>225</sup>, 44% coverage of the outer ER membrane proteome<sup>225</sup>, and 67% coverage of the mitochondrial intermembrane space proteome<sup>224</sup>. In light of this limitation, we used a subcellular fractionation step to isolate LD proteins from labeled cytosolic proteins. Although it remains possible that some peripherally associated LD proteins were lost during the fractionation procedure, we successfully identified peripheral proteins that are known to have both LD and cytosolic localization (e.g., VCP<sup>146,240,241</sup>, HSL<sup>219,242</sup>, and UBE2G2<sup>142,143</sup>). Together, these findings establish the utility of proximity labeling in investigating LD proteome dynamics and provide a foundation for future studies that will investigate how the LD proteome is remodeled in response to metabolic signals in diverse models of cellular metabolism.

## Materials and methods

### Cell Culture

U2OS, Huh7, and HEK293 cells were cultured in DMEM containing 4.5 g/L glucose and L-glutamine (Corning) supplemented with 10% fetal bovine serum (FBS, Thermo Fisher Scientific and Gemini Bio Products) at 37°C with 5% CO<sub>2</sub>.

Huh7 TetR expression lines were generated by infection with pLenti CMV TetR Blast virus (716-1) (Addgene plasmid #17492) and treatment with 8 µg/mL polybrene followed by selection in media containing 4 µg/mL blasticidin. Huh7 TetR cells were subsequently infected with pLenti CMV/TO Puro DEST virus (670-1) (Addgene plasmid #17293) containing V5-APEX2 fusion constructs and expressing cells were selected in media containing 2 µg/mL puromycin. Huh7 null

cell line was generated using CRISPR/Cas9 technology by transfection with pSpCas9(BB)-2A-Puro (PX459)<sup>243</sup>, a gift from Feng Zhang (Addgene plasmid # 48139), followed by selection in 1 ug/mL puromycin and isolation of individual clones by limited dilution.

### **Plasmids**

ATGL\*-V5-APEX2 and PLIN2-V5-APEX2 were generated by insertion of ATGL\* and PLIN2 between the NotI and BamHI sites in pcDNA3.1+ followed by insertion of V5-APEX2 between downstream BamHI and XhoI sites. V5-APEX2 was amplified by PCR from Mito-APEX2, a gift from Dr. Alice Ting (Stanford University). The resulting V5-APEX2 fusion constructs were cloned into pcDNA5/FRT/TO using polymerase incomplete primer extension (PIPE)<sup>244</sup>. Lentiviral constructs were generated by insertion of V5-APEX2 constructs between the NotI and XhoI sites in pLenti CMV/TO Puro DEST.

CRISPR guide RNA (sgRNA) sequence targeting p62 was designed using the online-available CRISPR design tool developed by the Zhang laboratory (<http://crispr.mit.edu/>). The seed sequence preceding the protospacer motif was: p62 guide 1, 5' CACCGACCGTGAAGGCCTACCTTCT 3'. Nucleotides in italics show the overhangs necessary for incorporation into the BbsI restriction site of PX459 vector.

Reagents used in this study include: doxycycline (Sigma), emetine (Sigma), oleic acid (Sigma), CB5083<sup>247</sup> (Cleave Biosciences), MLN-7243 (AOBIOUS, Inc.), biotin-phenol (Iris Biotech GmbH), puromycin (Invitrogen), hygromycin (Invitrogen), and MG132 (Enzo Life Sciences).

### **Immunoblotting**

Cells were washed in PBS, lysed in 1% SDS, sonicated for 10-30 sec, and boiled for 5 min at 100°C. Protein concentrations were determined using the bicinchoninic acid (BCA) protein assay (Thermo Fisher Scientific), and equal amounts of protein by weight were combined with 1X Laemmli buffer, separated on 4-20% polyacrylamide gradient gels (Bio-Rad Laboratories, Inc.), and transferred onto low fluorescence PVDF or nitrocellulose membranes (Bio-Rad Laboratories, Inc.). Membranes were washed in PBS with 0.1% Tween-20 (PBST) and blocked in PBST containing 5% (wt/vol) dried milk for 30 min. Membranes were incubated for 2-24 hr in PBST containing 5% bovine serum albumin (BSA) (Sigma Aldrich) and primary antibodies. After washing with PBST, membranes were incubated with fluorescent secondary antibodies diluted in 5% BSA/PBST at room temperature for 30-60 min. All immunoblots were imaged on a LI-COR imager (LI-COR Biosciences).

The following blotting reagents and antibodies were used: anti-V5 tag (Invitrogen), anti-Plin2 (Abgent), anti- $\alpha$ -tubulin (Cell Signaling Technology, Inc.), anti-GAPDH (EMD Millipore), IRDye800 conjugated streptavidin (LI-COR Biosciences), anti-rabbit IRDye800 conjugated secondary (LI-COR Biosciences), anti-mouse Alexa Fluor 680 conjugated secondary (Invitrogen).

### **Fluorescence Microscopy**

For fluorescence microscopy of fixed cells, cells grown on coverslips were incubated in the presence of 200  $\mu$ M oleate for 24 hr. Cells were washed 3X in PBS, fixed for 15 min in PBS



containing 4% (wt/vol) paraformaldehyde, and washed 3X with PBS. Cells were permeabilized and blocked for 15 min with 1% BSA/PBS containing 0.01% digitonin (prior to staining LDs) or for 5 min with 1% BSA/PBS containing 0.1% Triton-X100 (prior to staining ER) followed by blocking in 1% BSA/PBS for 15 min. Cells were washed 3X with 1% BSA/PBS and incubated in primary antibody for 2 hr at RT. Cells were washed 3X and incubated for 1 hr in blocking solution containing anti-rabbit or anti-mouse secondary antibodies conjugated to Alexa Fluor 488 or 594, or in solution containing streptavidin-568 (Thermo Fisher Scientific). Droplets were stained with 10  $\mu\text{g}/\text{ml}$  BODIPY 493/503 (Thermo Fisher Scientific) that was added to the secondary antibody solution. Cells were subsequently washed 3X and mounted using Fluoromount G (Southern Biotech).

For live-cell microscopy, cells were grown in 4-well or 8-well Lab-Tek II Chambered Coverglass (Thermo Fisher Scientific). To image LDs, cells were incubated for 24 hr with 200  $\mu\text{M}$  oleate and 1  $\mu\text{M}$  Bodipy-C12-568 (Thermo Fisher Scientific) or incubated with 100  $\mu\text{M}$  AUTODOT (Abgent). Cells were imaged using a Deltavision Elite widefield epifluorescence deconvolution microscope (GE Healthcare) equipped with a 60 $\times$  oil immersion objective (Olympus) using DAPI, FITC, Tx-Red and Cy5 filters. For live-cell microscopy, cells were imaged in an enclosure heated to 37 $^{\circ}\text{C}$  and exposed to continuous perfusion of a gas mixture containing 5%  $\text{CO}_2$ , 21%  $\text{O}_2$  and 74%  $\text{N}_2$  (BioBlend, Praxair). Images were analyzed using ImageJ (<http://imagej.nih.gov/ij/>) and line scan intensities were generated using softWoRx (GE Healthcare Life Sciences).

### **LD Proteome Labeling and LD Isolation**

For each APEX2 cell line, 18 15-cm plates of cells were treated with 5-10  $\text{ng}/\mu\text{L}$  doxycycline for 48 h followed by incubation in 200  $\mu\text{M}$  oleate and 7  $\mu\text{M}$  Hemin for 24 hr. Cells were subsequently treated with 500  $\mu\text{M}$  biotin-phenol for 45 min. Prior to harvesting, biotinylation of proteins was catalyzed by addition of 1  $\mu\text{M}$   $\text{H}_2\text{O}_2$  for 1 min, and the reaction was quenched by washing cells 2X with PBS containing 10 mM sodium ascorbate and 5 mM Trolox. Cells were harvested in PBS, centrifuged for 10 min at 500  $\times g$ , and cell pellets were incubated for 10 min in cold hypotonic lysis medium (HLM, 20 mM Tris-HCl pH 7.4 and 1 mM EDTA) containing Mini EDTA-free Protease Inhibitor Cocktail (Sigma-Aldrich). Cells were dounced 80X strokes in a 7 mL dounce and lysates were centrifuged at 1000  $\times g$  for 10 min. The supernatant was subsequently transferred to Ultra-Clear ultracentrifuge tubes (Beckman-Coulter), diluted to a final concentration of 20% sucrose/HLM, and overlaid by 4 mL of 5% sucrose/HLM followed by 4 mL of HLM. Overlaid samples were centrifuged for 30 min at 15,000  $\times g$  in an ultracentrifuge using an SW41 swinging bucket rotor (Beckman-Coulter). Buoyant fractions were isolated using a tube cutter (Beckman-Coulter), additional fractions were pipetted from the top of the sucrose gradient in 1 mL increments and pellets were resuspended in 1 mL HLM. 100  $\mu\text{L}$  of 10% SDS was added to each fraction, yielding a final concentration of 1% SDS. Samples were then sonicated for 15 sec. Buoyant fractions were additionally incubated at 37 $^{\circ}\text{C}$  for 1 hr with sonication every 20 min, followed by a final incubation for 10 min at 65 $^{\circ}\text{C}$ .

### **Proteomic Analysis of LD Proteins**

For isolation of biotinylated proteins from U2OS cells, buoyant fractions containing 1% SDS were diluted with PBS/0.1% Tween-20 (PBST) to a final concentration of 0.1% SDS. 0.4 mL of

streptavidin-conjugated agarose bead slurry (Thermo Fisher Scientific) was washed 3X with PBST and added to the diluted buoyant fractions for 4 hr at RT with constant mixing. Beads were centrifuged at 2000 × g and washed 5X with PBST, followed by 3X washes with PBS and 3X washes with 50 mM ammonium bicarbonate. The beads were resuspended in one bead volume of 50 mM ammonium bicarbonate containing 0.02% Rapigest (Waters) (w/v), heated at 65°C for 15 min and bound proteins were digested O/N at 37°C with 1 µg mass spectrometry grade trypsin (Promega). After protein digestion, beads were removed and the supernatant was acidified to pH < 2 by addition of 500 mM HCl and incubation at RT for 45 min. All precipitated material was removed by centrifugation at 20,000 × g for 15 min. Peptides were dried down to a final volume of 15-20 µl in a vacuum centrifuge.

For isolation of biotinylated proteins from Huh7 cells, an in-gel digestion protocol was used to minimize contamination of samples with streptavidin from the beads. Buoyant fractions containing 1% SDS were diluted with HLM buffer to a final concentration of 0.1% SDS. 0.2 mL of streptavidin-conjugated agarose bead slurry (Thermo Fisher Scientific) was washed 3X with PBST and 1X with HLM buffer and added to the diluted buoyant fractions for 4 hr at RT with constant mixing. Beads were centrifuged at 2000 × g and washed 5X with PBST, followed by 3X washes with PBS. Proteins were eluted with 2% SDS + 3 mM biotin by incubating at RT for 15 min with constant mixing followed by heating at 95°C for 15 min. The eluted proteins were mixed with 1X Laemmli buffer and run into a mini-PROTEAN TGX 4-20% polyacrylamide gel (Bio-Rad), and proteins were digested in-gel overnight with 0.5 µg trypsin in 5% acetonitrile/5 mM ammonium bicarbonate. Digested peptides were extracted by addition of 5% formic acid in acetonitrile and incubation at 37°C for 15 min with constant agitation. The resulting supernatant was dried down to a final volume of 15-20 µL in a vacuum centrifuge.

Total proteins from U2OS and Huh7 buoyant fractions were isolated by dilution of fractions to a final volume of 1% SDS and addition of trichloroacetic acid (TCA) to a final concentration of 15%. Precipitated proteins were pelleted by centrifuging at 20,000 × g for 30 min at 4°C, washed twice with cold acetone and resuspended in 0.02% Rapigest.

1 µg of peptides was analyzed by LC-MS/MS on a Thermo Scientific Q Exactive Orbitrap Mass spectrometer connected to a Proxeon Easy-nLC II HPLC (Thermo Fisher Scientific) and Proxeon nanospray source at the University of California, Davis Proteomics Core Facility. Peptide identity and MS/MS counts were determined by analyzing RAW output files in MaxQuant (Max Planck Institute of Biochemistry) using the reviewed human protein database obtained from UniProt. Variable modifications were set to include N-terminal acetylation and oxidation. The FDR was set to 1% and minimum peptide length was set to 6 amino acids. All proteomic data files are available through the PRoteomics IDentifications (PRIDE) database (Project PXD007695).

### **Bioinformatic Characterization of the LD Proteome**

A LD confidence score was calculated using the equations depicted in Figure 3-S5. This algorithm accounts for protein abundance (i.e. SAF), replication in multiple experiments with different LD-targeted APEX2 fusion proteins, and specificity (i.e. absence from Cyto-APEX2 samples). The

confidence score is equal to the sum of the SAF of a protein identified in the LD-targeted APEX2 samples (PLIN2 or ATGL\*) minus the SAF in the corresponding Cyto-APEX2 control sample, multiplied by the number of times the protein was identified in the LD-targeted APEX2 experimental replicates. Thus, proteins that are detected with high numbers of spectral counts in multiple LD-targeted APEX2 samples and are not detected in the Cyto-APEX2 sample are assigned a high LD confidence score. Proteins that have low spectral counts or have high abundance in the Cyto-APEX2 sample are assigned a low LD confidence score. The threshold value CST was manually determined to include the largest number of validated proteins while excluding likely contaminant proteins. Ultimately, the threshold is not a definitive cutoff and validated LD proteins are detected below the threshold, but with reduced likelihood.

Heatmaps were generated using Multiple Experiment Viewer Version 10.2. To represent the proteomics data on a heatmap for comparison we used a normalized SAF (NSAF) to account for the difference in protein abundance between the different samples. The NSAF was calculated by dividing the SAF by the average SAF in the sample (Figure 3-S5).

GO analysis of high confidence LD proteomes was performed using the Database for Annotation, Visualization and Integrated Discovery (DAVID) v6.8<sup>248</sup>. GO terms were then summarized, simplified, and visualized by analyzing the GO terms and the Benjamini corrected P-values using REVIGO<sup>249</sup>. GO networks were downloaded from REVIGO and the final GO networks were generated using cytoscape<sup>250</sup>.

## **QUANTIFICATION AND STATISTICAL ANALYSIS**

### **Quantification of LDs**

To quantify LD size distributions, cells were treated with 200  $\mu$ M oleate for 24 hr or treated with 200  $\mu$ M oleate for 24 hr and then starved in glucose-free DMEM (Life Technologies) supplemented with 10% FBS and 1X glutamate (Life Technologies) for 16 hr. Live cells were stained with BODIPY 493/503 and Hoechst, and >100 positions were automatically acquired in a grid pattern for each experimental condition using a 60 $\times$  objective. The resulting BODIPY 493/503 images were loaded into a custom package written in MATLAB (MathWorks) that uses a built-in algorithm to detect circular objects (LDs), a recursive segmentation algorithm to quantify nuclei number and a data analyzer to bin, normalize and compile the data of LD size distributions into histograms. All histograms were normalized by the number of nuclei to determine mean LD size distribution per cell. The MATLAB programs and supporting documentation can be found at <http://dropletproteome.org>.

### **Quantification of Immunoblotting**

All immunoblots were visualized using a LI-COR imager (LI-COR Biosciences). Band density was quantified using ImageJ software and the mean  $\pm$  SEM was determined from three independent experiments.

## Figures

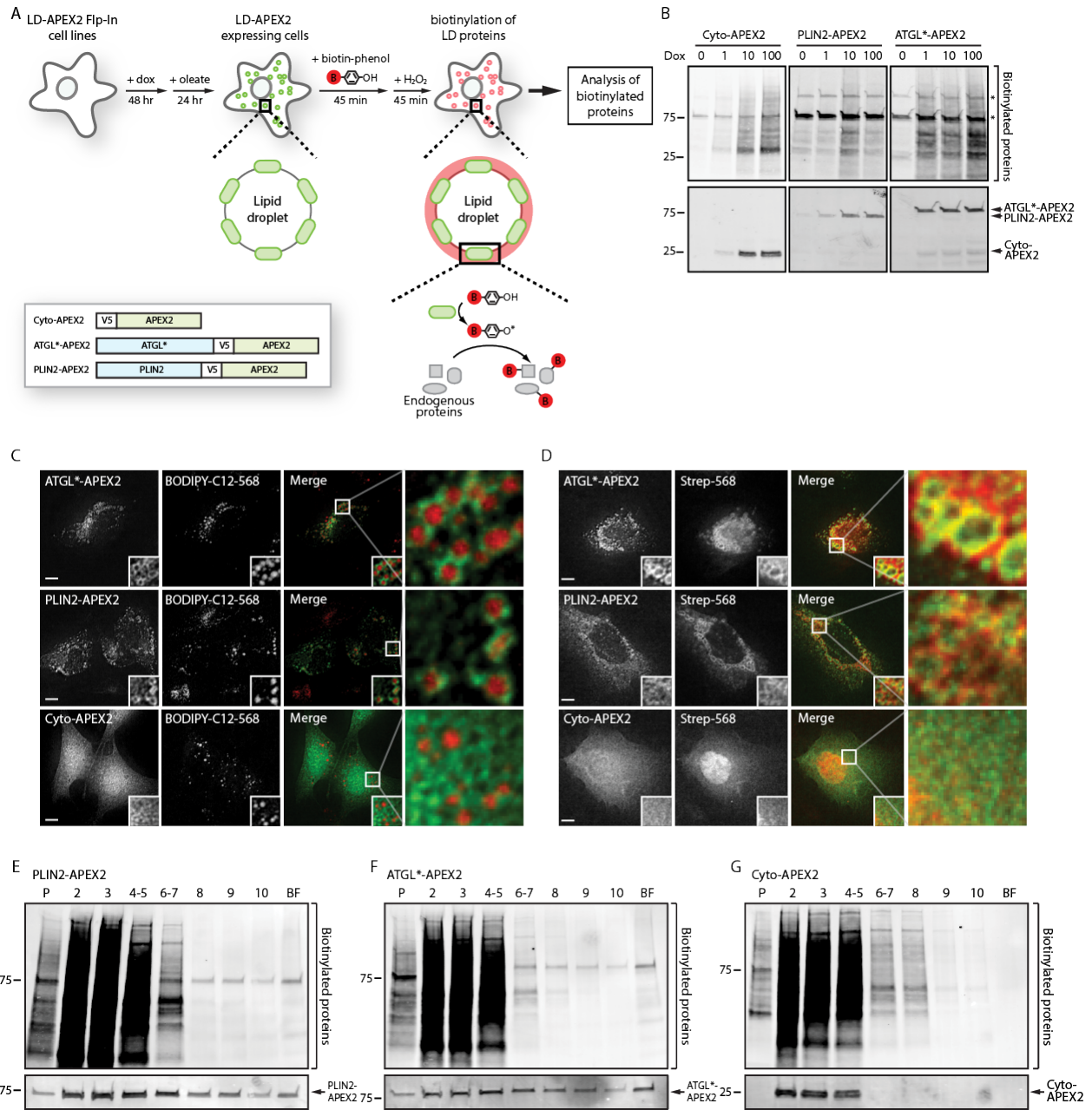


Figure 3-1: Lipid Droplet-Targeted APEX2 Biotinylates Proteins on Lipid Droplets. (A) Illustration of the proximity labeling strategy to identify lipid droplets (LD) proteins. Cells stably expressing ATGL\*-V5-APEX2, PLIN2-V5-APEX2, or Cyto-V5-APEX2 are treated with doxycycline (dox) for 48 hr to induce expression of LD-targeted or cytosolic APEX2 proteins, and then treated with oleate for 24 hr to induce formation of LDs. LD-targeted APEX2 covalently modifies proximal LD proteins with biotin upon addition of biotin-phenol and hydrogen peroxide (H<sub>2</sub>O<sub>2</sub>). Biotinylated proteins are subsequently affinity purified and identified by mass spectrometry. (B) U2OS cells stably expressing cytosolic or LD-targeted APEX2 were treated with 0–100 ng/mL dox for 48 hr and biotin-phenol/H<sub>2</sub>O<sub>2</sub>. Total proteins from lysed cells were separated by SDS-PAGE and analyzed by blotting with fluorescently labeled streptavidin and antibodies against the V5 epitope tag. (C) U2OS cells stably expressing cytosolic or LD-targeted APEX2 were treated with 200 μM oleate and 1 μM BODIPY-C12-568 for 24 hr to induce formation of BODIPY-C12-568-positive LDs (red). Cells were imaged by fluorescence microscopy and the APEX2 fusion proteins were detected using antibodies against the V5 epitope tag (green). Magnified insets show cellular regions with LDs. Scale bars represent 10 μm. (D) U2OS cells stably expressing cytosolic or LD-targeted APEX2 incubated with 200 μM oleate for 24 hr were treated with biotin-phenol/H<sub>2</sub>O<sub>2</sub> and imaged by fluorescence microscopy using fluorescent streptavidin-568 (red) and antibodies against the V5-epitope tag (green). Scale bars represent 10 μm. (E–G) Lysates from U2OS cells stably expressing LD-targeted or cytosolic APEX2 were fractionated by sucrose gradient centrifugation. Proteins in individual fractions were separated by SDS-PAGE and analyzed by blotting with fluorescent streptavidin-568 and antibodies against the V5 epitope tag.

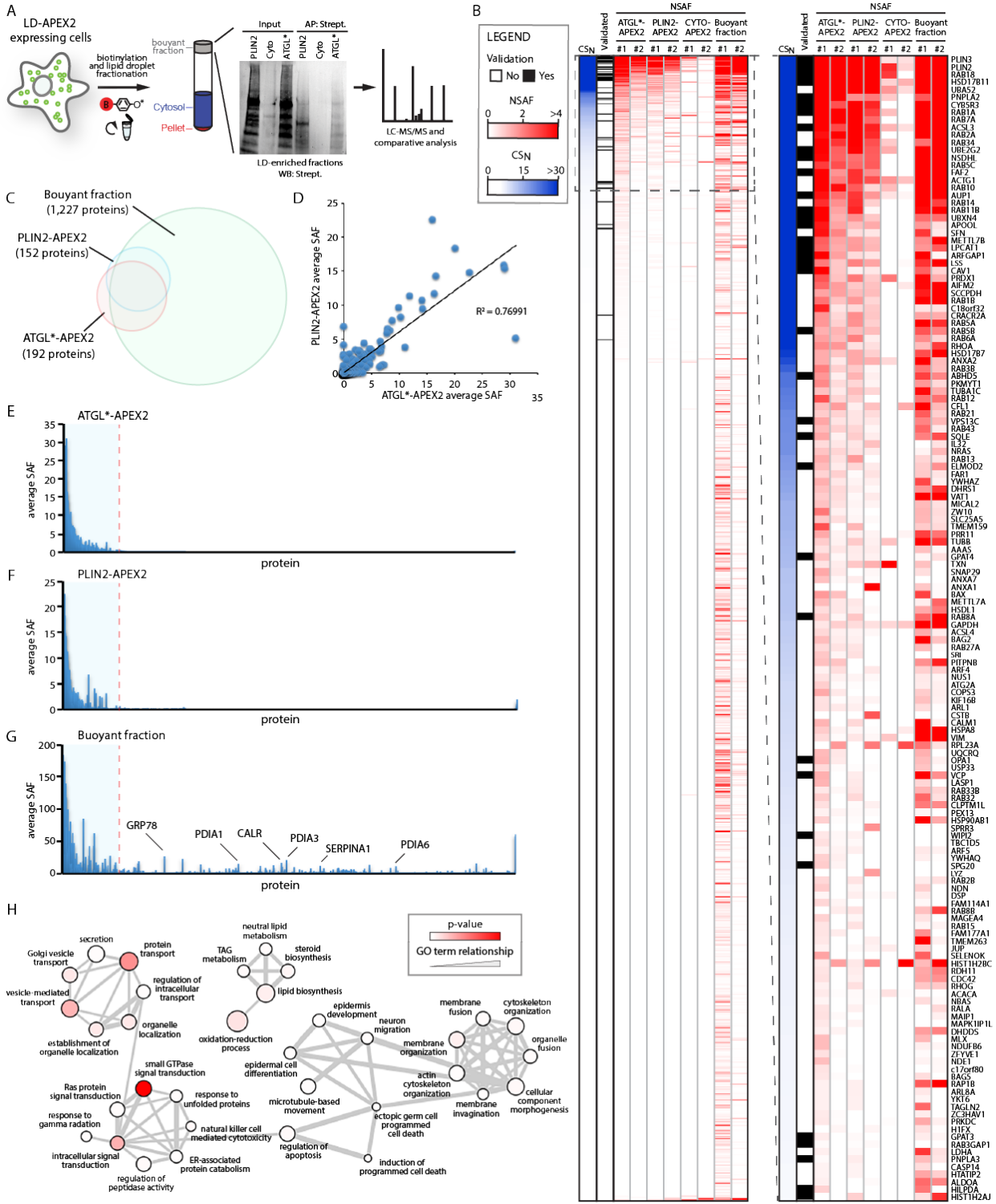


Figure 3-2: Proteomic Analysis of Biotinylated LD Proteins. (A) Illustration depicting the two-step strategy to identify biotinylated LD proteins. Following the induction of biotinylation in cells stably expressing cytosolic or LD-targeted APEX2, LD-enriched buoyant fractions are isolated by sucrose gradient centrifugation. Biotinylated proteins are then affinity purified from buoyant fractions using streptavidin-conjugated beads and identified by mass spectrometry. (B) Proteins identified in total buoyant fraction and in streptavidin affinity purifications from the indicated APEX2 cell lines were ranked by descending LD confidence score ( $CS_N$ ). Data from two independent experimental replicates for each sample are shown. The intensity of the blue color represents the  $CS_N$  value and the intensity of the red color represents the normalized spectral abundance factor (NSAF) value. The heatmap scale is linear. A black box indicates if a protein was previously validated as an LD protein by microscopy. The boxed inset shows the high-confidence LD proteins ( $CS_N > 1$ ). (C) Venn diagram illustrating the overlap between proteomes identified in the LD-targeted APEX2 cell lines and in the buoyant fraction. (D) Comparison of average spectral abundance factors (SAF) for proteins identified in the affinity purifications from ATGL\*-V5-APEX2 and PLIN2-V5-APEX2 cells. Each symbol corresponds to an LD protein identified in both cell lines. The  $R^2$  coefficient for the linear regression line is indicated. (E–G) The average SAF for proteins identified in the affinity purifications from the ATGL\*-V5-APEX2 (E) or PLIN2-V5-APEX2 (F) cells or in the total buoyant fractions isolated from parental cells (G). (H) Selected enriched gene ontology (GO)-term categories for high-confidence LD proteins.



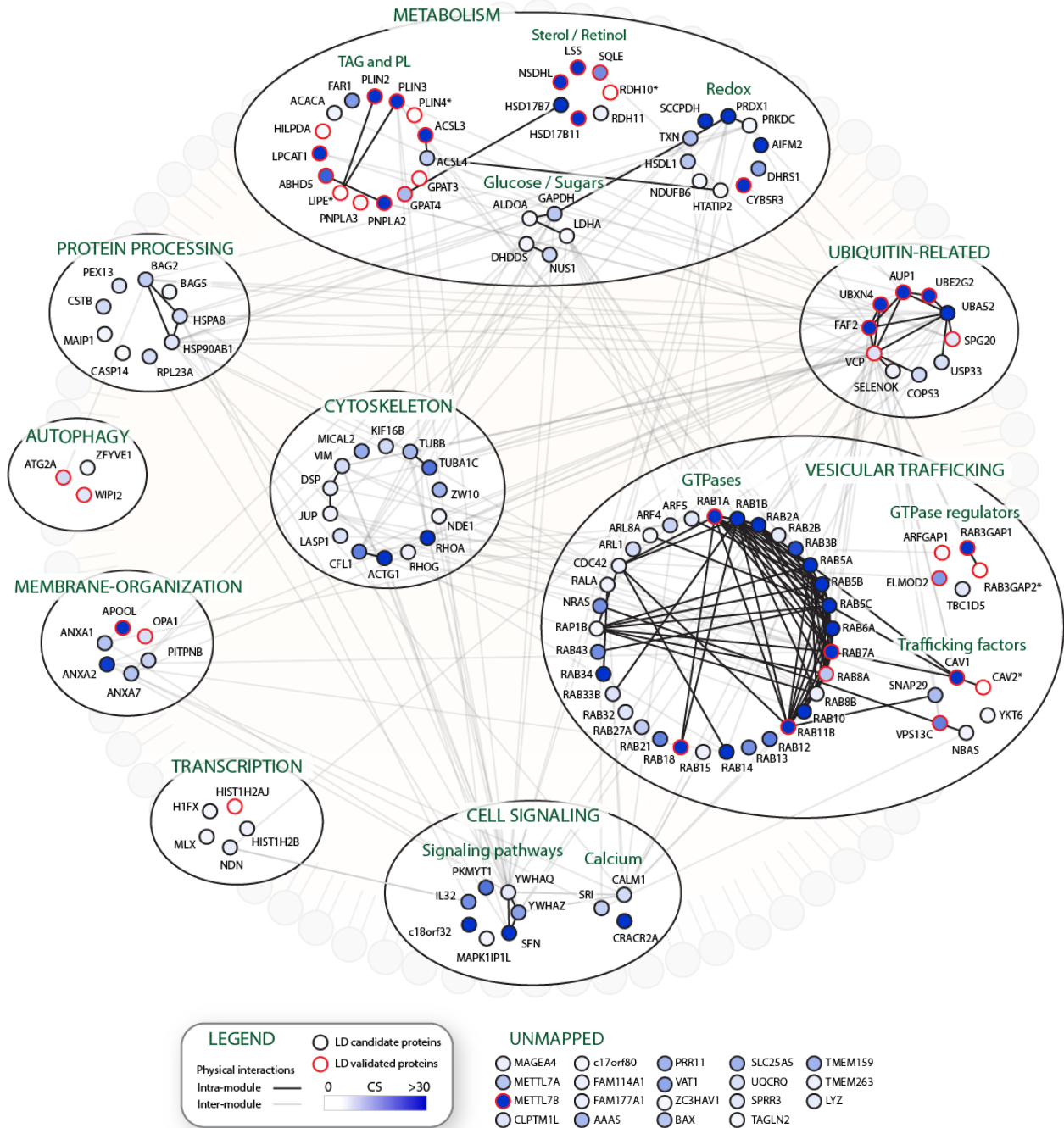


Figure 3-3: Illustration of the High-Confidence LD Proteome. High-confidence LD proteins are grouped into functional modules based on GO analysis and UNIPROT functional annotations. Solid lines represent physical interactions within functional modules and transparent lines represent interactions between proteins in distinct modules, as annotated in Bio-GRID. The intensity of the blue color in a node indicates the confidence score. Nodes outlined in red represent proteins that have been previously validated to localize to LDs by microscopy.

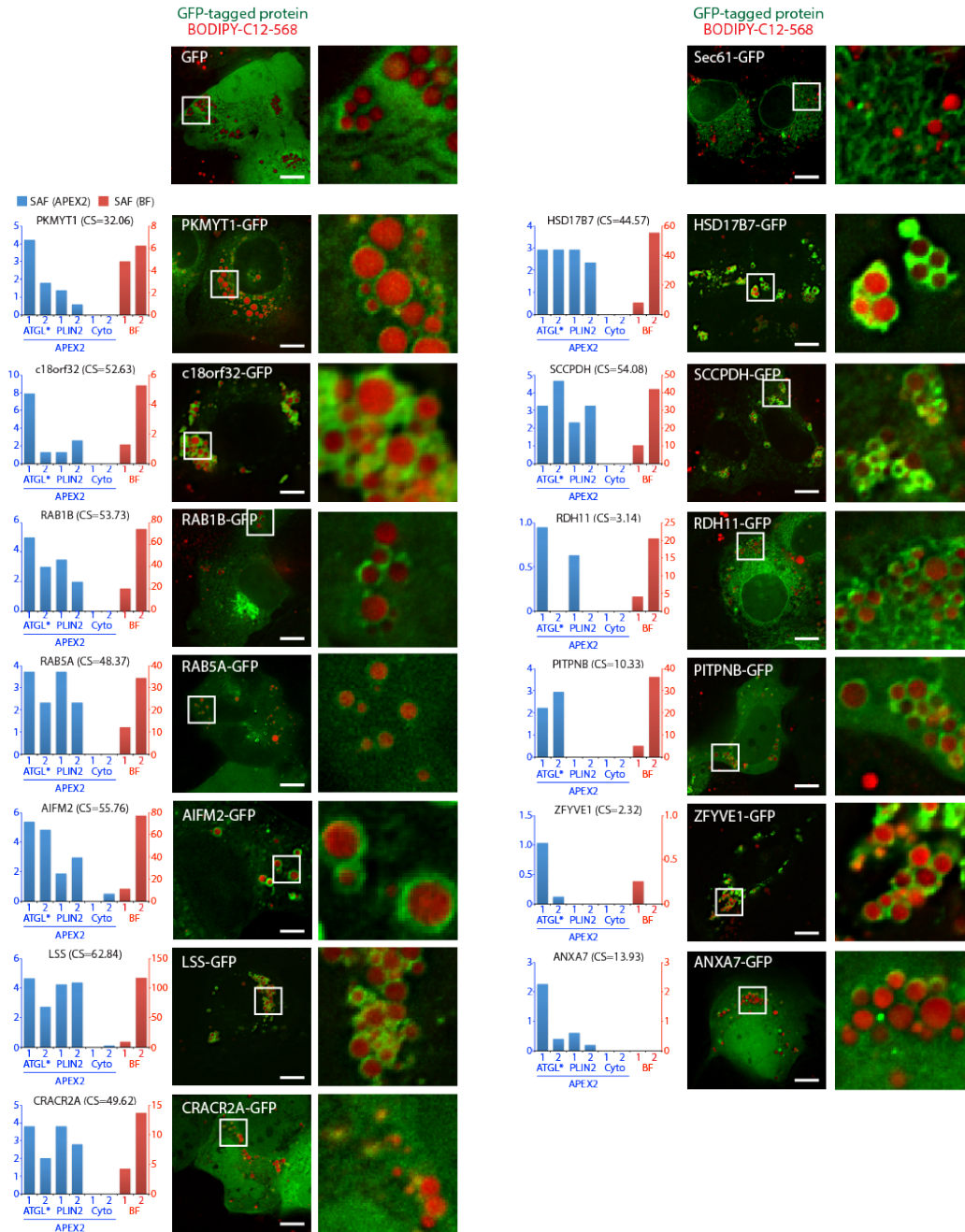


Figure 3-4: Combined High-Confidence LD Proteomes from U2OS and Huh7 Cells. Composite illustration of high-confidence LD proteins identified in U2OS and Huh7 cells. Proteins are grouped into functional modules. Boxes indicate U2OS-specific proteins (green), Huh7-specific proteins (blue), and shared proteins (red). Microscopic validation of individual nodes at LDs in previous studies (red circle) and in this study (shaded red circle) is also indicated. Asterisk indicates that the protein was identified, but was below the high-confidence threshold ( $CS_N < 1$ ) in one or both cell lines.

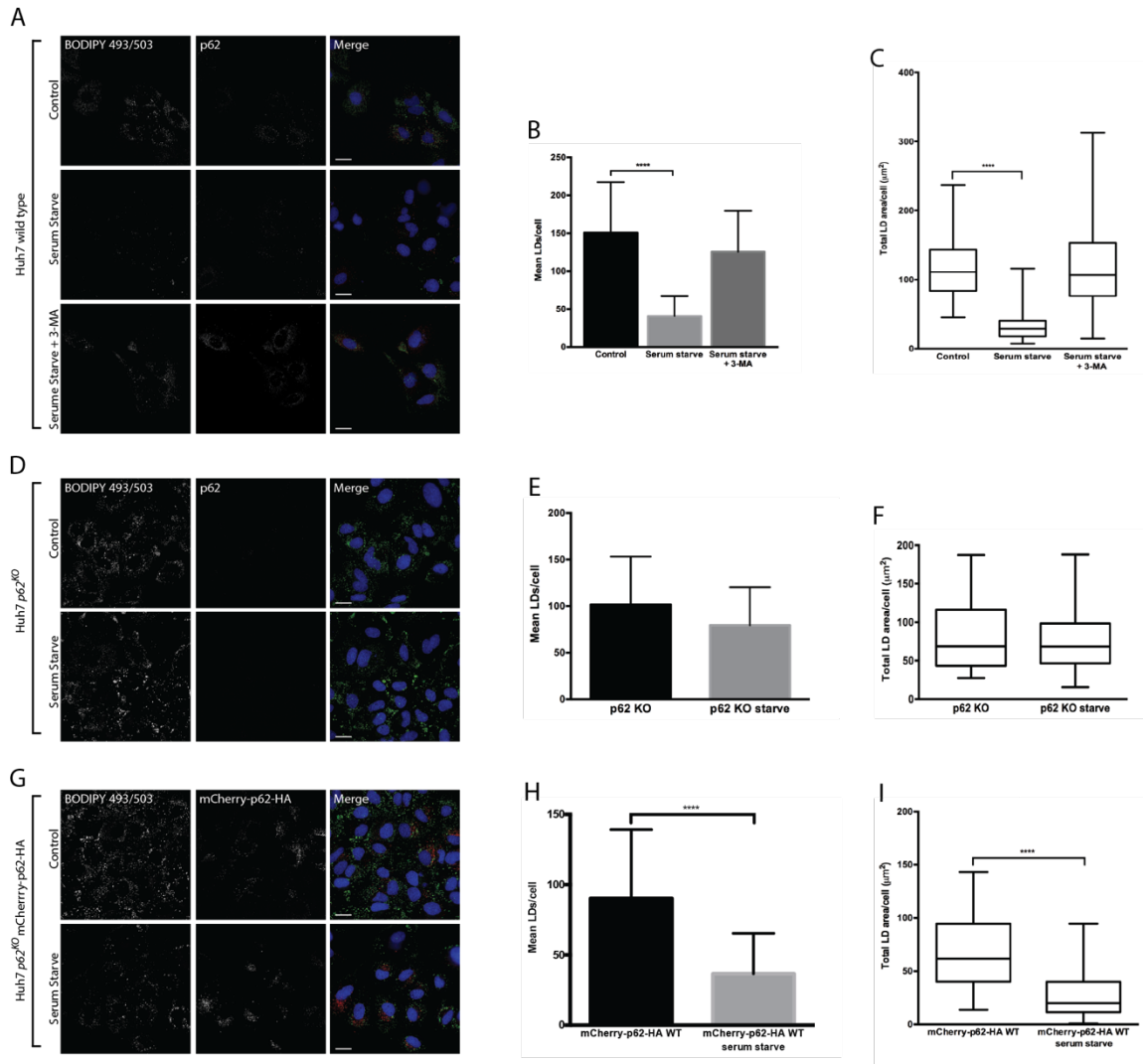


Figure 3-5: p62 is required for LD catabolism in hepatocytes. (A-C) Fluorescence imaging of Huh7 cells grown for 48-h in control medium containing DMEM supplemented with 10% FBS or serum starved medium containing DMEM supplemented with 0.2% FBS in the presence or absence of the autophagy inhibitor 3-MA and the corresponding quantifications of LD number and size per cell. Cells were visualized by addition of  $1 \mu\text{g mL}^{-1}$  BODIPY 493/503 to detect LDs and using antibodies direct against p62. (D-F) Images and quantifications of a similar starvation experiment performed in Huh7 p62<sup>KO</sup> cells. (G-I) Images and quantifications of a similar starvation performed in Huh7 p62<sup>KO</sup> cells expressing the mCherry-p62-HA construct. p62 was observed through direct visualization of mCherry. Scale bars = 40  $\mu\text{m}$ .

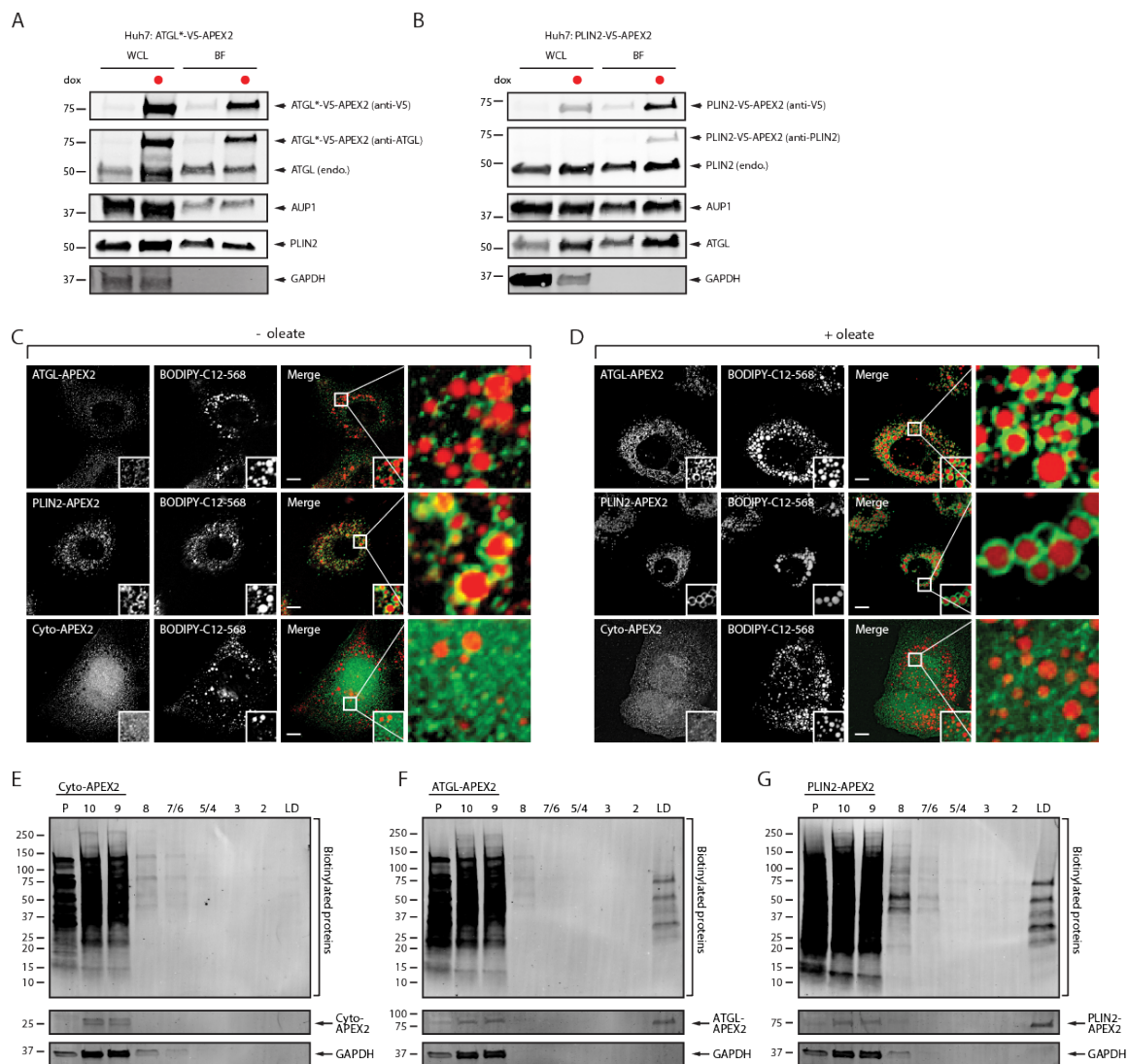


Figure 3-S1: Lipid droplet-targeted APEX2 biotinylates lipid droplet proteins in Huh7 cells. (A and B) Huh7 cells stably expressing ATGL\*-APEX2 or PLIN2-APEX2 were treated with 10 ng/mL dox for 48 hr. Whole cell lysates (WCL, normalized by total protein levels) or buoyant fractions (BF, normalized by AUP1 levels) were separated by SDS-PAGE and analyzed by blotting with the indicated antibodies. Endo., endogenous protein. 6 (C and D) Huh7 cells stably expressing cytosolic or LD-targeted APEX2 were treated for 24 hr with 1  $\mu$ M BODIPY-C12-568 or 200  $\mu$ M oleate and 1  $\mu$ M BODIPY-C12-568 (red). Cells were imaged by fluorescence microscopy using antibodies against the V5 epitope tag (green). Magnified insets show cellular regions with LDs. Scale bars represent 10  $\mu$ m. (E-G) Lysates from Huh7 cells stably expressing LD-targeted or cytosolic APEX2 were fractionated by sucrose gradient centrifugation. Proteins in individual fractions were separated by SDS-PAGE and analyzed by blotting with fluorescent streptavidin-568 and antibody against the V5 epitope tag.



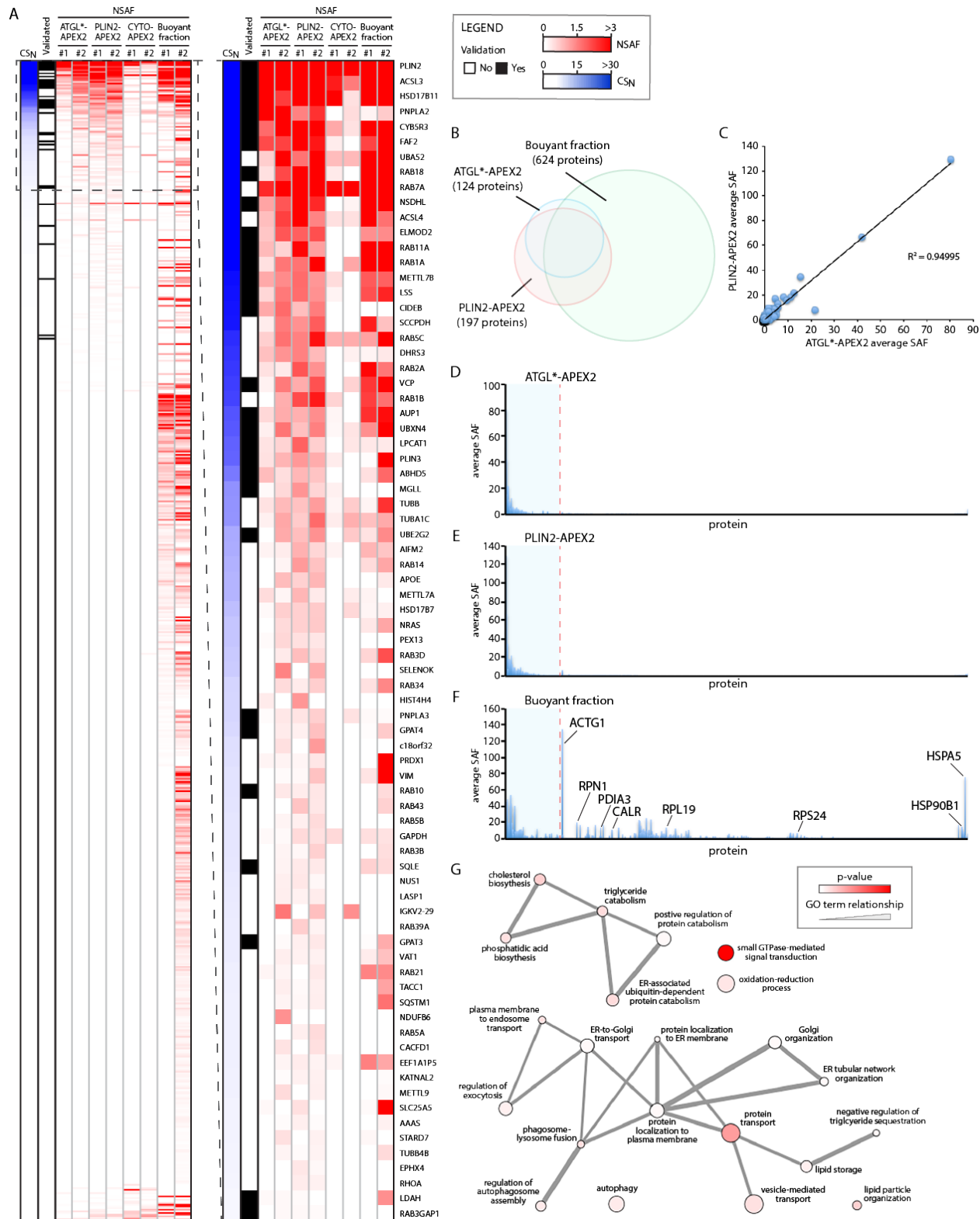


Figure 3-S2: Proteomic analysis of biotinylated lipid droplet proteins in Huh7 cells. (A) Proteins identified in total buoyant fractions and in streptavidin affinity purifications from the indicated Huh7 APEX2 cell lines were ranked by descending LD confidence score (CSN). Data from two independent experimental replicates for each sample are shown. The intensity of the blue color represents the CSN value and the intensity of the red color represents the normalized spectral abundance factor (NSAF) value. The heat map scale is linear. The black color indicates if a protein was previously validated as an LD protein by microscopy. The boxed inset shows the high confidence LD proteins (CSN > 1). (B) Venn diagram illustrating the degree of overlap between proteomes identified in the Huh7 LD-targeted APEX2 cell lines and in the buoyant fraction. (C) Comparison of average spectral abundance factors (SAF) for proteins identified in the affinity purifications from ATGL\*-V5-APEX2 and PLIN2-V5-APEX2 Huh7 cells. Each symbol corresponds to an LD protein identified in both cell lines. The R2 coefficient for the linear regression line is indicated. (D-F) The average SAF for proteins identified in the affinity purifications from ATGL\*-V5-APEX2 (D) or PLIN2-V5-APEX2 (E) Huh7 cells or in the total buoyant fractions isolated from parental cells (F). (G) Selected enriched GO-Term categories for high confidence LD proteins in Huh7 cells.

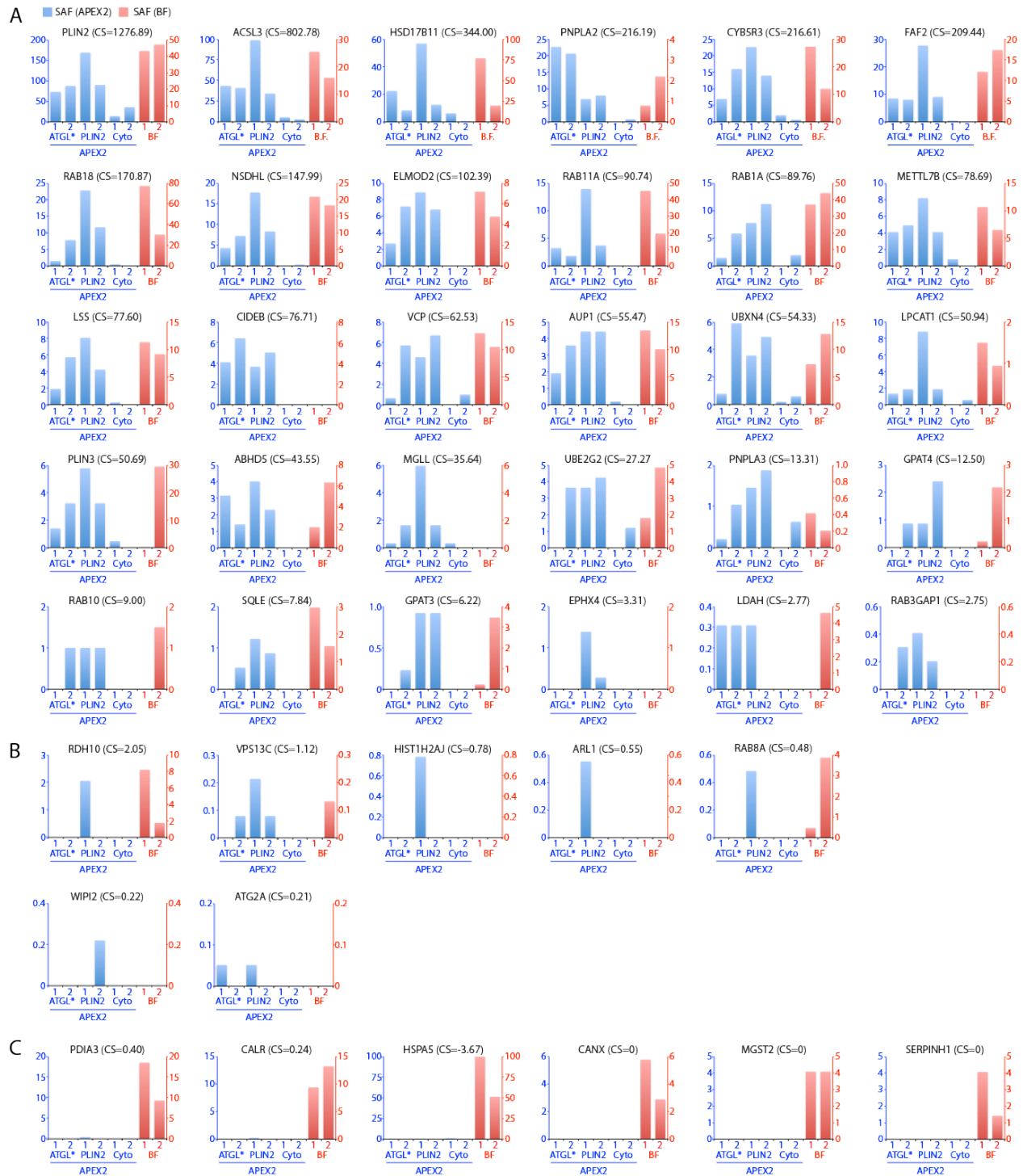
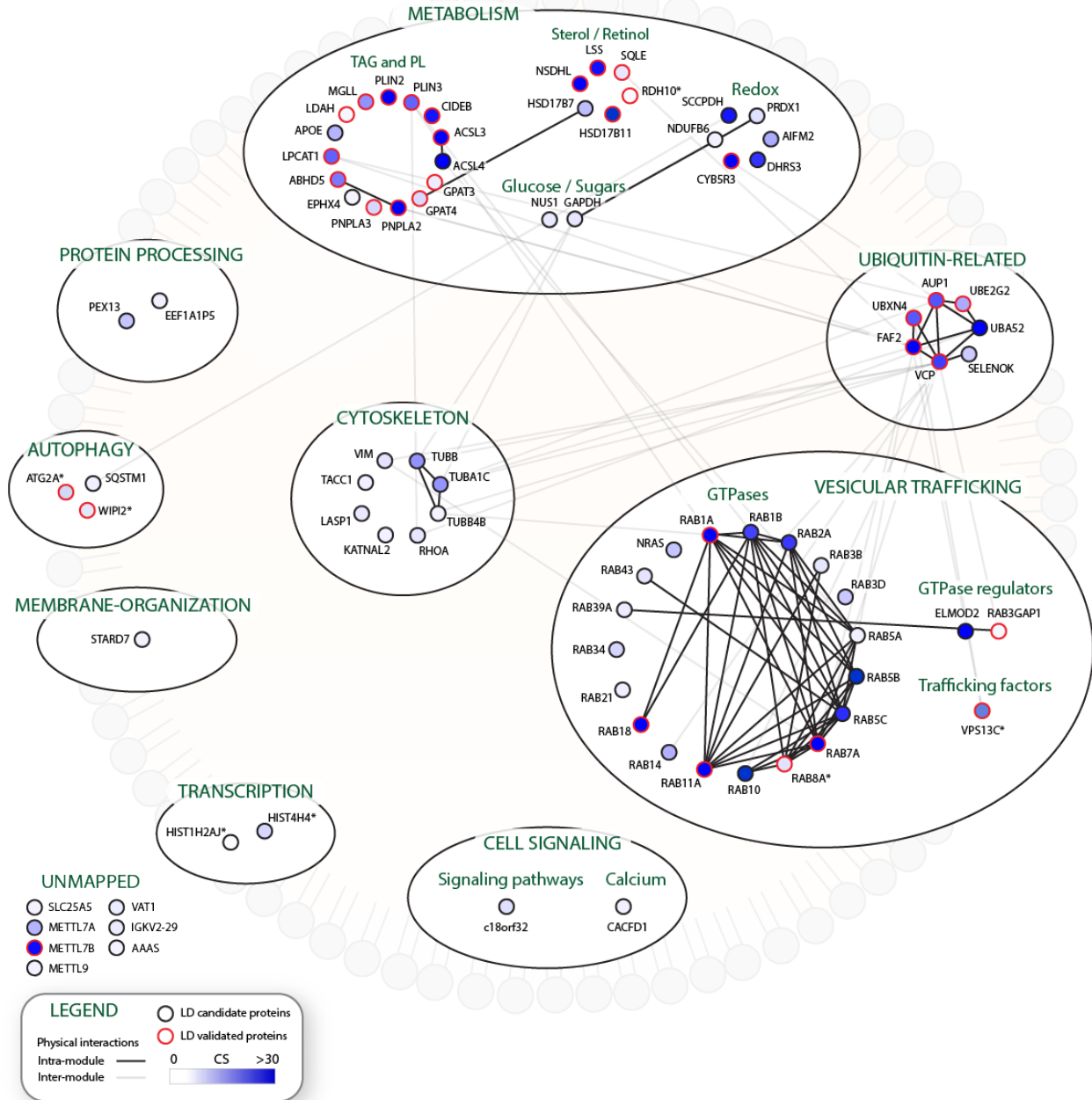
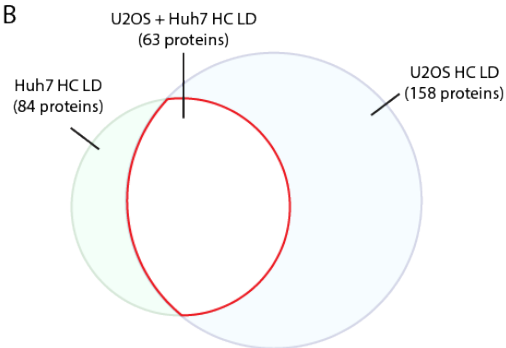


Figure 3-S3: Spectral profiles of validated lipid droplet proteins and select contaminants in Huh7 cells. (A-C) Graphs indicating the SAF in APEX2 (blue) and BF (red) samples for (A) validated proteins identified as high confidence LD proteins, (B) validated proteins that were detected, but were below the threshold value and were not designated as high confidence LD proteins, and (C) select common contaminant proteins. CS, confidence score.

A



B



C

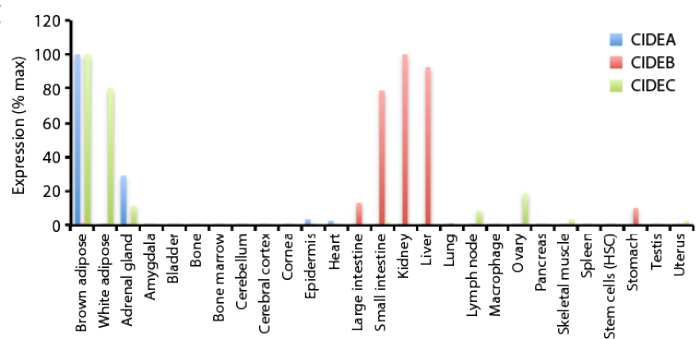




Figure 3-S4: Illustration of the high confidence lipid droplet proteome in Huh7 cells. (A) High confidence LD proteins identified in Huh7 cells (CSN > 1) are grouped into functional modules based on GO analysis and UNIPROT functional annotations. Solid lines represent physical interactions within functional modules and transparent lines represent interactions between proteins in distinct modules, as annotated in BIOGRID. The intensity of the blue color in a node indicates the confidence score. Nodes outlined in red represent proteins that have been previously validated to localize to LDs by microscopy. (B) Venn diagram illustrating the degree of overlap between high confidence LD proteins identified in U2OS and Huh7 cells. (C) Expression of CIDEA, CIDEB, and CIDEA transcripts in mouse tissues. Expression data was downloaded from BioGPS and normalized to the maximum expression level.

$$CS = \text{Eq. 1} \times \text{Eq. 2}$$

$$\text{Eq. 1} = \sum_{LD=1}^{LD=k} R_{LD,P}$$

$$\text{Eq. 2} = \sum_{LD=1}^{LD=k} (X_{LD,P} - X_{C,P})$$

$$CS_N = \frac{CS}{CS_T}$$

$$X_{LD,P} \begin{cases} \text{SAF for protein P from LD-APEX2} \\ \text{fusion protein (ATGL* or PLIN2)} \end{cases}$$

$$X_{C,P} \begin{cases} \text{SAF for protein P from Cyto-APEX2} \\ \text{fusion protein} \\ 0; X_{LD,P} = 0 \end{cases}$$

$$R_{LD,P} \begin{cases} 0; X_{LD,P} = 0 \\ 1; X_{LD,P} > 0 \end{cases}$$

$$SAF = TSC / \#aa \times 10$$

$$NSAF = SAF / (\text{average SAF, if } SAF > 0)$$

k = total number of  
LD-target APEX2 runs

$$15\% \text{ validated} < CS_T < 85\% \text{ validated}$$

Figure 3-S5: Calculation of LD confidence score. The LD confidence score (CS) for a protein “P” is calculated by multiplying a replication value (Eq. 1), which is the sum of the number of times the protein was detected in LD-targeted APEX2 samples ( $R_{LD,P}$ ), by an abundance value (Eq. 2), which is the sum of the spectral abundance factor (SAF) for the protein in the LD-targeted APEX2 samples ( $X_{LD,P}$ ) minus the SAF for the protein in the corresponding control Cyto-APEX2 sample ( $X_{C,P}$ ). SAF is calculated by dividing the total spectral counts (TSC) by the number of amino acids (aa) in the protein, multiplied by 10. The normalized SAF 2 (NSAF) is calculated by dividing the SAF by the average SAF for proteins in the sample (based on proteins with an SAF > 0).

## CONCLUSION

The ability to respond to changes in protein and lipid metabolism involves a complex network of inter-organelle regulation vital for maintaining cellular homeostasis. Dysregulation of endoplasmic reticulum-associated degradation (ERAD) and proteostasis in the ER has been implicated in the pathology of many diseases, including Alzheimer's and Parkinson's Disease, while neutral lipid storage disorders such as obesity and non-alcoholic fatty liver disease (NAFLD) are becoming increasingly prevalent in today's society. Understanding the various mechanisms by which these fundamental pathways are regulated and respond to fluctuations in nutrition is essential in efforts to help combat such diseases.

In chapter two, we disentangle the underlying mechanisms surrounding the impairment of ERAD and lipid droplet (LD) biogenesis following inhibition of acyl-CoA synthetases (ACSL) with the chemical inhibitor triacsin c, finding these effects are rather due to broad alterations in the cellular lipid landscape producing divergent complications in downstream protein and lipid homeostasis. Our findings indicate that triacsin c impairs the glycan trimming process of CD147 and its delivery to the Hrd1 complex, suggesting that a failure to establish the properly trimmed glycan structure leads to impairments in ERAD. Moreover, while ACSLs are required for triacylglycerol (TAG) synthesis and LD biogenesis, genetic disruption of DGAT-mediated LD biogenesis in cells did not lead to an impact in CD147 degradation, indicating that LDs are not required for ERAD, arguing against a previously proposed model<sup>159</sup>.

The observed overlap of pathways pursuant to ERAD and LD biogenesis in chapter two demonstrate an intimate connection between protein and lipid metabolism in the cell. ACSL activation of fatty acids has been similarly shown to have regulatory effects on various components involved in the ERAD pathway through the reversible addition of a palmitate moiety to the protein<sup>103,104</sup>. Indeed, we have identified several additional ERAD components that appear to be modified by palmitoylation as well, indicating a potentially unrecognized level of regulation involved in ERAD. However, whether the palmitoylation status of these proteins has an impact on their functionality and the full extent of this modification occurring throughout the ERAD pathway remains unanswered.

In chapter three, we employed a proximity-labeling approach using modified ascorbate peroxidase (APEX2) to biotinylate proteins LD proteins in living cells and identify a high-confidence LD proteome in two metabolically divergent cell types. In addition to identifying the majority of previously identified LD proteins, this approach provides an improved method for discriminating the large number of contaminant proteins that frequently plague LD preparations. We were also able to use this technique to identify new LD proteins whose functions involved with LDs have previously been uncharacterized, including the autophagy adapter protein p62/SQSTM1. Further analysis indicated that that p62 indeed functions as adapter protein mediating the recruitment of autophagosomal membranes to LDs and is required for starvation-induced lipophagy in hepatocytes.

In summary, the work presented in this dissertation illustrates the intricate relationship between protein and lipid homeostasis and identified important aspects involving in their regulation, including the previously uncharacterized requirement of the adapter protein p62 in mediating

lipid droplet autophagy in hepatocytes. Together these approaches provide new insight into the development of novel therapeutic targets of metabolic disease.

## REFERENCES

1. Roberts, Melissa A, and James A Olzmann. "Protein Quality Control and Lipid Droplet Metabolism." *Annual review of cell and developmental biology* vol. 36 (2020): 115-139. doi:10.1146/annurev-cellbio-031320-101827
2. Jacquemyn, Julie et al. "The ins and outs of endoplasmic reticulum-controlled lipid biosynthesis." *EMBO reports* vol. 18,11 (2017): 1905-1921. doi:10.15252/embr.201643426
3. Goder, Veit et al. "Lipids and their (un)known effects on ER-associated protein degradation (ERAD)." *Biochimica et biophysica acta. Molecular and cell biology of lipids* vol. 1865,1 (2020): 158488. doi:10.1016/j.bbalip.2019.06.014
4. Vembar, Shruthi S, and Jeffrey L Brodsky. "One step at a time: endoplasmic reticulum-associated degradation." *Nature reviews. Molecular cell biology* vol. 9,12 (2008): 944-57. doi:10.1038/nrm2546
5. Osowski, Christine M, and Fumihiko Urano. "Measuring ER stress and the unfolded protein response using mammalian tissue culture system." *Methods in enzymology* vol. 490 (2011): 71-92. doi:10.1016/B978-0-12-385114-7.00004-0
6. Lemus, Leticia, and Veit Goder. "Regulation of Endoplasmic Reticulum-Associated Protein Degradation (ERAD) by Ubiquitin." *Cells* vol. 3,3 824-47. 5 Aug. 2014, doi:10.3390/cells3030824
7. Fu, Suneng et al. "The role of endoplasmic reticulum in hepatic lipid homeostasis and stress signaling." *Cell metabolism* vol. 15,5 (2012): 623-34. doi:10.1016/j.cmet.2012.03.007
8. Fouillen, Laetitia et al. "ER Membrane Lipid Composition and Metabolism: Lipidomic Analysis." *Methods in molecular biology (Clifton, N.J.)* vol. 1691 (2018): 125-137. doi:10.1007/978-1-4939-7389-7\_10
9. Balla, Tamas et al. "Lipid Dynamics at Contact Sites Between the Endoplasmic Reticulum and Other Organelles." *Annual review of cell and developmental biology* vol. 35 (2019): 85-109. doi:10.1146/annurev-cellbio-100818-125251
10. Balla, Tamas et al. "Lipid synthesis and transport are coupled to regulate membrane lipid dynamics in the endoplasmic reticulum." *Biochimica et biophysica acta. Molecular and cell biology of lipids* vol. 1865,1 (2020): 158461. doi:10.1016/j.bbalip.2019.05.005
11. DeBose-Boyd, R. Feedback regulation of cholesterol synthesis: sterol-accelerated ubiquitination and degradation of HMG CoA reductase. *Cell Res* **18**, 609–621 (2008). <https://doi.org/10.1038/cr.2008.61>

12. Tsai, Yien Che et al. "Differential regulation of HMG-CoA reductase and Insig-1 by enzymes of the ubiquitin-proteasome system." *Molecular biology of the cell* vol. 23,23 (2012): 4484-94. doi:10.1091/mbc.E12-08-0631
13. Kounakis, Konstantinos et al. "Emerging Roles of Lipophagy in Health and Disease." *Frontiers in cell and developmental biology* vol. 7 185. 10 Sep. 2019, doi:10.3389/fcell.2019.00185
14. Schott, Micah B et al. "Lipid droplet size directs lipolysis and lipophagy catabolism in hepatocytes." *The Journal of cell biology* vol. 218,10 (2019): 3320-3335. doi:10.1083/jcb.201803153
15. Olzmann, James A, and Pedro Carvalho. "Dynamics and functions of lipid droplets." *Nature reviews. Molecular cell biology* vol. 20,3 (2019): 137-155. doi:10.1038/s41580-018-0085-z
16. Li, Zhihuan et al. "Lipid droplets control the maternal histone supply of Drosophila embryos." *Current biology : CB* vol. 22,22 (2012): 2104-13. doi:10.1016/j.cub.2012.09.018
17. Fukasawa, Masayoshi. "Cellular lipid droplets and hepatitis C virus life cycle." *Biological & pharmaceutical bulletin* vol. 33,3 (2010): 355-9. doi:10.1248/bpb.33.355
18. Yang XJ, Zhang LL. [Roles of lipid droplets in hepatitis C virus life cycle]. *Bing Du Xue Bao*. 2014 Jan;30(1):91-7. Chinese. PMID: 24772905.
19. Renne, Mike F et al. "Lipid droplet biogenesis: A mystery "unmixing"?" *Seminars in cell & developmental biology*, S1084-9521(18)30318-5. 17 Mar. 2020, doi:10.1016/j.semcd.2020.03.001
20. Chapman, Kent D et al. "Mechanisms of lipid droplet biogenesis." *The Biochemical journal* vol. 476,13 1929-1942. 9 Jul. 2019, doi:10.1042/BCJ20180021
21. Chang TY, Chang CC, Lin S, Yu C, Li BL, Miyazaki A. Roles of acyl-coenzyme A:cholesterol acyltransferase-1 and -2. *Curr Opin Lipidol*. 2001 Jun;12(3):289-96. doi: 10.1097/00041433-200106000-00008. PMID: 11353332.
22. Zhang C, Liu P. The New Face of the Lipid Droplet: Lipid Droplet Proteins. *Proteomics*. 2019 May;19(10):e1700223. doi: 10.1002/pmic.201700223. Epub 2018 Oct 8. PMID: 30216670.
23. Ding, Yunfeng et al. "Identification of the major functional proteins of prokaryotic lipid droplets." *Journal of lipid research* vol. 53,3 (2012): 399-411. doi:10.1194/jlr.M021899
24. Itabe, Hiroyuki et al. "Perilipins: a diversity of intracellular lipid droplet proteins." *Lipids in health and disease* vol. 16,1 83. 28 Apr. 2017, doi:10.1186/s12944-017-0473-y

25. Sztalryd, Carole, and Dawn L Brasaemle. "The perilipin family of lipid droplet proteins: Gatekeepers of intracellular lipolysis." *Biochimica et biophysica acta. Molecular and cell biology of lipids* vol. 1862,10 Pt B (2017): 1221-1232. doi:10.1016/j.bbalip.2017.07.009
26. Brasaemle, D L et al. "Perilipin A increases triacylglycerol storage by decreasing the rate of triacylglycerol hydrolysis." *The Journal of biological chemistry* vol. 275,49 (2000): 38486-93. doi:10.1074/jbc.M007322200
27. Zechner, Rudolf et al. "Cytosolic lipolysis and lipophagy: two sides of the same coin." *Nature reviews. Molecular cell biology* vol. 18,11 (2017): 671-684. doi:10.1038/nrm.2017.76
28. Kimmel AR, Sztalryd C. Perilipin 5, a lipid droplet protein adapted to mitochondrial energy utilization. *Curr Opin Lipidol.* 2014 Apr;25(2):110-7. doi: 10.1097/MOL.000000000000057. PMID: 24535284; PMCID: PMC4517968.
29. Gallardo-Montejano, Violeta I et al. "Nuclear Perilipin 5 integrates lipid droplet lipolysis with PGC-1 $\alpha$ /SIRT1-dependent transcriptional regulation of mitochondrial function." *Nature communications* vol. 7 12723. 24 Aug. 2016, doi:10.1038/ncomms12723
30. Mardani, Ismena et al. "Plin2-deficiency reduces lipophagy and results in increased lipid accumulation in the heart." *Scientific reports* vol. 9,1 6909. 6 May. 2019, doi:10.1038/s41598-019-43335-y
31. Pingitore, Piero, and Stefano Romeo. "The role of PNPLA3 in health and disease." *Biochimica et biophysica acta. Molecular and cell biology of lipids* vol. 1864,6 (2019): 900-906. doi:10.1016/j.bbalip.2018.06.018
32. Yen, Chi-Liang Eric, and Robert V Farese Jr. "Fat breakdown: a function for CGI-58 (ABHD5) provides a new piece of the puzzle." *Cell metabolism* vol. 3,5 (2006): 305-7. doi:10.1016/j.cmet.2006.04.001
33. Guo Y, Cordes KR, Farese RV Jr, Walther TC. Lipid droplets at a glance. *J Cell Sci.* 2009 Mar 15;122(Pt 6):749-52. doi: 10.1242/jcs.037630. PMID: 19261844; PMCID: PMC2714424.
34. Bersuker, Kirill, and James A Olzmann. "Establishing the lipid droplet proteome: Mechanisms of lipid droplet protein targeting and degradation." *Biochimica et biophysica acta. Molecular and cell biology of lipids* vol. 1862,10 Pt B (2017): 1166-1177. doi:10.1016/j.bbalip.2017.06.006
35. Fujimoto, Toyoshi et al. "Lipid droplets: a classic organelle with new outfits." *Histochemistry and cell biology* vol. 130,2 (2008): 263-79. doi:10.1007/s00418-008-0449-0



36. Krahmer, Natalie et al. "Phosphatidylcholine synthesis for lipid droplet expansion is mediated by localized activation of CTP:phosphocholine cytidyltransferase." *Cell metabolism* vol. 14,4 (2011): 504-15. doi:10.1016/j.cmet.2011.07.013
37. Walther, Tobias C, and Robert V Farese Jr. "Lipid droplets and cellular lipid metabolism." *Annual review of biochemistry* vol. 81 (2012): 687-714. doi:10.1146/annurev-biochem-061009-102430
38. Boscher, Cécile, and Ivan Robert Nabi. "Caveolin-1: role in cell signaling." *Advances in experimental medicine and biology* vol. 729 (2012): 29-50. doi:10.1007/978-1-4614-1222-9\_3
39. Cohen, Alex W et al. "Role of caveolin-1 in the modulation of lipolysis and lipid droplet formation." *Diabetes* vol. 53,5 (2004): 1261-70. doi:10.2337/diabetes.53.5.1261
40. Stone, Scot J et al. "The endoplasmic reticulum enzyme DGAT2 is found in mitochondria-associated membranes and has a mitochondrial targeting signal that promotes its association with mitochondria." *The Journal of biological chemistry* vol. 284,8 (2009): 5352-61. doi:10.1074/jbc.M805768200
41. Robenek, Mirko J et al. "Lipids partition caveolin-1 from ER membranes into lipid droplets: updating the model of lipid droplet biogenesis." *FASEB journal : official publication of the Federation of American Societies for Experimental Biology* vol. 18,7 (2004): 866-8. doi:10.1096/fj.03-0782fje
42. Barneda, David et al. "The brown adipocyte protein CIDEA promotes lipid droplet fusion via a phosphatidic acid-binding amphipathic helix." *eLife* vol. 4 e07485. 26 Nov. 2015, doi:10.7554/eLife.07485
43. Prévost, Coline et al. "Mechanism and Determinants of Amphipathic Helix-Containing Protein Targeting to Lipid Droplets." *Developmental cell* vol. 44,1 (2018): 73-86.e4. doi:10.1016/j.devcel.2017.12.011
44. Hickenbottom, Sabrina J et al. "Structure of a lipid droplet protein; the PAT family member TIP47." *Structure (London, England : 1993)* vol. 12,7 (2004): 1199-207. doi:10.1016/j.str.2004.04.021
45. Welte, Michael A et al. "Regulation of lipid-droplet transport by the perilipin homolog LSD2." *Current biology : CB* vol. 15,14 (2005): 1266-75. doi:10.1016/j.cub.2005.06.062
46. Schuldiner, Maya, and Maria Bohnert. "A different kind of love - lipid droplet contact sites." *Biochimica et biophysica acta. Molecular and cell biology of lipids* vol. 1862,10 Pt B (2017): 1188-1196. doi:10.1016/j.bbalip.2017.06.005

47. Nguyen, Truc B et al. "DGAT1-Dependent Lipid Droplet Biogenesis Protects Mitochondrial Function during Starvation-Induced Autophagy." *Developmental cell* vol. 42,1 (2017): 9-21.e5. doi:10.1016/j.devcel.2017.06.003
48. Benador, Ilan Y et al. "Mitochondria Bound to Lipid Droplets: Where Mitochondrial Dynamics Regulate Lipid Storage and Utilization." *Cell metabolism* vol. 29,4 (2019): 827-835. doi:10.1016/j.cmet.2019.02.011
49. Kimmel, Alan R, and Carole Sztalryd. "Perilipin 5, a lipid droplet protein adapted to mitochondrial energy utilization." *Current opinion in lipidology* vol. 25,2 (2014): 110-7. doi:10.1097/MOL.0000000000000057
50. Boutant, Marie et al. "Mfn2 is critical for brown adipose tissue thermogenic function." *The EMBO journal* vol. 36,11 (2017): 1543-1558. doi:10.15252/embj.201694914
51. Ikura, Yoshihiro, and Stephen H Caldwell. "Lipid droplet-associated proteins in alcoholic liver disease: a potential linkage with hepatocellular damage." *International journal of clinical and experimental pathology* vol. 8,8 8699-708. 1 Aug. 2015
52. Wang, Hong et al. "Perilipin 5, a lipid droplet-associated protein, provides physical and metabolic linkage to mitochondria." *Journal of lipid research* vol. 52,12 (2011): 2159-68. doi:10.1194/jlr.M017939
53. Poulos, A et al. "Very long-chain fatty acids in peroxisomal disease." *Advances in experimental medicine and biology* vol. 318 (1992): 331-40. doi:10.1007/978-1-4615-3426-6\_30
54. Rambold, Angelika S et al. "Fatty acid trafficking in starved cells: regulation by lipid droplet lipolysis, autophagy, and mitochondrial fusion dynamics." *Developmental cell* vol. 32,6 (2015): 678-92. doi:10.1016/j.devcel.2015.01.029
55. Singh, Rajat, and Ana Maria Cuervo. "Lipophagy: connecting autophagy and lipid metabolism." *International journal of cell biology* vol. 2012 (2012): 282041. doi:10.1155/2012/282041
56. Weidberg, Hilla et al. "Lipophagy: selective catabolism designed for lipids." *Developmental cell* vol. 16,5 (2009): 628-30. doi:10.1016/j.devcel.2009.05.001
57. Zechner, Rudolf et al. "Adipose triglyceride lipase and the lipolytic catabolism of cellular fat stores." *Journal of lipid research* vol. 50,1 (2009): 3-21. doi:10.1194/jlr.R800031-JLR200
58. Zimmermann, Robert et al. "Fat mobilization in adipose tissue is promoted by adipose triglyceride lipase." *Science (New York, N.Y.)* vol. 306,5700 (2004): 1383-6. doi:10.1126/science.1100747

59. Lee, Jung Hyun et al. "Lipid droplet protein LID-1 mediates ATGL-1-dependent lipolysis during fasting in *Caenorhabditis elegans*." *Molecular and cellular biology* vol. 34,22 (2014): 4165-76. doi:10.1128/MCB.00722-14
60. Lass, Achim et al. "Adipose triglyceride lipase-mediated lipolysis of cellular fat stores is activated by CGI-58 and defective in Chanarin-Dorfman Syndrome." *Cell metabolism* vol. 3,5 (2006): 309-19. doi:10.1016/j.cmet.2006.03.005
61. Chen, Yingfei et al. "Carboxylic ester hydrolases: Classification and database derived from their primary, secondary, and tertiary structures." *Protein science : a publication of the Protein Society* vol. 25,11 (2016): 1942-1953. doi:10.1002/pro.3016
62. Li, Fang, and Hanrui Zhang. "Lysosomal Acid Lipase in Lipid Metabolism and Beyond." *Arteriosclerosis, thrombosis, and vascular biology* vol. 39,5 (2019): 850-856. doi:10.1161/ATVBAHA.119.312136
63. Holm, C. "Molecular mechanisms regulating hormone-sensitive lipase and lipolysis." *Biochemical Society transactions* vol. 31,Pt 6 (2003): 1120-4. doi:10.1042/bst0311120
64. Shen, Wen-Jun et al. "Interaction of hormone-sensitive lipase with steroidogenic acute regulatory protein: facilitation of cholesterol transfer in adrenal." *The Journal of biological chemistry* vol. 278,44 (2003): 43870-6. doi:10.1074/jbc.M303934200
65. Shen WJ, Patel S, Natu V, Hong R, Wang J, Azhar S, Kraemer FB. Interaction of hormone-sensitive lipase with steroidogenic acute regulatory protein: facilitation of cholesterol transfer in adrenal. *J Biol Chem*. 2003 Oct 31;278(44):43870-6. doi: 10.1074/jbc.M303934200. Epub 2003 Aug 18. PMID: 12925534.
66. Meijssen, S et al. "Insulin mediated inhibition of hormone sensitive lipase activity in vivo in relation to endogenous catecholamines in healthy subjects." *The Journal of clinical endocrinology and metabolism* vol. 86,9 (2001): 4193-7. doi:10.1210/jcem.86.9.7794
67. Douglass, John D et al. "Erratum: Global deletion of MGL in mice delays lipid absorption and alters energy homeostasis and diet-induced obesity." *Journal of lipid research* vol. 60,3 (2019): 717. doi:10.1194/jlr.M058586ERR
68. Douglass, John D et al. "Global deletion of MGL in mice delays lipid absorption and alters energy homeostasis and diet-induced obesity." *Journal of lipid research* vol. 56,6 (2015): 1153-71. doi:10.1194/jlr.M058586
69. Taschler, Ulrike et al. "Monoglyceride lipase deficiency in mice impairs lipolysis and attenuates diet-induced insulin resistance." *The Journal of biological chemistry* vol. 286,20 (2011): 17467-77. doi:10.1074/jbc.M110.215434

70. Glick, Danielle et al. "Autophagy: cellular and molecular mechanisms." *The Journal of pathology* vol. 221,1 (2010): 3-12. doi:10.1002/path.2697
71. Lim CY, Zoncu R. The lysosome as a command-and-control center for cellular metabolism. *J Cell Biol.* 2016 Sep 12;214(6):653-64. doi: 10.1083/jcb.201607005. PMID: 27621362; PMCID: PMC5021098.
72. Dunn, W A Jr. "Autophagy and related mechanisms of lysosome-mediated protein degradation." *Trends in cell biology* vol. 4,4 (1994): 139-43. doi:10.1016/0962-8924(94)90069-8
73. Yim, Willa Wen-You, and Noboru Mizushima. "Lysosome biology in autophagy." *Cell discovery* vol. 6 6. 11 Feb. 2020, doi:10.1038/s41421-020-0141-7
74. Brown, M S, and J L Goldstein. "The SREBP pathway: regulation of cholesterol metabolism by proteolysis of a membrane-bound transcription factor." *Cell* vol. 89,3 (1997): 331-40. doi:10.1016/s0092-8674(00)80213-5
75. Li WW, Li J, Bao JK. Microautophagy: lesser-known self-eating. *Cell Mol Life Sci.* 2012 Apr;69(7):1125-36. doi: 10.1007/s00018-011-0865-5. Epub 2011 Nov 12. PMID: 22080117.
76. Li WW, Li J, Bao JK. Microautophagy: lesser-known self-eating. *Cell Mol Life Sci.* 2012 Apr;69(7):1125-36. doi: 10.1007/s00018-011-0865-5. Epub 2011 Nov 12. PMID: 22080117.
77. Dice JF. Chaperone-mediated autophagy. *Autophagy.* 2007 Jul-Aug;3(4):295-9. doi: 10.4161/auto.4144. Epub 2007 Jul 15. PMID: 17404494.
78. Zachari M, Ganley IG. The mammalian ULK1 complex and autophagy initiation. *Essays Biochem.* 2017 Dec 12;61(6):585-596. doi: 10.1042/EBC20170021. PMID: 29233870; PMCID: PMC5869855.
79. Tanida I, Ueno T, Kominami E. LC3 and Autophagy. *Methods Mol Biol.* 2008;445:77-88. doi: 10.1007/978-1-59745-157-4\_4. PMID: 18425443.
80. Kriegenburg F, Ungermann C, Reggiori F. Coordination of Autophagosome-Lysosome Fusion by Atg8 Family Members. *Curr Biol.* 2018 Apr 23;28(8):R512-R518. doi: 10.1016/j.cub.2018.02.034. PMID: 29689234.
81. Johansen T, Lamark T. Selective autophagy mediated by autophagic adapter proteins. *Autophagy.* 2011 Mar;7(3):279-96. doi: 10.4161/auto.7.3.14487. PMID: 21189453; PMCID: PMC3060413.

82. Anding AL, Baehrecke EH. Cleaning House: Selective Autophagy of Organelles. *Dev Cell*. 2017 Apr 10;41(1):10-22. doi: 10.1016/j.devcel.2017.02.016. PMID: 28399394; PMCID: PMC5395098.
83. Filimonenko, Maria et al. "The selective macroautophagic degradation of aggregated proteins requires the PI3P-binding protein Alfy." *Molecular cell* vol. 38,2 (2010): 265-79. doi:10.1016/j.molcel.2010.04.007
84. Geisler, Sven et al. "PINK1/Parkin-mediated mitophagy is dependent on VDAC1 and p62/SQSTM1." *Nature cell biology* vol. 12,2 (2010): 119-31. doi:10.1038/ncb2012
85. Wong, Yvette C, and Erika L F Holzbaur. "Optineurin is an autophagy receptor for damaged mitochondria in parkin-mediated mitophagy that is disrupted by an ALS-linked mutation." *Proceedings of the National Academy of Sciences of the United States of America* vol. 111,42 (2014): E4439-48.
86. Iwata, Jun-ichi et al. "Excess peroxisomes are degraded by autophagic machinery in mammals." *The Journal of biological chemistry* vol. 281,7 (2006): 4035-41. doi:10.1074/jbc.M512283200
87. Kraft, Claudine et al. "Mature ribosomes are selectively degraded upon starvation by an autophagy pathway requiring the Ubp3p/Bre5p ubiquitin protease." *Nature cell biology* vol. 10,5 (2008): 602-10. doi:10.1038/ncb1723
88. Bernales, Sebastián et al. "Autophagy counterbalances endoplasmic reticulum expansion during the unfolded protein response." *PLoS biology* vol. 4,12 (2006): e423. doi:10.1371/journal.pbio.0040423
89. Pankiv, Serhiy et al. "p62/SQSTM1 binds directly to Atg8/LC3 to facilitate degradation of ubiquitinated protein aggregates by autophagy." *The Journal of biological chemistry* vol. 282,33 (2007): 24131-45. doi:10.1074/jbc.M702824200
90. Walinda, Erik et al. "Solution structure of the ubiquitin-associated (UBA) domain of human autophagy receptor NBR1 and its interaction with ubiquitin and polyubiquitin." *The Journal of biological chemistry* vol. 289,20 (2014): 13890-902. doi:10.1074/jbc.M114.555441
91. Viret, Christophe et al. "Novel Insights into NDP52 Autophagy Receptor Functioning." *Trends in cell biology* vol. 28,4 (2018): 255-257. doi:10.1016/j.tcb.2018.01.003
92. Ju, Jeong-Sun et al. "Valosin-containing protein (VCP) is required for autophagy and is disrupted in VCP disease." *The Journal of cell biology* vol. 187,6 (2009): 875-88. doi:10.1083/jcb.200908115

93. Singh, Rajat et al. "Autophagy regulates lipid metabolism." *Nature* vol. 458,7242 (2009): 1131-5. doi:10.1038/nature07976
94. Kaushik, Susmita et al. "Autophagy in hypothalamic AgRP neurons regulates food intake and energy balance." *Cell metabolism* vol. 14,2 (2011): 173-83. doi:10.1016/j.cmet.2011.06.008
95. Jeong SJ, Lee MN, Oh GT. The Role of Macrophage Lipophagy in Reverse Cholesterol Transport. *Endocrinol Metab (Seoul)*. 2017 Mar;32(1):41-46. doi: 10.3803/EnM.2017.32.1.41. PMID: 28345315; PMCID: PMC5368120.
96. Martinez-Lopez, Nuria, and Rajat Singh. "Autophagy and Lipid Droplets in the Liver." *Annual review of nutrition* vol. 35 (2015): 215-37. doi:10.1146/annurev-nutr-071813-105336
97. Klemm, Elizabeth J et al. "Dual role of ancient ubiquitous protein 1 (AUP1) in lipid droplet accumulation and endoplasmic reticulum (ER) protein quality control." *The Journal of biological chemistry* vol. 286,43 (2011): 37602-14. doi:10.1074/jbc.M111.284794
98. Spandl, Johanna et al. "Ancient ubiquitous protein 1 (AUP1) localizes to lipid droplets and binds the E2 ubiquitin conjugase G2 (Ube2g2) via its G2 binding region." *The Journal of biological chemistry* vol. 286,7 (2011): 5599-606. doi:10.1074/jbc.M110.190785
99. Lam, T et al. "Reversal of intramyocellular lipid accumulation by lipophagy and a p62-mediated pathway." *Cell death discovery* vol. 2 16061. 22 Aug. 2016, doi:10.1038/cddiscovery.2016.61
100. Tatsumi, Takayuki et al. "Forced lipophagy reveals that lipid droplets are required for early embryonic development in mouse." *Development (Cambridge, England)* vol. 145,4 dev161893. 23 Feb. 2018, doi:10.1242/dev.161893
101. Martinez-Lopez, Nuria et al. "Autophagy in the CNS and Periphery Coordinate Lipophagy and Lipolysis in the Brown Adipose Tissue and Liver." *Cell metabolism* vol. 23,1 (2016): 113-27. doi:10.1016/j.cmet.2015.10.008
102. Anand, Preetha et al. "A novel role for lipid droplets in the organismal antibacterial response." *eLife* vol. 1 e00003. 13 Nov. 2012, doi:10.7554/eLife.00003
103. Fairbank M, Huang K, El-Husseini A, Nabi IR. RING finger palmitoylation of the endoplasmic reticulum Gp78 E3 ubiquitin ligase. *FEBS Lett*. 2012 Jul 30;586(16):2488-93. doi: 10.1016/j.febslet.2012.06.011. Epub 2012 Jun 21. PMID: 22728137.
104. Lynes EM, Raturi A, Shenkman M, Ortiz Sandoval C, Yap MC, Wu J, Janowicz A, Myhill N, Benson MD, Campbell RE, Berthiaume LG, Lederkremer GZ, Simmen T. Palmitoylation is

- the switch that assigns calnexin to quality control or ER Ca<sup>2+</sup> signaling. *J Cell Sci.* 2013 Sep 1;126(Pt 17):3893-903. doi: 10.1242/jcs.125856. Epub 2013 Jul 10. PMID: 23843619.
105. Guerriero, Christopher J, and Jeffrey L Brodsky. "The delicate balance between secreted protein folding and endoplasmic reticulum-associated degradation in human physiology." *Physiological reviews* vol. 92,2 (2012): 537-76. doi:10.1152/physrev.00027.2011
  106. Olzmann, James A et al. "The mammalian endoplasmic reticulum-associated degradation system." *Cold Spring Harbor perspectives in biology* vol. 5,9 a013185. 1 Sep. 2013, doi:10.1101/cshperspect.a013185
  107. Christianson, John C, and Yihong Ye. "Cleaning up in the endoplasmic reticulum: ubiquitin in charge." *Nature structural & molecular biology* vol. 21,4 (2014): 325-35. doi:10.1038/nsmb.2793
  108. Lin, Jonathan H et al. "Divergent effects of PERK and IRE1 signaling on cell viability." *PloS one* vol. 4,1 (2009): e4170. doi:10.1371/journal.pone.0004170
  109. Wang, Miao, and Randal J Kaufman. "Protein misfolding in the endoplasmic reticulum as a conduit to human disease." *Nature* vol. 529,7586 (2016): 326-35. doi:10.1038/nature17041
  110. Xu, Chengchao, and Davis T W Ng. "Glycosylation-directed quality control of protein folding." *Nature reviews. Molecular cell biology* vol. 16,12 (2015): 742-52. doi:10.1038/nrm4073
  111. Cherepanova, Natalia et al. "N-linked glycosylation and homeostasis of the endoplasmic reticulum." *Current opinion in cell biology* vol. 41 (2016): 57-65. doi:10.1016/j.ceb.2016.03.021
  112. Satoh, Tadashi et al. "Structural basis for oligosaccharide recognition of misfolded glycoproteins by OS-9 in ER-associated degradation." *Molecular cell* vol. 40,6 (2010): 905-16. doi:10.1016/j.molcel.2010.11.017
  113. Christianson, John C et al. "OS-9 and GRP94 deliver mutant alpha1-antitrypsin to the Hrd1-SEL1L ubiquitin ligase complex for ERAD." *Nature cell biology* vol. 10,3 (2008): 272-82. doi:10.1038/ncb1689
  114. Mueller, Britta et al. "SEL1L nucleates a protein complex required for dislocation of misfolded glycoproteins." *Proceedings of the National Academy of Sciences of the United States of America* vol. 105,34 (2008): 12325-30. doi:10.1073/pnas.08053711105
  115. Tyler, Ryan E et al. "Unassembled CD147 is an endogenous endoplasmic reticulum-associated degradation substrate." *Molecular biology of the cell* vol. 23,24 (2012): 4668-78. doi:10.1091/mbc.E12-06-0428

116. Carvalho, Pedro et al. "Retrotranslocation of a misfolded luminal ER protein by the ubiquitin-ligase Hrd1p." *Cell* vol. 143,4 (2010): 579-91. doi:10.1016/j.cell.2010.10.028
117. Stein A, Ruggiano A, Carvalho P, Rapoport TA. Key steps in ERAD of luminal ER proteins reconstituted with purified components. *Cell*. 2014 Sep 11;158(6):1375-1388. doi: 10.1016/j.cell.2014.07.050. PMID: 25215493; PMCID: PMC4163015.
118. Baldrige, Ryan D, and Tom A Rapoport. "Autoubiquitination of the Hrd1 Ligase Triggers Protein Retrotranslocation in ERAD." *Cell* vol. 166,2 (2016): 394-407. doi:10.1016/j.cell.2016.05.048
119. Lilley, Brendan N, and Hidde L Ploegh. "A membrane protein required for dislocation of misfolded proteins from the ER." *Nature* vol. 429,6994 (2004): 834-40. doi:10.1038/nature02592
120. Ye, Yihong et al. "A membrane protein complex mediates retro-translocation from the ER lumen into the cytosol." *Nature* vol. 429,6994 (2004): 841-7. doi:10.1038/nature02656
121. Greenblatt, Ethan J et al. "Derlin-1 is a rhomboid pseudoprotease required for the dislocation of mutant  $\alpha$ -1 antitrypsin from the endoplasmic reticulum." *Nature structural & molecular biology* vol. 18,10 1147-52. 11 Sep. 2011, doi:10.1038/nsmb.2111
122. Mehnert, Martin et al. "Der1 promotes movement of misfolded proteins through the endoplasmic reticulum membrane." *Nature cell biology* vol. 16,1 (2014): 77-86. doi:10.1038/ncb2882
123. Plemper, R K et al. "Mutant analysis links the translocon and BiP to retrograde protein transport for ER degradation." *Nature* vol. 388,6645 (1997): 891-5. doi:10.1038/42276
124. Scott, Daniel C, and Randy Schekman. "Role of Sec61p in the ER-associated degradation of short-lived transmembrane proteins." *The Journal of cell biology* vol. 181,7 (2008): 1095-105. doi:10.1083/jcb.200804053
125. Walther, Tobias C, and Robert V Farese Jr. "Lipid droplets and cellular lipid metabolism." *Annual review of biochemistry* vol. 81 (2012): 687-714. doi:10.1146/annurev-biochem-061009-102430
126. Pol, Albert et al. "Review: biogenesis of the multifunctional lipid droplet: lipids, proteins, and sites." *The Journal of cell biology* vol. 204,5 (2014): 635-46. doi:10.1083/jcb.201311051
127. Hashemi, Hayaa F, and Joel M Goodman. "The life cycle of lipid droplets." *Current opinion in cell biology* vol. 33 (2015): 119-24. doi:10.1016/j.ceb.2015.02.002



128. Listenberger, Laura L et al. "Triglyceride accumulation protects against fatty acid-induced lipotoxicity." *Proceedings of the National Academy of Sciences of the United States of America* vol. 100,6 (2003): 3077-82. doi:10.1073/pnas.0630588100
129. Kurat, Christoph F et al. "Cdk1/Cdc28-dependent activation of the major triacylglycerol lipase Tgl4 in yeast links lipolysis to cell-cycle progression." *Molecular cell* vol. 33,1 (2009): 53-63. doi:10.1016/j.molcel.2008.12.019
130. Rambold, Angelika S et al. "Fatty acid trafficking in starved cells: regulation by lipid droplet lipolysis, autophagy, and mitochondrial fusion dynamics." *Developmental cell* vol. 32,6 (2015): 678-92. doi:10.1016/j.devcel.2015.01.029
131. Haemmerle, Guenter et al. "ATGL-mediated fat catabolism regulates cardiac mitochondrial function via PPAR- $\alpha$  and PGC-1." *Nature medicine* vol. 17,9 1076-85. 21 Aug. 2011, doi:10.1038/nm.2439
132. Tang, Tianyi et al. "Desnutrin/ATGL activates PPAR $\delta$  to promote mitochondrial function for insulin secretion in islet  $\beta$  cells." *Cell metabolism* vol. 18,6 (2013): 883-95. doi:10.1016/j.cmet.2013.10.012
133. Miyanari, Yusuke et al. "The lipid droplet is an important organelle for hepatitis C virus production." *Nature cell biology* vol. 9,9 (2007): 1089-97. doi:10.1038/ncb1631
134. Herker, Eva et al. "Efficient hepatitis C virus particle formation requires diacylglycerol acyltransferase-1." *Nature medicine* vol. 16,11 (2010): 1295-8. doi:10.1038/nm.2238
135. Cermelli, Silvia et al. "The lipid-droplet proteome reveals that droplets are a protein-storage depot." *Current biology : CB* vol. 16,18 (2006): 1783-95. doi:10.1016/j.cub.2006.07.062
136. Anand, Preetha et al. "A novel role for lipid droplets in the organismal antibacterial response." *eLife* vol. 1 e00003. 13 Nov. 2012, doi:10.7554/eLife.00003
137. Moldavski, Ofer et al. "Lipid Droplets Are Essential for Efficient Clearance of Cytosolic Inclusion Bodies." *Developmental cell* vol. 33,5 (2015): 603-10. doi:10.1016/j.devcel.2015.04.015
138. Brasaemle, Dawn L et al. "Proteomic analysis of proteins associated with lipid droplets of basal and lipolytically stimulated 3T3-L1 adipocytes." *The Journal of biological chemistry* vol. 279,45 (2004): 46835-42. doi:10.1074/jbc.M409340200
139. Liu, Pingsheng et al. "Chinese hamster ovary K2 cell lipid droplets appear to be metabolic organelles involved in membrane traffic." *The Journal of biological chemistry* vol. 279,5 (2004): 3787-92. doi:10.1074/jbc.M311945200

140. Hodges, Brittany D M, and Christine C Wu. "Proteomic insights into an expanded cellular role for cytoplasmic lipid droplets." *Journal of lipid research* vol. 51,2 (2010): 262-73. doi:10.1194/jlr.R003582
141. Zehmer, John K et al. "Targeting sequences of UBXD8 and AAM-B reveal that the ER has a direct role in the emergence and regression of lipid droplets." *Journal of cell science* vol. 122,Pt 20 (2009): 3694-702. doi:10.1242/jcs.054700
142. Klemm, Elizabeth J et al. "Dual role of ancient ubiquitous protein 1 (AUP1) in lipid droplet accumulation and endoplasmic reticulum (ER) protein quality control." *The Journal of biological chemistry* vol. 286,43 (2011): 37602-14. doi:10.1074/jbc.M111.284794
143. Spandl, Johanna et al. "Ancient ubiquitous protein 1 (AUP1) localizes to lipid droplets and binds the E2 ubiquitin conjugase G2 (Ube2g2) via its G2 binding region." *The Journal of biological chemistry* vol. 286,7 (2011): 5599-606. doi:10.1074/jbc.M110.190785
144. Suzuki, Michitaka et al. "Derlin-1 and UBXD8 are engaged in dislocation and degradation of lipidated ApoB-100 at lipid droplets." *Molecular biology of the cell* vol. 23,5 (2012): 800-10. doi:10.1091/mbc.E11-11-0950
145. Jo, Youngah et al. "Ancient ubiquitous protein-1 mediates sterol-induced ubiquitination of 3-hydroxy-3-methylglutaryl CoA reductase in lipid droplet-associated endoplasmic reticulum membranes." *Molecular biology of the cell* vol. 24,3 (2013): 169-83. doi:10.1091/mbc.E12-07-0564
146. Olzmann, James A et al. "Spatial regulation of UBXD8 and p97/VCP controls ATGL-mediated lipid droplet turnover." *Proceedings of the National Academy of Sciences of the United States of America* vol. 110,4 (2013): 1345-50. doi:10.1073/pnas.1213738110
147. Ohsaki, Yuki et al. "Cytoplasmic lipid droplets are sites of convergence of proteasomal and autophagic degradation of apolipoprotein B." *Molecular biology of the cell* vol. 17,6 (2006): 2674-83. doi:10.1091/mbc.e05-07-0659
148. Hartman, Isamu Z et al. "Sterol-induced dislocation of 3-hydroxy-3-methylglutaryl coenzyme A reductase from endoplasmic reticulum membranes into the cytosol through a subcellular compartment resembling lipid droplets." *The Journal of biological chemistry* vol. 285,25 (2010): 19288-98.
149. Fei, Weihua et al. "Conditions of endoplasmic reticulum stress stimulate lipid droplet formation in *Saccharomyces cerevisiae*." *The Biochemical journal* vol. 424,1 61-7. 23 Oct. 2009, doi:10.1042/BJ20090785
150. Vevea, Jason D et al. "Role for Lipid Droplet Biogenesis and Microlipophagy in Adaptation to Lipid Imbalance in Yeast." *Developmental cell* vol. 35,5 (2015): 584-599. doi:10.1016/j.devcel.2015.11.010

151. Garbarino, Jeanne et al. "Sterol and diacylglycerol acyltransferase deficiency triggers fatty acid-mediated cell death." *The Journal of biological chemistry* vol. 284,45 (2009): 30994-1005. doi:10.1074/jbc.M109.050443
152. Petschnigg, Julia et al. "Good fat, essential cellular requirements for triacylglycerol synthesis to maintain membrane homeostasis in yeast." *The Journal of biological chemistry* vol. 284,45 (2009): 30981-93. doi:10.1074/jbc.M109.024752
153. Olzmann, James A, and Ron R Kopito. "Lipid droplet formation is dispensable for endoplasmic reticulum-associated degradation." *The Journal of biological chemistry* vol. 286,32 (2011): 27872-4. doi:10.1074/jbc.C111.266452
154. Velázquez, Ariadna P et al. "Lipid droplet-mediated ER homeostasis regulates autophagy and cell survival during starvation." *The Journal of cell biology* vol. 212,6 (2016): 621-31. doi:10.1083/jcb.201508102
155. Tomoda, H et al. "Inhibition of acyl-CoA synthetase by triacsins." *Biochimica et biophysica acta* vol. 921,3 (1987): 595-8.
156. Igal, R A et al. "Triacsin C blocks de novo synthesis of glycerolipids and cholesterol esters but not recycling of fatty acid into phospholipid: evidence for functionally separate pools of acyl-CoA." *The Biochemical journal* vol. 324 ( Pt 2),Pt 2 (1997): 529-34. doi:10.1042/bj3240529
157. Fujimoto, Yasuyuki et al. "Involvement of ACSL in local synthesis of neutral lipids in cytoplasmic lipid droplets in human hepatocyte HuH7." *Journal of lipid research* vol. 48,6 (2007): 1280-92. doi:10.1194/jlr.M700050-JLR200
158. Kassan, Adam et al. "Acyl-CoA synthetase 3 promotes lipid droplet biogenesis in ER microdomains." *The Journal of cell biology* vol. 203,6 (2013): 985-1001. doi:10.1083/jcb.201305142
159. Ploegh, Hidde L. "A lipid-based model for the creation of an escape hatch from the endoplasmic reticulum." *Nature* vol. 448,7152 (2007): 435-8. doi:10.1038/nature06004
160. Nakatsukasa, Kunio, and Takumi Kamura. "Subcellular Fractionation Analysis of the Extraction of Ubiquitinated Polytopic Membrane Substrate during ER-Associated Degradation." *PloS one* vol. 11,2 e0148327. 5 Feb. 2016, doi:10.1371/journal.pone.0148327
161. Hosokawa, Nobuko et al. "Human XTP3-B forms an endoplasmic reticulum quality control scaffold with the HRD1-SEL1L ubiquitin ligase complex and BiP." *The Journal of biological chemistry* vol. 283,30 (2008): 20914-24. doi:10.1074/jbc.M709336200

162. Meacham, G C et al. "The Hsc70 co-chaperone CHIP targets immature CFTR for proteasomal degradation." *Nature cell biology* vol. 3,1 (2001): 100-5. doi:10.1038/35050509
163. Younger, J Michael et al. "Sequential quality-control checkpoints triage misfolded cystic fibrosis transmembrane conductance regulator." *Cell* vol. 126,3 (2006): 571-82. doi:10.1016/j.cell.2006.06.041
164. Morito, Daisuke et al. "Gp78 cooperates with RMA1 in endoplasmic reticulum-associated degradation of CFTRDeltaF508." *Molecular biology of the cell* vol. 19,4 (2008): 1328-36. doi:10.1091/mbc.e07-06-0601
165. Tang, Wei et al. "Links between CD147 function, glycosylation, and caveolin-1." *Molecular biology of the cell* vol. 15,9 (2004): 4043-50. doi:10.1091/mbc.e04-05-0402
166. Banaszynski, Laura A et al. "A rapid, reversible, and tunable method to regulate protein function in living cells using synthetic small molecules." *Cell* vol. 126,5 (2006): 995-1004. doi:10.1016/j.cell.2006.07.025
167. Egeler, Emily L et al. "Ligand-switchable substrates for a ubiquitin-proteasome system." *The Journal of biological chemistry* vol. 286,36 (2011): 31328-36. doi:10.1074/jbc.M111.264101
168. Bersuker, Kirill et al. "Protein misfolding specifies recruitment to cytoplasmic inclusion bodies." *The Journal of cell biology* vol. 213,2 (2016): 229-41. doi:10.1083/jcb.201511024
169. Han, Gil-Soo et al. "An unconventional diacylglycerol kinase that regulates phospholipid synthesis and nuclear membrane growth." *The Journal of biological chemistry* vol. 283,29 (2008): 20433-42. doi:10.1074/jbc.M802903200
170. Adeyo, Oludotun et al. "The yeast lipin orthologue Pah1p is important for biogenesis of lipid droplets." *The Journal of cell biology* vol. 192,6 (2011): 1043-55. doi:10.1083/jcb.201010111
171. Thibault, Guillaume et al. "The membrane stress response buffers lethal effects of lipid disequilibrium by reprogramming the protein homeostasis network." *Molecular cell* vol. 48,1 (2012): 16-27. doi:10.1016/j.molcel.2012.08.016
172. Caldwell, S R et al. "Degradation of endoplasmic reticulum (ER) quality control substrates requires transport between the ER and Golgi." *The Journal of biological chemistry* vol. 276,26 (2001): 23296-303. doi:10.1074/jbc.M102962200

173. Vashist, S et al. "Distinct retrieval and retention mechanisms are required for the quality control of endoplasmic reticulum protein folding." *The Journal of cell biology* vol. 155,3 (2001): 355-68. doi:10.1083/jcb.200106123
174. Taxis, Christof et al. "ER-golgi traffic is a prerequisite for efficient ER degradation." *Molecular biology of the cell* vol. 13,6 (2002): 1806-18. doi:10.1091/mbc.01-08-0399
175. Christianson, John C et al. "Defining human ERAD networks through an integrative mapping strategy." *Nature cell biology* vol. 14,1 93-105. 27 Nov. 2011, doi:10.1038/ncb2383
176. Bogdanov, Mikhail et al. "Lipids in the assembly of membrane proteins and organization of protein supercomplexes: implications for lipid-linked disorders." *Sub-cellular biochemistry* vol. 49 (2008): 197-239. doi:10.1007/978-1-4020-8831-5\_8
177. Contreras, Francesc-Xabier et al. "Specificity of intramembrane protein-lipid interactions." *Cold Spring Harbor perspectives in biology* vol. 3,6 a004705. 1 Jun. 2011, doi:10.1101/cshperspect.a004705
178. Harris, Charles A et al. "DGAT enzymes are required for triacylglycerol synthesis and lipid droplets in adipocytes." *Journal of lipid research* vol. 52,4 (2011): 657-67. doi:10.1194/jlr.M013003
179. Grotzke, Jeff E et al. "Deglycosylation-dependent fluorescent proteins provide unique tools for the study of ER-associated degradation." *Proceedings of the National Academy of Sciences of the United States of America* vol. 110,9 (2013): 3393-8. doi:10.1073/pnas.1300328110
180. Cao, Jingsong et al. "Targeting Acyl-CoA:diacylglycerol acyltransferase 1 (DGAT1) with small molecule inhibitors for the treatment of metabolic diseases." *The Journal of biological chemistry* vol. 286,48 (2011): 41838-51. doi:10.1074/jbc.M111.245456
181. Stone, Scot J et al. "Lipopenia and skin barrier abnormalities in DGAT2-deficient mice." *The Journal of biological chemistry* vol. 279,12 (2004): 11767-76. doi:10.1074/jbc.M311000200
182. Xu, Guoheng et al. "Post-translational regulation of adipose differentiation-related protein by the ubiquitin/proteasome pathway." *The Journal of biological chemistry* vol. 280,52 (2005): 42841-7. doi:10.1074/jbc.M506569200
183. Masuda, Yutaka et al. "ADRP/adipophilin is degraded through the proteasome-dependent pathway during regression of lipid-storing cells." *Journal of lipid research* vol. 47,1 (2006): 87-98. doi:10.1194/jlr.M500170-JLR200

184. Takahashi, Yu et al. "Perilipin2 plays a positive role in adipocytes during lipolysis by escaping proteasomal degradation." *Scientific reports* vol. 6 20975. 15 Feb. 2016, doi:10.1038/srep20975
185. Velázquez, Ariadna P et al. "Lipid droplet-mediated ER homeostasis regulates autophagy and cell survival during starvation." *The Journal of cell biology* vol. 212,6 (2016): 621-31. doi:10.1083/jcb.201508102
186. Li, Zhaoyu et al. "The ratio of phosphatidylcholine to phosphatidylethanolamine influences membrane integrity and steatohepatitis." *Cell metabolism* vol. 3,5 (2006): 321-31. doi:10.1016/j.cmet.2006.03.007
187. Fu, Suneng et al. "Aberrant lipid metabolism disrupts calcium homeostasis causing liver endoplasmic reticulum stress in obesity." *Nature* vol. 473,7348 (2011): 528-31. doi:10.1038/nature09968
188. Volmer, Romain, and David Ron. "Lipid-dependent regulation of the unfolded protein response." *Current opinion in cell biology* vol. 33 (2015): 67-73. doi:10.1016/j.ceb.2014.12.002
189. Jonikas, Martin C et al. "Comprehensive characterization of genes required for protein folding in the endoplasmic reticulum." *Science (New York, N.Y.)* vol. 323,5922 (2009): 1693-7. doi:10.1126/science.1167983
190. Hiramatsu, Nobuhiko et al. "Multiple Mechanisms of Unfolded Protein Response-Induced Cell Death." *The American journal of pathology* vol. 185,7 (2015): 1800-8. doi:10.1016/j.ajpath.2015.03.009
191. Novoa, I et al. "Feedback inhibition of the unfolded protein response by GADD34-mediated dephosphorylation of eIF2alpha." *The Journal of cell biology* vol. 153,5 (2001): 1011-22. doi:10.1083/jcb.153.5.1011
192. Lin, Jonathan H et al. "IRE1 signaling affects cell fate during the unfolded protein response." *Science (New York, N.Y.)* vol. 318,5852 (2007): 944-9. doi:10.1126/science.1146361
193. Han, Dan et al. "IRE1alpha kinase activation modes control alternate endoribonuclease outputs to determine divergent cell fates." *Cell* vol. 138,3 (2009): 562-75. doi:10.1016/j.cell.2009.07.017
194. Yen, Chi-Liang Eric et al. "Thematic review series: glycerolipids. DGAT enzymes and triacylglycerol biosynthesis." *Journal of lipid research* vol. 49,11 (2008): 2283-301. doi:10.1194/jlr.R800018-JLR200

195. Benyair, Ron et al. "Glycan regulation of ER-associated degradation through compartmentalization." *Seminars in cell & developmental biology* vol. 41 (2015): 99-109. doi:10.1016/j.semcdb.2014.11.006
196. Tamura, Taku et al. "Characterization of early EDEM1 protein maturation events and their functional implications." *The Journal of biological chemistry* vol. 286,28 (2011): 24906-15. doi:10.1074/jbc.M111.243998
197. Lakkaraju, Asvin Kk et al. "Palmitoylated calnexin is a key component of the ribosome-translocon complex." *The EMBO journal* vol. 31,7 (2012): 1823-35. doi:10.1038/emboj.2012.15
198. Lynes, Emily M et al. "Palmitoylated TMX and calnexin target to the mitochondria-associated membrane." *The EMBO journal* vol. 31,2 (2012): 457-70. doi:10.1038/emboj.2011.384
199. Fairbank, Maria et al. "RING finger palmitoylation of the endoplasmic reticulum Gp78 E3 ubiquitin ligase." *FEBS letters* vol. 586,16 (2012): 2488-93. doi:10.1016/j.febslet.2012.06.011
200. Hetz, Claudio. "The unfolded protein response: controlling cell fate decisions under ER stress and beyond." *Nature reviews. Molecular cell biology* vol. 13,2 89-102. 18 Jan. 2012, doi:10.1038/nrm3270
201. Lu, Min et al. "Opposing unfolded-protein-response signals converge on death receptor 5 to control apoptosis." *Science (New York, N.Y.)* vol. 345,6192 (2014): 98-101. doi:10.1126/science.1254312
202. Urano, F et al. "Coupling of stress in the ER to activation of JNK protein kinases by transmembrane protein kinase IRE1." *Science (New York, N.Y.)* vol. 287,5453 (2000): 664-6. doi:10.1126/science.287.5453.664
203. Volmer, Romain et al. "Membrane lipid saturation activates endoplasmic reticulum unfolded protein response transducers through their transmembrane domains." *Proceedings of the National Academy of Sciences of the United States of America* vol. 110,12 (2013): 4628-33. doi:10.1073/pnas.1217611110
204. Hetz, Claudio et al. "Targeting the unfolded protein response in disease." *Nature reviews. Drug discovery* vol. 12,9 (2013): 703-19. doi:10.1038/nrd3976
205. Menendez, Javier A, and Ruth Lupu. "Fatty acid synthase and the lipogenic phenotype in cancer pathogenesis." *Nature reviews. Cancer* vol. 7,10 (2007): 763-77. doi:10.1038/nrc2222
206. Currie, Erin et al. "Cellular fatty acid metabolism and cancer." *Cell metabolism* vol. 18,2 (2013): 153-61. doi:10.1016/j.cmet.2013.05.017

207. Benjamin, Daniel I et al. "Diacylglycerol Metabolism and Signaling Is a Driving Force Underlying FASN Inhibitor Sensitivity in Cancer Cells." *ACS chemical biology* vol. 10,7 (2015): 1616-23. doi:10.1021/acscchembio.5b00240
208. Anderson, Daniel J et al. "Targeting the AAA ATPase p97 as an Approach to Treat Cancer through Disruption of Protein Homeostasis." *Cancer cell* vol. 28,5 (2015): 653-665. doi:10.1016/j.ccell.2015.10.002
209. Schneider, Caroline A et al. "NIH Image to ImageJ: 25 years of image analysis." *Nature methods* vol. 9,7 (2012): 671-5. doi:10.1038/nmeth.2089
210. Benjamin, Daniel I et al. "Ether lipid generating enzyme AGPS alters the balance of structural and signaling lipids to fuel cancer pathogenicity." *Proceedings of the National Academy of Sciences of the United States of America* vol. 110,37 (2013): 14912-7. doi:10.1073/pnas.1310894110
211. Mulvihill, Melinda M et al. "Metabolic profiling reveals PAFAH1B3 as a critical driver of breast cancer pathogenicity." *Chemistry & biology* vol. 21,7 (2014): 831-40. doi:10.1016/j.chembiol.2014.05.008
212. Chen, Xiao, and Joel M Goodman. "The collaborative work of droplet assembly." *Biochimica et biophysica acta. Molecular and cell biology of lipids* vol. 1862,10 Pt B (2017): 1205-1211. doi:10.1016/j.bbalip.2017.07.003
213. Koliwad, Suneil K et al. "DGAT1-dependent triacylglycerol storage by macrophages protects mice from diet-induced insulin resistance and inflammation." *The Journal of clinical investigation* vol. 120,3 (2010): 756-67. doi:10.1172/JCI36066
214. Senkal, Can E et al. "Ceramide Is Metabolized to Acylceramide and Stored in Lipid Droplets." *Cell metabolism* vol. 25,3 (2017): 686-697. doi:10.1016/j.cmet.2017.02.010
215. Greenberg, Andrew S et al. "The role of lipid droplets in metabolic disease in rodents and humans." *The Journal of clinical investigation* vol. 121,6 (2011): 2102-10. doi:10.1172/JCI46069
216. Krahmer, Natalie et al. "Balancing the fat: lipid droplets and human disease." *EMBO molecular medicine* vol. 5,7 (2013): 973-83. doi:10.1002/emmm.201100671
217. Wilfling, Florian et al. "Triacylglycerol synthesis enzymes mediate lipid droplet growth by relocalizing from the ER to lipid droplets." *Developmental cell* vol. 24,4 (2013): 384-99. doi:10.1016/j.devcel.2013.01.013
218. Lass, Achim et al. "Lipolysis - a highly regulated multi-enzyme complex mediates the catabolism of cellular fat stores." *Progress in lipid research* vol. 50,1 (2011): 14-27. doi:10.1016/j.plipres.2010.10.004



219. Sztalryd, Carole et al. "Perilipin A is essential for the translocation of hormone-sensitive lipase during lipolytic activation." *The Journal of cell biology* vol. 161,6 (2003): 1093-103. doi:10.1083/jcb.200210169
220. Kim, Dae In, and Kyle J Roux. "Filling the Void: Proximity-Based Labeling of Proteins in Living Cells." *Trends in cell biology* vol. 26,11 (2016): 804-817. doi:10.1016/j.tcb.2016.09.004
221. Rees, Johanna S et al. "Protein Neighbors and Proximity Proteomics." *Molecular & cellular proteomics : MCP* vol. 14,11 (2015): 2848-56. doi:10.1074/mcp.R115.052902
222. Lam, Stephanie S et al. "Directed evolution of APEX2 for electron microscopy and proximity labeling." *Nature methods* vol. 12,1 (2015): 51-4. doi:10.1038/nmeth.3179
223. Rhee, Hyun-Woo et al. "Proteomic mapping of mitochondria in living cells via spatially restricted enzymatic tagging." *Science (New York, N.Y.)* vol. 339,6125 (2013): 1328-1331. doi:10.1126/science.1230593
224. Hung, Victoria et al. "Proteomic mapping of the human mitochondrial intermembrane space in live cells via ratiometric APEX tagging." *Molecular cell* vol. 55,2 (2014): 332-41. doi:10.1016/j.molcel.2014.06.003
225. Hung, Victoria et al. "Proteomic mapping of cytosol-facing outer mitochondrial and ER membranes in living human cells by proximity biotinylation." *eLife* vol. 6 e24463. 25 Apr. 2017, doi:10.7554/eLife.24463
226. Le Guerroué, François et al. "Autophagosomal Content Profiling Reveals an LC3C-Dependent Piecemeal Mitophagy Pathway." *Molecular cell* vol. 68,4 (2017): 786-796.e6. doi:10.1016/j.molcel.2017.10.029
227. Mick, David U et al. "Proteomics of Primary Cilia by Proximity Labeling." *Developmental cell* vol. 35,4 (2015): 497-512. doi:10.1016/j.devcel.2015.10.015
228. Bendayan, M. "Tech.Sight. Worth its weight in gold." *Science (New York, N.Y.)* vol. 291,5507 (2001): 1363-5. doi:10.1126/science.291.5507.1363
229. Ruggiano, Annamaria et al. "Spatial control of lipid droplet proteins by the ERAD ubiquitin ligase Doa10." *The EMBO journal* vol. 35,15 (2016): 1644-55. doi:10.15252/embj.201593106
230. Stevenson, Julian et al. "Endoplasmic Reticulum-Associated Degradation and Lipid Homeostasis." *Annual review of nutrition* vol. 36 (2016): 511-42. doi:10.1146/annurev-nutr-071715-051030

231. Eastman, Scott W et al. "A role for ubiquitin ligases and Spartin/SPG20 in lipid droplet turnover." *The Journal of cell biology* vol. 184,6 (2009): 881-94. doi:10.1083/jcb.200808041
232. Bartz, René et al. "Dynamic activity of lipid droplets: protein phosphorylation and GTP-mediated protein translocation." *Journal of proteome research* vol. 6,8 (2007): 3256-65. doi:10.1021/pr070158j
233. Liu, Pingsheng et al. "Rab-regulated interaction of early endosomes with lipid droplets." *Biochimica et biophysica acta* vol. 1773,6 (2007): 784-93. doi:10.1016/j.bbamcr.2007.02.004
234. Gluchowski, Nina L et al. "Lipid droplets and liver disease: from basic biology to clinical implications." *Nature reviews. Gastroenterology & hepatology* vol. 14,6 (2017): 343-355. doi:10.1038/nrgastro.2017.32
235. Gao, Guangang et al. "Control of lipid droplet fusion and growth by CIDE family proteins." *Biochimica et biophysica acta. Molecular and cell biology of lipids* vol. 1862,10 Pt B (2017): 1197-1204. doi:10.1016/j.bbalip.2017.06.009
236. Li, Zhipeng et al. "A novel Rab10-EHBP1-EHD2 complex essential for the autophagic engulfment of lipid droplets." *Science advances* vol. 2,12 e1601470. 16 Dec. 2016, doi:10.1126/sciadv.1601470
237. Krahmer, Natalie et al. "Protein correlation profiles identify lipid droplet proteins with high confidence." *Molecular & cellular proteomics : MCP* vol. 12,5 (2013): 1115-26. doi:10.1074/mcp.M112.020230
238. Currie, Erin et al. "High confidence proteomic analysis of yeast LDs identifies additional droplet proteins and reveals connections to dolichol synthesis and sterol acetylation." *Journal of lipid research* vol. 55,7 (2014): 1465-77. doi:10.1194/jlr.M050229
239. Zhang, Shuyan et al. "Morphologically and Functionally Distinct Lipid Droplet Subpopulations." *Scientific reports* vol. 6 29539. 8 Jul. 2016, doi:10.1038/srep29539
240. Meyer, Hemmo et al. "Emerging functions of the VCP/p97 AAA-ATPase in the ubiquitin system." *Nature cell biology* vol. 14,2 117-23. 2 Feb. 2012, doi:10.1038/ncb2407
241. Peters, J M et al. "An abundant and ubiquitous homo-oligomeric ring-shaped ATPase particle related to the putative vesicle fusion proteins Sec18p and NSF." *The EMBO journal* vol. 9,6 (1990): 1757-67.
242. Egan, J J et al. "Mechanism of hormone-stimulated lipolysis in adipocytes: translocation of hormone-sensitive lipase to the lipid storage droplet." *Proceedings of the National*

- Academy of Sciences of the United States of America* vol. 89,18 (1992): 8537-41. doi:10.1073/pnas.89.18.8537
243. Ran, F Ann et al. "Genome engineering using the CRISPR-Cas9 system." *Nature protocols* vol. 8,11 (2013): 2281-2308. doi:10.1038/nprot.2013.143
  244. Stevenson, Julian et al. "A practical comparison of ligation-independent cloning techniques." *PloS one* vol. 8,12 e83888. 23 Dec. 2013, doi:10.1371/journal.pone.0083888
  245. Wang, Huajin et al. "Seipin is required for converting nascent to mature lipid droplets." *eLife* vol. 5 e16582. 26 Aug. 2016, doi:10.7554/eLife.16582
  246. Zurek, Nesia et al. "Reticulon short hairpin transmembrane domains are used to shape ER tubules." *Traffic (Copenhagen, Denmark)* vol. 12,1 (2011): 28-41. doi:10.1111/j.1600-0854.2010.01134.x
  247. Anderson, Daniel J et al. "Targeting the AAA ATPase p97 as an Approach to Treat Cancer through Disruption of Protein Homeostasis." *Cancer cell* vol. 28,5 (2015): 653-665. doi:10.1016/j.ccell.2015.10.002
  248. Huang, Da Wei et al. "Systematic and integrative analysis of large gene lists using DAVID bioinformatics resources." *Nature protocols* vol. 4,1 (2009): 44-57. doi:10.1038/nprot.2008.211
  249. Supek, Fran et al. "REVIGO summarizes and visualizes long lists of gene ontology terms." *PloS one* vol. 6,7 (2011): e21800. doi:10.1371/journal.pone.0021800
  250. Shannon, Paul et al. "Cytoscape: a software environment for integrated models of biomolecular interaction networks." *Genome research* vol. 13,11 (2003): 2498-504. doi:10.1101/gr.1239303
  251. To, Milton et al. "Lipid disequilibrium disrupts ER proteostasis by impairing ERAD substrate glycan trimming and dislocation." *Molecular biology of the cell* vol. 28,2 (2017): 270-284. doi:10.1091/mbc.E16-07-0483
  252. Saraswathi, Viswanathan, and Alyssa H Hasty. "Inhibition of long-chain acyl coenzyme A synthetases during fatty acid loading induces lipotoxicity in macrophages." *Arteriosclerosis, thrombosis, and vascular biology* vol. 29,11 (2009): 1937-43. doi:10.1161/ATVBAHA.109.195362
  253. Klaus, Christina et al. "Modulating effects of acyl-CoA synthetase 5-derived mitochondrial Wnt2B palmitoylation on intestinal Wnt activity." *World journal of gastroenterology* vol. 20,40 (2014): 14855-64. doi:10.3748/wjg.v20.i40.14855

254. Ruiz, Mario et al. "Evolutionarily conserved long-chain Acyl-CoA synthetases regulate membrane composition and fluidity." *eLife* vol. 8 e47733. 26 Nov. 2019, doi:10.7554/eLife.47733
255. Grevengoed, Trisha J et al. "Acyl-CoA metabolism and partitioning." *Annual review of nutrition* vol. 34 (2014): 1-30. doi:10.1146/annurev-nutr-071813-105541